To the Graduate Council:

I am submitting herewith a dissertation written by Ming Zhang entitled "Study of Shape Coexistence in Lead and Thallium Isotopes." I have examined the final copy of this dissertation for form and content and recommend that it be accepted in partial fulfillment of the requirements for the degree of Doctor of Philosophy, with a major in Physics.

Carrol Bingham

Carrol R. Bingham, Major professor

We have read this dissertation
and recommend its acceptance:

Wasil Nazarewicz

D. V. Blelock

Leo T. Rudinger

Accepted for the Council:

Associate Vice Chancellor
and Dean of the Graduate School

STUDY OF SHAPE COEXISTENCE IN LEAD AND THALLIUM ISOTOPES

A Dissertation

Presented for the

Doctor of Philosophy

Degree

The University of Tennessee, Knoxville

Ming Zhang

May 1995

This dissertation

is

dedicated

to my parents

and

to my wife

Yi Yu

ACKNOWLEDGEMENTS

First of all I would like to acknowledge the Nuclear Physics Group at the University of Tennessee of which I have been a member of for the past five years. It is the constant support from this group by offering me the position of a research assistant that enabled me to finish my Ph.D. degree studies. I would like to thank the committee members for carefully reading this manuscript and giving many very valuable comments and suggestion. Thanks go to Dr. L. L. Riedinger and other professors in the nuclear physics group for their support and encouragement. My sincere gratitude goes to Dr. C. R. Bingham, not only because he is my thesis advisor who introduced me to the aspects of this thesis work, but also for his help and encouragement in my study and daily life here for all past years.

I greatly appreciate the opportunity to meet with the many theoreticians both through Oak Ridge National Laboratory and the Joint Institute for Heavy-Ion Research. I would particularly like to thank Dr. J.-y. Zhang for his willingness to answer the many questions which arose during this work. Many theoretical calculations and discussion part in my thesis work were critically dependent upon his help. I would like to thank our collaborators at Oak Ridge National Laboratory for giving me the opportunity to learn and practice experimental nuclear science at the Holifield Heavy Ion Research Facility. Thanks should be expressed to Drs. H.K. Carter, J. Kormicki, P. Mantica, L. Rayburn, and many other people who helped in setting up the experiments and taking data for this thesis work. Thanks should go to Dr. J.L. Wood particularly for his help and suggestions in the experiment and relating to his experience on ^{195}Pb and shape coexistence.

Thanks should go to the postdoctoral fellow, Dr. B. Zimmerman for many useful discussions about my thesis work. I am also thankful to Dr. H. Jin and Mr.

W.F. Mueller and X.-Z. Wang for help on many occasions in last few years. Dr. Jin's program 'lipha' was very useful in the preparing figures in this thesis and many other works. Mr. Mueller's experience on the TRS' plotting just helped me on time. To others whose names are not mentioned, I owe thanks for the many friendships I have gained during my stay at the University of Tennessee.

Finally, I would like to express my personal gratitude to my wife, Yi, for her support, encouragement and love throughout my academic years.

ABSTRACT

The β^+/EC decays of mass-separated ^{199}Bi and ^{193}Bi were studied at the Oak Ridge Holifield Heavy-Ion Research Facility. In these experiments the heavy-ion fusion reactions $^{187}Re(^{16}O, 4n)$ and $^{185}Re(^{16}O, 8n)$ were used. Time-sequenced spectra of γ-rays, X-rays, conversion electrons and $\gamma\gamma$t, γXt, eγt, eXt coincidence data have been obtained. The decay schemes of ^{199}Bi consisting of 67 excited states and 216 transitions and of ^{193}Bi consisting of 41 excited states and 61 transitions in were constructed . Several very-converted transitions interpreted to have E0 multipole admixtures, an indicator of shape coexistence, were found to de-excite positive-parity levels at 1705 and 1754 keV in ^{199}Bi and levels 757 and 1023 keV higher than the isomer state in ^{193}Bi. One possible deformed state with negative parity was found at 739 keV in ^{193}Bi.

The systematics of the lower excited states in odd-mass Pb isotopes were discussed. The good agreement were found for $p_{3/2}$, $f_{5/2}$ and $i_{13/2}$ energies as compared with the theoretical deformed harmonic-oscillator potential predictions. The systematics of shape coexistent states in odd-mass Pb isotopes were discussed in both positive and negative parities states and compares was made with even-mass isotopes. The odd-A states were interpreted in terms of a single neutron weakly coupled with the spherical and oblate deformed even-core. The Nilsson model and Total Routhian Surface calculations were used to studied the nuclear shape of Pb isotopes.

As a by-product of the ^{193}Bi experiment, a decay scheme of ^{193}Pb with 56 excited states and 86 transitions was established. Two bands of $\pi h_{9/2}$ $9/2^-[505]$ and $\pi h_{9/2}$ $7/2[514]$ were expanded. The particle-rotor model was applied to calculate

level energies and and transition rates. The calculation with $\varepsilon_2 = -0.145$ and $\gamma = 0°$ gave a good fit to the experimental relative intensities for K=9/2 band.

Contents

List of Tables

List of Figures

CHAPTER 1

INTRODUCTION

Nuclear shape, a semi-classical concept, is used to describe the property of general, collective structure in nuclei. As with many other nuclear properties, e.g., single particle orbitals, different nuclear shapes can coexist among the eigenstates of a nucleus. It means there is more than one stable nuclear shape existing in some excitation region, rather than a shape change as the excitation energy changes. The main point of this paper is the study of the shape coexistence in odd-A Pb isotopes.

The phenomenon of nuclear shape coexistence was found first in the nucleus ^{16}O about 40 years ago. Morinaga [Mor56] explained the first excited $J^\pi = 0^+$ at 6.05 MeV as a deformed state in 1956. In about ten years, Brown and Green [Bro64,66a,66b] and Engeland [Eng65] developed this idea in theory. The first excited $J^\pi = 0^+$, the collective rotational-like band built on it and the B(E2) values related with this band were explained very well, using two particle-two hole (2p-2h) and 4p-4h configurations which mixed with the spherical ground state. After that, coexistent states in the ^{40}Ca region were studied by the same process. Federman [Fed69] made a comprehensive review of this region. Before 1970, the main study of coexistence phenomena was limited to the light nuclei ($\leq^{56}$Ni). In this period, the main theoretical considerations started from the Nilsson model and included the pairing part from the residual interaction which induces the BCS pairing correlations in the nuclear system. A quadrupole deformed static field combined with pairing correlations create the necessary minima in the potential energy surface of

the nucleus. Spherical states and quadrupole deformed excited states will co-exist in the same nucleus.

After understanding shape coexistence in the light mass region, many coexistence phenomena were found in the heavy nuclide region from the 1970's, especially in heavy nuclei near closed shells. The presence of low-lying shell-model intruder states and rotational bands occurring in nuclei with spherical or near-spherical ground states constituted the main evidence of coexistence in this region. In the 1980's and 90's, more shape coexistence was found and superdeformed high spin states proliferated. With the development of experimental techniques, in fact, coexistence phenomena were found in (nearly) every nucleus. Heyde *et al.*[Hey83] had a comprehensive review in odd-mass nuclei and Wood *et al.*[Woo92] had another comprehensive review in even-mass nuclei. Large amounts of experimental results have pushed the development of the theory on coexistence. There are many theoretical descriptions of coexistence in nuclei. But usually these theories can be placed in two major categories: shell model plus a residual proton-neutron force and deformed mean-field descriptions.

For lead isotopes, the first evidence of shape coexistence was obtained only ten years ago [Dup84]. In even-mass isotopes, the deformed 0^+ excited state is explained as a π(2p-2h) intruder state. A proton pair jumps from $3s_{1/2}$ state to next shell $1h_{9/2}$ state. Excited 0^+ deformed state systematics of even-A lead isotopes compared with intruder states in $^{A-1}$Tl and $^{A+1}$Bi are shown in Fig. 1.1. B(E2) values for decay from the deformed 2^+ state to the ground state and deformed 0^+ state and the E0 transition components are used to support the existence of collective bands and shape coexistence (Fig. 1.2). ρ^2(E0), given in the figure 1.2, is the reduced electric monopole transition probability and will be discussed in section 2.7.

In the odd-mass lead isotopes, there is evidence for shape coexistence only

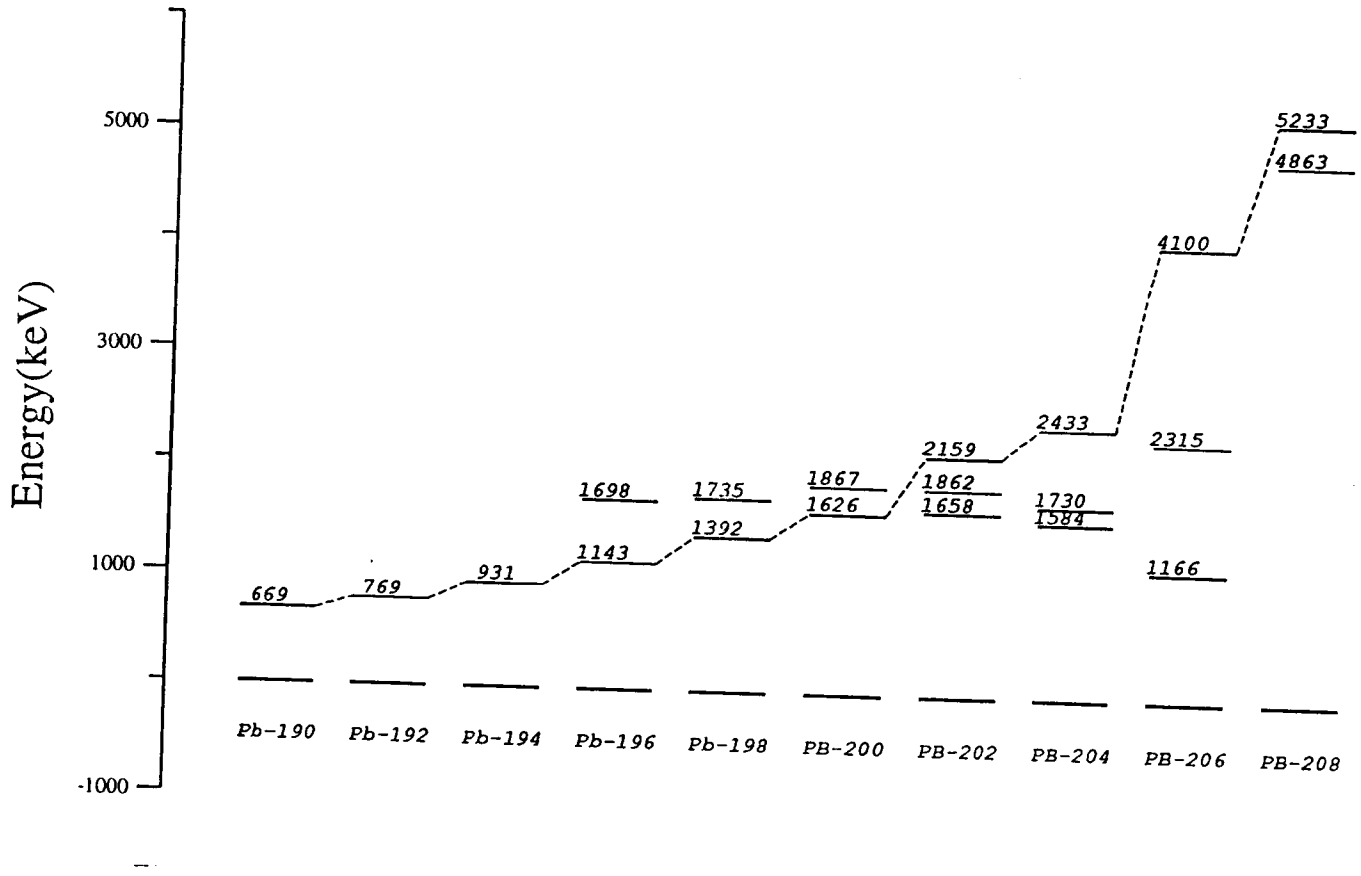

Figure 1.1: The excitation energy of the 0^+ states in the $^{190\text{-}208}$Pb nuclei. The candidates for the intruder states π(2p-2h) are connected with the dashed line.

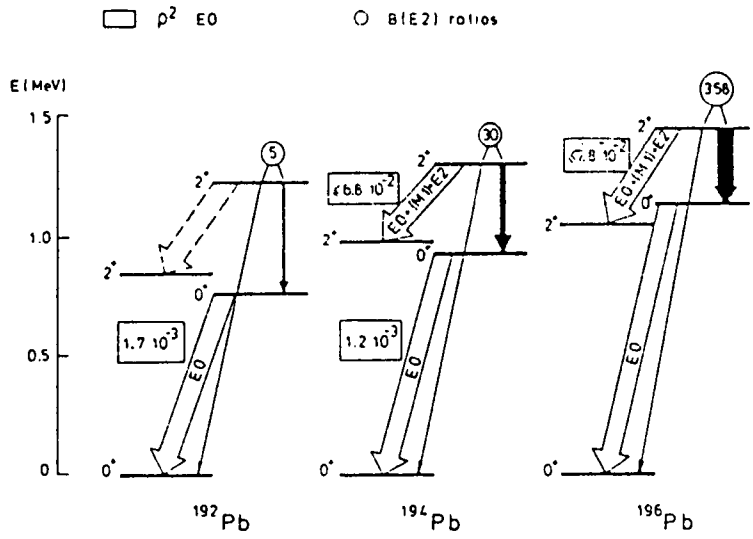

Figure 1.2: Electromagnetic decay for low-spin candidates of the deformed bands in $^{192-196}$Pb. The ratios $B(\mathrm{E2}; 2_2^+ \rightarrow 0_2^+)/B(\mathrm{E2}; 2_2^+ \rightarrow 0_1^+)$ are shown in circles above the 2_2^+ levels. Electric monopole transitions and their $\rho^2(\mathrm{E0})$ values are also shown. (from [Woo92])

in ^{195}Pb [Gri91] and ^{197}Pb [Van91]. Some positive parity shape coexisting states in these nuclei can be interpreted in terms of an $i_{13/2}$ neutron coupled to the shape coexisting states of the even mass cores.

The main objective of this study is to utilize β-decay from neutron-deficient Bismuth isotopes 193 and 199, to set up more complete level schemes of ^{193,199}Pb, to search for evidence of coexistence in these isotopes and to extend the systematics in odd-mass lead isotopes.

The development of nuclear physics depends on both theoretical and experimental studies. Chapter 2 is devoted to the nuclear theory. In the first four sections, some theoretical descriptions related with the shape coexistence phenomenon will be discussed. In the second half some nuclear decay theories related with this experiment will be introduced.

In Chapter 3, the experimental set up at Oak Ridge National Laboratory will be described including components for the production of radionuclides, mass

separation, tape transfer of activities and detection of γ-rays and electrons. In the last two sections, the data-acquisition system used for this work and the techniques of data analysis will be discussed in detail.

In Chapter 4 the experimental results are reported. From the β decay of ^{199}Bi and ^{193}Bi and γ de-excitation, more complete level schemes of ^{199}Pb and ^{193}Pb were developed and several possible E0 transitions were found, which serve as the indicator of nuclear deformation. The ^{193}Bi decays to ^{193}Pb and it, in turn, decays to ^{193}Tl. As the by-product of this experiment and combined with some early works of this group, a new level scheme of ^{193}Tl is presented.

The most important results, shape coexistence in ^{193,199}Pb, are discussed in the chapter 5. The systematics of coexistence and low levels in odd-mass Pb isotopes are discussed and compared with even- mass isotopes. Finally the single particle states of ^{193}Tl will be considered and calculated and the negative parity states will be discussed in terms of a particle-core coupling model.

Finally, the primary conclusions from the current work and some suggestions regarding future directions are discussed in the last chapter.

CHAPTER 2

THEORETICAL BACKGROUND

The essential challenge of nuclear physics is to explain the nucleus as a *many-body system of strongly interacting particles.* There are three fundamental forces in nature: *strong, electroweak and gravitation forces.* The short-ranged strong interaction which is the main force functioning in the nucleus, is still not understood in sufficient detail. The many-body($n > 3$) problem can not be solved mathematically. The nucleon number of a nucleus is lower than a few hundred, which is not enough to get a precise solution by statistical methods. Because of these difficulties in nuclear physics, many approximation methods have been adopted. Theoretically, many simplifying mathematical models are constructed to make the many-body problem tractable. According to the treatment of particles in the nucleus, these models can be divided to two kinds: *independent-particle models* and *collective models.* Experimentally, through nuclear spectroscopy and the analysis of different nuclear reactions, attempts are made to understand the nuclear structure and fundamental interactions among the particles moving in the nucleus.

2.1 Shell Model

The nuclear shell model is the best-known independent-particle model and usually is taken as the fundamental model of all other nuclear models in the low energy region. In this model, every nucleon is assumed to move independently in a single, smoothly varying central potential field, representing the average interaction

with all other nucleons in nucleus. It is a good approximation, because of the short-range property of the strong force and the Pauli exclusion principle which limits the interaction between the nucleons. This potential field has roughly the shape of a square well with a depth of about 50MeV and a radius equal to that of the nucleus.

For the single-particle moving in this approximately spherical potential, the Schrödiger equation is:

$$H\psi = \left(\frac{\mathbf{P}^2}{2M} + U(\mathbf{r})\right)\psi_{nlm}(\mathbf{r}) = E_{nlm}\psi_{nlm}(\mathbf{r}) \tag{2.1}$$

If the potential $U(\mathbf{r})$ is taken as a 3D harmonic oscillator or square well, this equation can be solved analytically. Solutions exist only for certain energies (eigenvalues) which are functions of quantum numbers. With the harmonic oscillator potential, the states are evenly distributed by the main quantum number $< n >$ and solutions are degenerate in l and m. In finite or infinite square wells, the states are further separated by different orbital angular momentum number $< l >$.

The Woods-Saxon potential:

$$U_{WS}(\mathbf{r}) = \frac{V_0}{1 + exp\left(\frac{\mathrm{r-R}}{a}\right)} \tag{2.2}$$

gives a better description to the real potential field. V_0 is the depth of the potential, R is the half-depth radius, and a is the diffuseness parameter which describes the rate of radial decrease in the nuclear potential at its surface. With this potential a numerical solution is required. There is some shift in the energy eigenvalues, but no big difference with solutions utilizing the finite square well. The rounded edge of the Woods-Saxon potential and the spin-orbit coupling interaction separates the states further by the direction of spin. The corresponding single-particle Woods-Saxon Hamiltonian is

$$H_{WS} = \frac{\mathbf{P}^2}{2M} + U_{WS}(\mathbf{r}) - v_{ls}\left(\frac{\hbar}{2Mc}\right)^2 gradU_{WS}(r)(\sigma \times p) \tag{2.3}$$

v_{ls} is the constant of spin-orbit interaction, σ is the spin matrix. The spin-orbit coupling interaction is a surface phenomenon. It is only connected with outside nucleons near the potential surface. An energy splitting proportional to $\sigma \cdot l$ is introduced where

$$\begin{aligned} \sigma \cdot l &= 2(s \cdot l) \\ &= j^2 - l^2 - s^2 \\ &= \begin{cases} l, & j = l + 1/2; \\ -(l+1), & j = l - 1/2. \end{cases} \end{aligned} \tag{2.4}$$

The energy splitting from the spin-orbit coupling interaction is proportional to l for different orbit quantum numbers $< l >$. The selection of the proper v_{ls} of this potential will create appropriate big gaps in the energy levels at neutron or proton numbers 2, 8, 20, 28, 50, 82 and 126(Fig. 2.1). The splitting of higher orbit states of $1f$, $1g$, $1h$ and $1i$ are responsible for gaps of 28, 50, 82 and 126. These magic numbers are fitted with experimental results perfectly. This is the most astonishing and important result from the shell model.

In this model, the nucleons filling the states under the major gap constitute a spherical "core" and are difficult to be excited. Nucleons outside of the major gap or unfilled holes under it are called valence particles and rearrangement of these is used to describe most low energy nuclear phenomena. This method simplified a very complicated many-body problem. The properties of ground states of nuclei and the structure of light or near closed shell nuclei can be explained successfully. But for nuclei far from closed shells, the more valence particles may occupy many j shells. The size of matrices for shell model calculations is too big to be solved. This is the limitation of single-particle shell model.

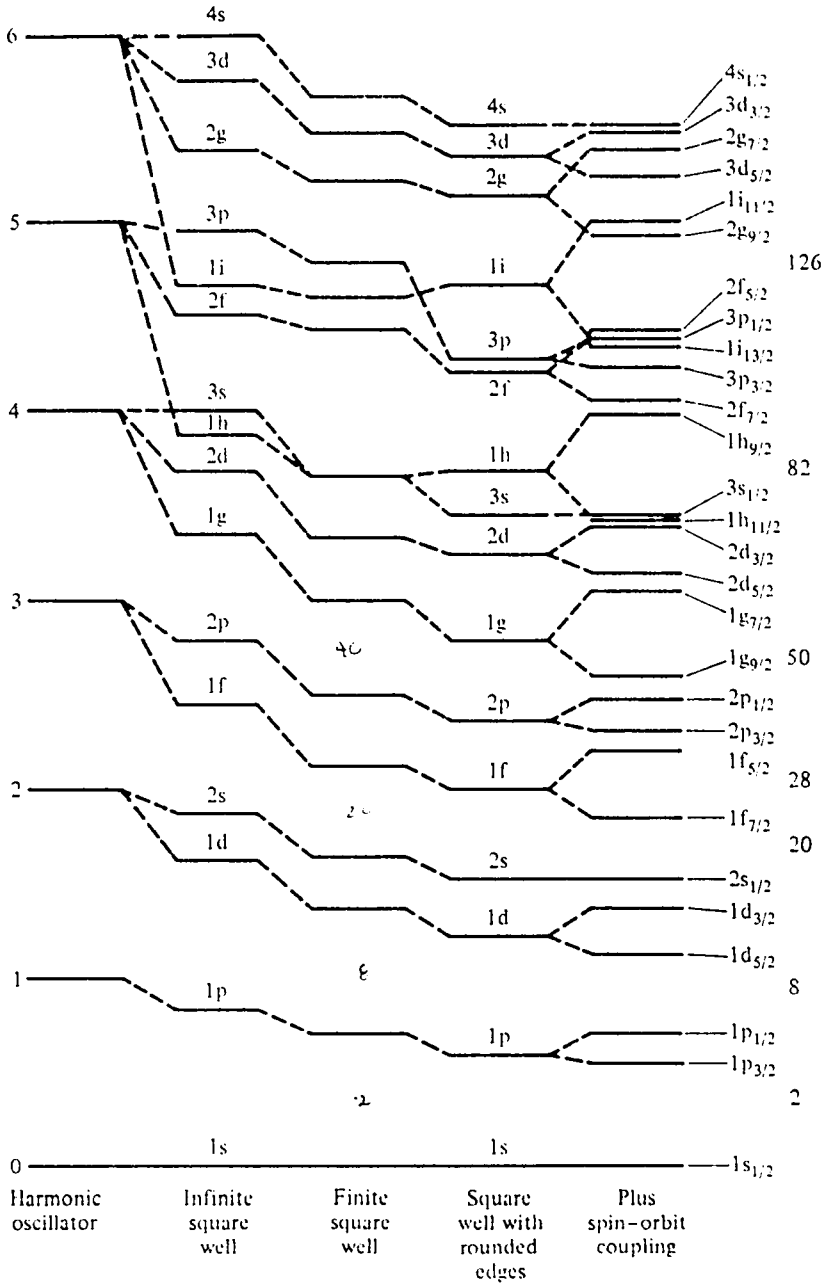

Figure 2.1: Ordering of states according to the shell model, using various potentials(schematic). From [JEL90]

2.2 Collective Model

The collective model was introduced by Bohr and Mottelson, mainly as a basic macroscopic nuclear structure model in the medium and heavy mass region. At the regions far from closed shells the collective motion of many valence nucleons is approximated with a few collective degrees of freedom. For regions relatively near closed shells ($60 < A < 150, 190 < A < 220$), the experimental low energy excited levels resemble those of a vibrating harmonic oscillator. For regions far from closed shells ($150 < A < 190, A > 220$), the experimental levels are similar to those of a rigid rotor. Thus the collective model is divided into two parts: the *vibrational* model and *rotational* model.

2.2.1 Vibrational Model

When a nucleus is easy to deform about its lowest equilibrium shape, vibrations about this shape will be the important motion mode at low excited energy. For small deformation at constant volume, the shape of a nucleus is described by a radius vector $R(\theta, \phi)$ from the origin to the surface.

$$R(\theta, \phi) = R_0[1 + \sum_{\lambda=2}^{\infty} \sum_{\mu=-\lambda}^{\lambda} \alpha^*_{\lambda\mu} Y_{\lambda\mu}(\theta, \phi)] \tag{2.5}$$

$\lambda = 1$, which corresponds to a translation of the nucleus, is not considered here. For the small harmonic vibration, the total Hamiltonian is[Nat65]

$$H = E_0 + \frac{1}{2B_\lambda} \sum_\mu \pi^+_{\lambda\mu} \pi_{\lambda\mu} + \frac{1}{2} C_\lambda \sum_\mu \alpha^+_{\lambda\mu} \alpha_{\lambda\mu} \tag{2.6}$$

E_0 is the energy of nucleus at the ground state; the second and third items are kinetic and potential energies of collective vibration. The classical oscillation frequency ω_λ equals $\sqrt{C_\lambda / B_\lambda}$. Introducing phonon creation and annihilation operators $(\beta^+_{\lambda\mu}, \beta_{\lambda\mu})$,

which satisfy the relations:

$$\left.\begin{aligned}\left[\beta_{\lambda'\mu'}, \beta^{+}_{\lambda\mu}\right] &= \delta_{\lambda'\lambda}\delta_{\mu'\mu} \\ [\beta_{\lambda'\mu'}, \beta_{\lambda\mu}] &= \left[\beta^{+}_{\lambda'\mu'}, \beta^{+}_{\lambda\mu}\right] = 0\end{aligned}\right\} \tag{2.7}$$

and letting

$$\left.\begin{aligned}\alpha_{\lambda\mu} &= \sqrt{\frac{\hbar}{2B_\lambda\omega_\lambda}}(\beta^{+}_{\lambda\mu} + (-1)^{\mu}\beta_{\lambda-\mu}) \\ \pi_{\lambda\mu} &= i\sqrt{\frac{\hbar B_\lambda\omega_\lambda}{2}}((-1)^{\mu}\beta^{+}_{\lambda-\mu} - \beta_{\lambda\mu})\end{aligned}\right\} \tag{2.8}$$

the quantized vibration Hamiltonian becomes

$$H_{vib} = H - E_0 = \hbar\omega_\lambda \sum_{\mu}(\beta^{+}_{\lambda\mu}\beta_{\lambda\mu} + \frac{1}{2}) \tag{2.9}$$

The total energy eigenvalues are

$$E = E_0 + \sum_{\lambda\mu}(n_{\lambda\mu} + \frac{1}{2})\hbar\omega_\lambda \tag{2.10}$$

where $n_{\lambda\mu}$ is the number of phonons in the $\lambda\mu$-mode of vibration. Modes with $\lambda = 2$ and 3 are called quadrupole and octupole vibrations, respectively. The excited energy spectra are shown in figure 2.2. The selection rule for the decay of a vibrational excited state limits the change in phonon number to one, or $\Delta n_\lambda = \pm 1$.

The main vibrational mode found in the experimental results is the quadrupole vibration($\lambda = 2$). Usually the orientation of the coordinate axes is chosen so that $\alpha_{21} = \alpha_{2-1} = 0$ and $\alpha_{22} = \alpha_{2-2}$. The parameters $\alpha_{2\mu}$ are related by the expressions:

$$\begin{aligned}\alpha_{20} &= \beta cos\gamma \\ \alpha_{22} &= \alpha_{2-2} = \tfrac{1}{\sqrt{2}}\beta sin\gamma\end{aligned} \tag{2.11}$$

An axially-symmetric nucleus has $\gamma = 0$. Oscillations in α_{20} and α_{22} are called β and γ vibrations, respectively.

2.2.2 Rotational Model

The total Hamiltonian of a collective rotational nucleus is

$$H = H_{rot} + H_{int} + H_{coup} \tag{2.12}$$

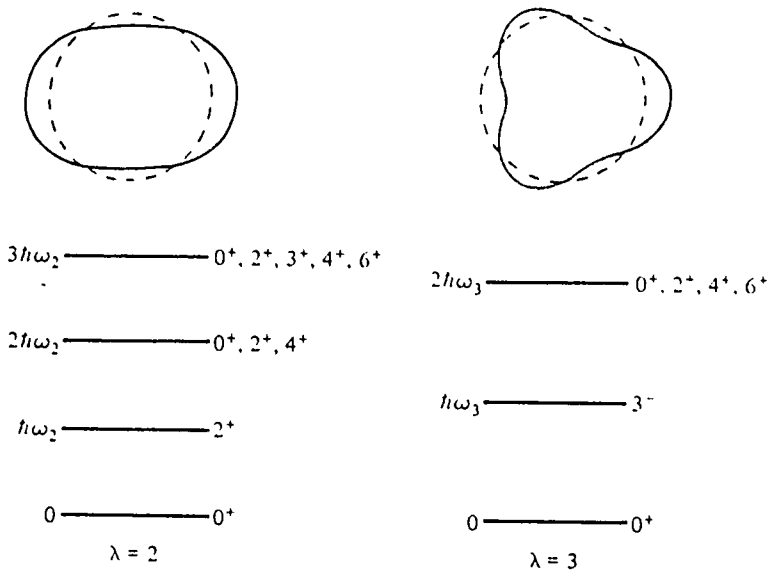

Figure 2.2: Energy spectra for the quadrupole and octupole surface vibration

where H_{rot} represents the collective rotation of the nucleus, H_{int} describes the internal motion of the nucleons and H_{coup} is the coupling between the rotational and intrinsic motion.

Usually for a nucleus far from closed shells, the nuclear deformation is large and the excitation energies of the rotational states are much lower than the single particle states. The characteristic frequency of rotation of the whole nucleus is much less than that of the internal nucleon motion. The coupling interaction is weak. Under the adiabatic approximation ($H_{coup} \sim 0$)

$$H = H_{rot} + H_{int} \tag{2.13}$$

The deformed nuclear shape or potential field is the first condition of nuclear collective rotation. A nucleus can not rotate along the symmetry axis, because a change in orientation is not detectable in quantum mechanics. Any collective rotational angular momentum $\mathbf{R}$ is perpendicular to the symmetry axis(Figure 2.3).

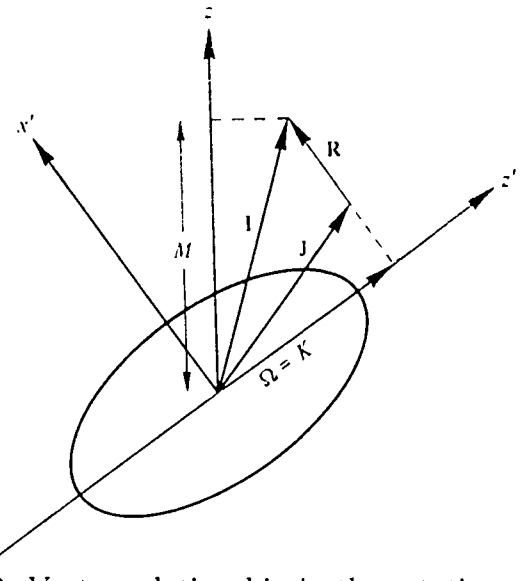

Figure 2.3: Vector relationship in the rotation model

The rotational Hamiltonian and corresponding energy eigenvalues are given by

$$\begin{aligned} H_{rot} &= \tfrac{1}{2\mathcal{J}}\mathbf{R}^2 \\ E_{rot} &= \tfrac{\hbar^2}{2\mathcal{J}}[I(I+1)+J(J+1)-2K^2] \end{aligned} \tag{2.14}$$

where $\mathcal{J}$ is the moment of inertia of the nucleus. In general, it lies between the moment of inertia of a rigid body and that for irrotational nucleon motion. For particular values of J and K, the sequence of energy levels just looks like a molecular rotational band.

For an even-even nucleus, the intrinsic angular momentum **J** is zero. The total angular momentum **I** equals **R**. So

$$\begin{aligned} H_{rot} &= \tfrac{1}{2\mathcal{J}}\mathbf{I}^2 \\ E_{rot} &= \tfrac{\hbar^2}{2\mathcal{J}}I(I+1) \end{aligned} \tag{2.15}$$

At higher energy, the adiabatic approximation will be worse and the moment of inertia will increase due to centrifugal stretching. The excited energy is modified as

$$E_{rot} = \frac{\hbar^2}{2\mathcal{J}}I(I+1) - BI^2(I+1)^2 \tag{2.16}$$

B is a fitting constant and can be decided by the experimental data. The rotational band can be set up on the collective vibrational states. Depending on the type, they are called the β or γ bands.

There have been many interesting phenomena found in the high spin rotational states in recent years. The description of high-spin phenomena has become a big topic in nuclear theory and lies outside of the scope of this work.

2.3 Nilsson Model

The deformed shell model is called the Nilsson model because a significant advance was made by Nilsson. The model assumes that all nucleons move in an axially deformed harmonic oscillator potential *V(x,y,z)* with spin-orbit and orbital angular momentum dependent terms. The Nilsson Hamiltonian is

$$H = \frac{-\hbar^2}{2m}\nabla^2 + V(x,y,z) - C\mathbf{l}\cdot\mathbf{s} - D\mathbf{l}^2 \tag{2.17}$$

where $V(x,y,z) = \frac{1}{2}m(\omega_x^2x^2 + \omega_y^2y^2 + \omega_z^2z^2)$ and $\omega_x = \omega_y = \omega_\perp$. Further, the frequencies can be written as

$$\left.\begin{aligned}\omega_\perp &= \omega_0(\varepsilon)(1+\tfrac{1}{3}\varepsilon)\\ \omega_z &= \omega_0(\varepsilon)(1-\tfrac{2}{3}\varepsilon)\end{aligned}\right\} \tag{2.18}$$

where ε is the deformation parameter in the Nilsson model. Keeping the nuclear volume as a constant

$$\omega_x\omega_y\omega_z = \omega_{00}^3 \tag{2.19}$$

Comparing the last two equations, one obtains

$$\omega_0(\varepsilon) = \omega_{00}(1 - \frac{1}{3}\varepsilon^2 - \frac{2}{27}\varepsilon^3)^{-1/3} \tag{2.20}$$

where ω_{00} is a constant which represents the frequency of the spherical nucleus.

For the case of a 3-D harmonic oscillator potential, the three frequencies can be written as

$$\left.\begin{aligned}\omega_x &= \omega_0(\varepsilon,\gamma)(1+\tfrac{1}{3}\varepsilon cos\gamma+\tfrac{1}{\sqrt{3}}\varepsilon sin\gamma)\\ \omega_y &= \omega_0(\varepsilon,\gamma)(1+\tfrac{1}{3}\varepsilon cos\gamma-\tfrac{1}{\sqrt{3}}\varepsilon sin\gamma)\\ \omega_z &= \omega_0(\varepsilon,\gamma)(1-\tfrac{2}{3}\varepsilon cos\gamma)\end{aligned}\right\} \tag{2.21}$$

where ε and γ are deformation parameters. For the axially symmetric system ($\gamma = 0$), it will return to the basic Nilsson model.

Using the polar coordinate system to describe a quadrupole deformed nucleus(Fig. 2.4), the deformed harmonic potential is

$$V_h(r,\theta,\phi) = \frac{1}{2}M\omega_0^2 r^2\{1-2\beta[cos\gamma\, Y_{20}(\theta,\phi)+\frac{1}{\sqrt{2}}sin\gamma(Y_{22}+Y_{2-2})]\} \tag{2.22}$$

The relationship between the different deformed parameters (β, ε) under the first-order approximation is

$$\varepsilon = \frac{3}{2}\sqrt{\frac{5}{4\pi}}\beta = 0.95\beta \tag{2.23}$$

The deformed Woods-Saxon potential is

$$V_{WS}(r,\theta,\phi) = \frac{V_0}{1+exp\left(\frac{r-R(\theta,\phi)}{a(\theta,\phi)}\right)} \tag{2.24}$$

where *R(θ, φ)* is defined by Eq. 2.5. In a deformed potential well, the nucleons in the same j subshell but having a different projection (Ω) on the symmetry axis have different wave functions and energies. The degeneracy of $(2j+1)$ for a j subshell is lifted to $(j+1/2)$ states. The resulting doubly degenerate states will split in the case of nuclear rotation. The calculated Nilsson diagram with the Woods-Saxon potential for both neutrons and protons are shown in Fig. 2.5.

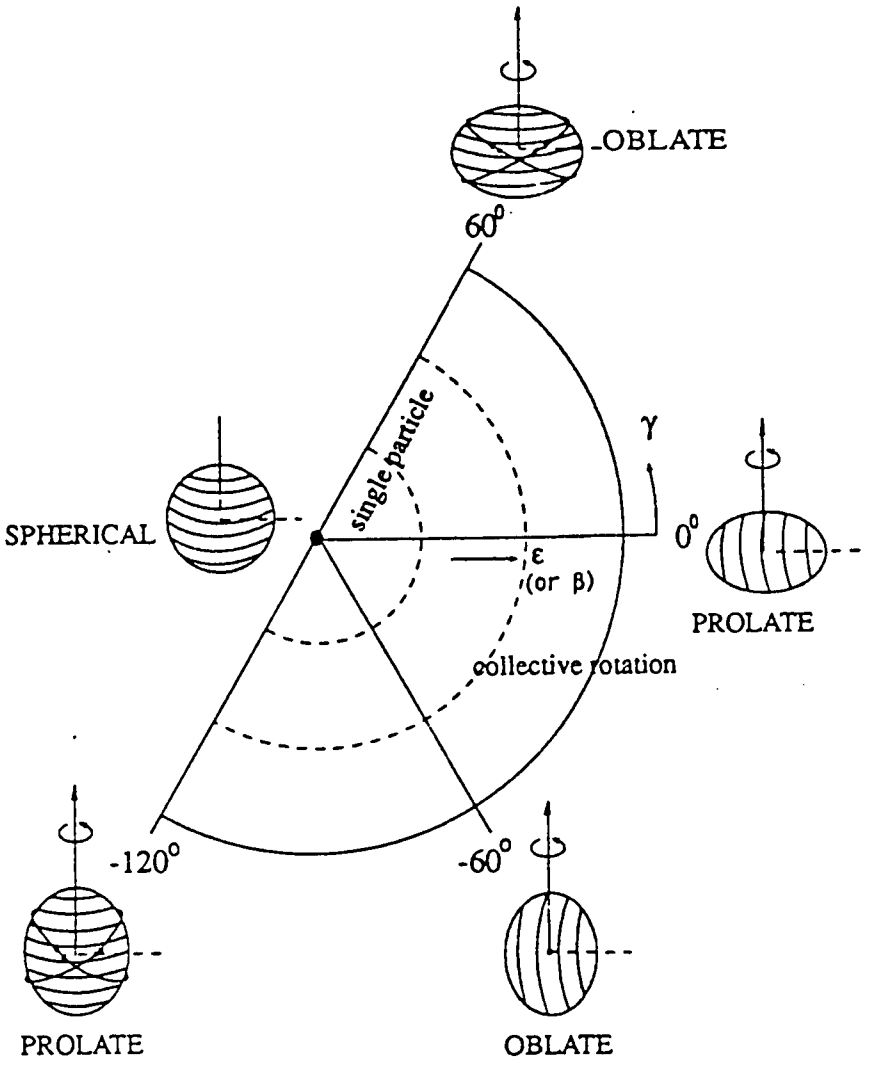

Figure 2.4: Lund-Warsaw convention of quadrupole deformation.

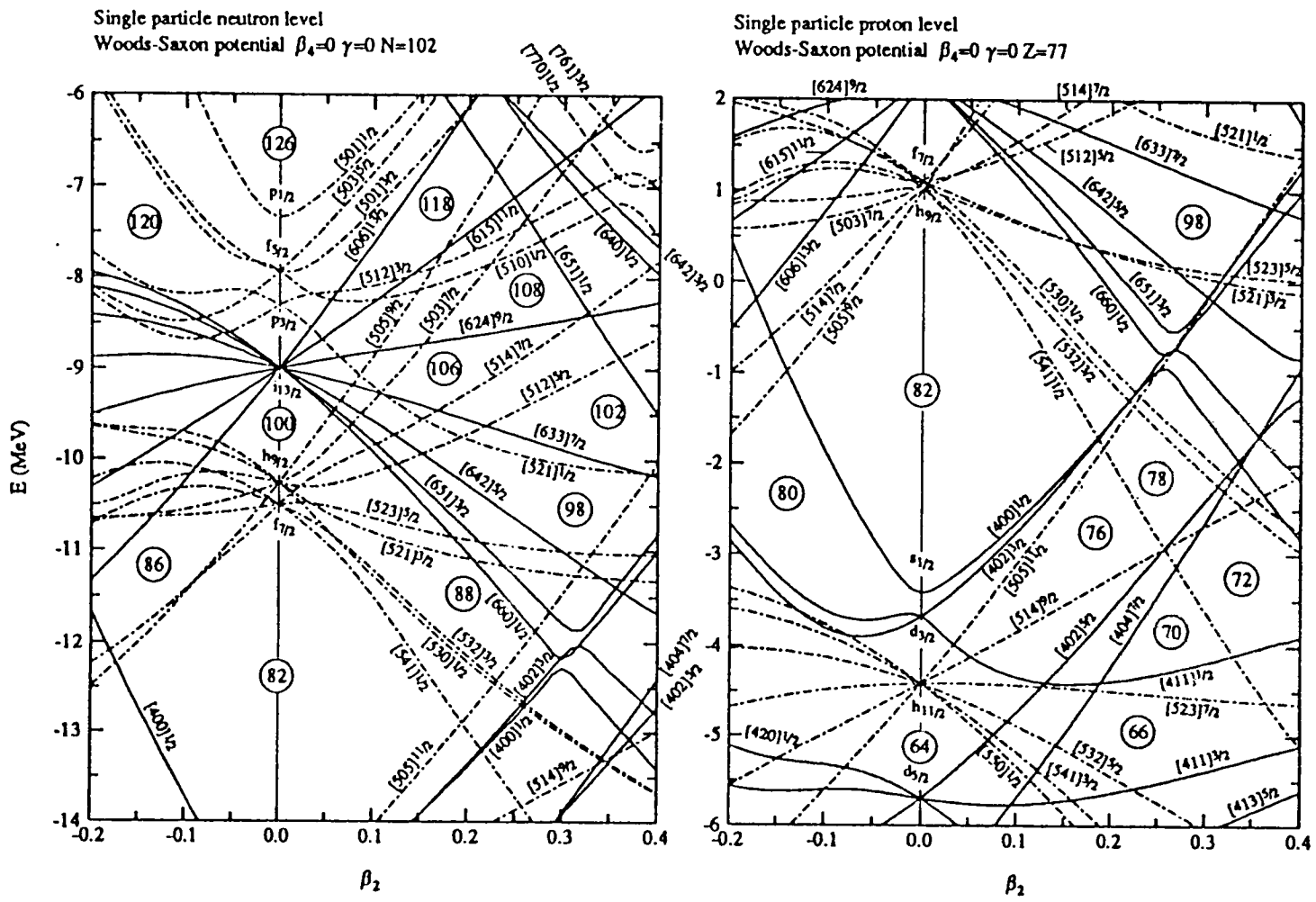

Figure 2.5: The Nilsson diagram for neutrons and protons in the large mass region.

2.4 Shape Coexistence

In the last two sections, the deformed nuclear shape has been discussed. The spherical or deformed potential field is used to describe the interaction among the nucleons effectively. But this is still an approximation. Usually the energy gap at closed shell can separate the nucleus as an "inert" core plus "valence" nucleons. The Hamiltonian can be written

$$H = H_{core} + H_{val} + H_{coup} \tag{2.25}$$

where H_{core} and H_{val} are Hamiltonians of the core part and valence nucleons, and H_{coup} represents the interaction between the core and valence nucleons. For a system with more than one valence nucleon, the "residual" two-body interactions between the valence nucleons are very important. H_{val} is written as

$$\begin{aligned} H_{val} &= H_{shell} + H_{res} \\ &= \textstyle\sum_i (\frac{p_i^2}{2m} + V(\mathbf{r}_i) \quad + \epsilon \mathbf{l}_i \cdot \mathbf{s}_i) + \sum_{i,j} V(\mathbf{r}_i, \mathbf{r}_j) \end{aligned} \tag{2.26}$$

There are two kinds of nucleons (proton and neutron) in the nucleus. Residual interactions can be divided further as

$$H_{res} = H_{\pi\pi} + H_{\nu\nu} + H_{\pi\nu} \tag{2.27}$$

The short-ranged "pairing" force is the most important interaction between the like valence nucleons, which produces a strongly pair-correlated structure as the nuclear ground state. In this case, a large amount of energy is needed to break a pair of nucleons to produce an excited state. The residual proton-neutron interaction is the main force responsible for the deformation in nuclei[Sha53].

Most of shape coexistence phenomena at low-excitation energy are found at and near closed shell regions. The proton-neutron residual interaction is the key to understand the coexistence in the shell model theory. In single closed-shell

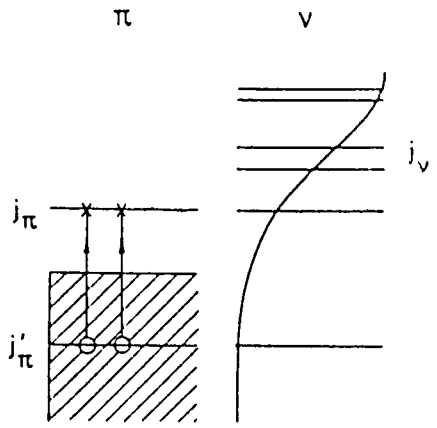

Figure 2.6: Schematic representation of a proton intruder 2p-2h 0^+ configuration where j_π and j'_π denote the intruder particle and hole orbitals, and j_ν denotes the neutron orbitals filled with a BCS-like pair distribution.

nuclei there is only one kind of valence nucleon, the deformation producing force is zero($H_{\pi\nu} \sim 0$). The ground states of tin and lead isotopes are spherical or near spherical shapes. However for the isotopes like tin or lead, when a proton pair is excited out of the closed shell to the next higher shell(Fig. 2.6), it is called an "intruder" state. The strong proton-neutron residual force will create the deformed nuclear structure.

For medium and heavy nuclei, even single closed-shell isotopes, the number of valence nucleons is big enough to make the shell model calculation difficult or impossible. Empirically the energy of the proton intruder 2p-2h 0^+ state can be written as[Hey87]

$$\begin{aligned} E_{intr}(0^+) &= 2(\varepsilon_{j_\pi} - \varepsilon_{j'_\pi}) - \Delta\mathrm{E_{pair}} + \Delta\mathrm{E_M} + \Delta\mathrm{E_Q} \\ &= 2(\varepsilon_{j_\pi} - \varepsilon_{j'_\pi}) - \Delta\mathrm{E_{pair}} + 2\sum_{j_\nu}(2j_\nu+1)v^2_{j_\nu}[\overline{E}(j_\pi j_\nu) - \overline{E}(j'_\pi j_\nu)] \\ &\quad + \begin{cases} \frac{2}{5}\frac{\overline{\kappa}^2}{\Delta\overline{E}}\sum_{j_\nu}\frac{(2j_\nu+1)u^2_{j_\nu}v^2_{j_\nu}}{2(2j_\nu-1)}F(j_\pi, j_\nu, j'_\pi, n_\pi) \\ 4\kappa_0\sqrt{\Omega_\pi - N_\pi}\sqrt{\Omega_\nu - N_\nu}N_\nu \end{cases} \end{aligned} \tag{2.28}$$

where ε_{j_π} is the energy of the proton single particle state at j subshell; ΔE_M and

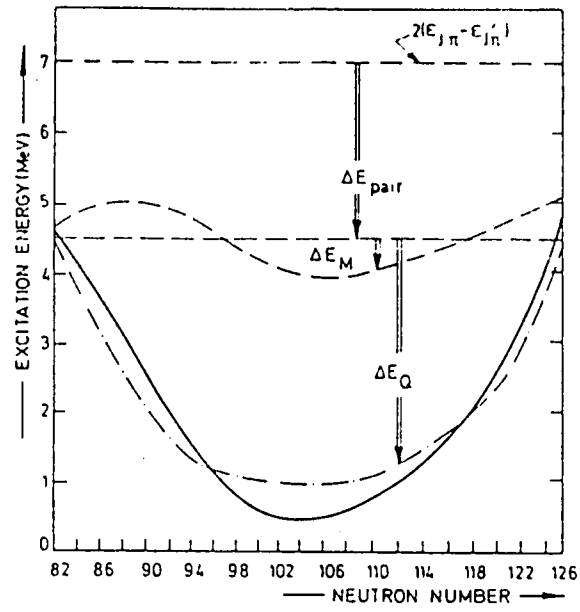

Figure 2.7: The total energy correction (full line) for the lowest 0^+ intruder state. The different contributions due to the pairing energy (straight dashed line); the monopole correction(dashed line) and the quadrupole correction (dot-dashed line) are given in a schematic way for the $Z = 82$ region. (from [Hey87])

ΔE_Q are monopole and quadrupole proton-neutron interaction energy corrections; $v^2_{j\nu}$ is neutron pair BCS distribution probability at j subshell; N is the number of valence pairs and $\Omega = j + \frac{1}{2}$ is the orbital degeneracy; and, $\overline{E}$ denotes the spin-averaged proton-neutron matrix element;

$$\overline{E}(j_\pi j_\nu) = \frac{\sum_J (2J+1)\langle j_\pi j_\nu; J \mid V_{\pi\nu} \mid j_\pi j_\nu; J\rangle}{\sum_J (2J+1)} \tag{2.29}$$

The total energy correction applied to the Pb region is shown in Fig 2.7. Under the IBM-2 SU(3) limit (lower line of Eq. 2.28), using subshell ($N = 114$) correction, the excited energy intruder 0^+ of Pb isotopes are fitted(Fig. 2.8).

The Nilsson single-particle energies depend sensitively on the deformation. There is more than one local minimum of the total energy as a function of deformation for a given nucleus. From the Nilsson diagram(Fig. 2.5), on the oblate side the high-j, high-Ω orbitals and on the prolate side the high-j, low-Ω orbitals drop

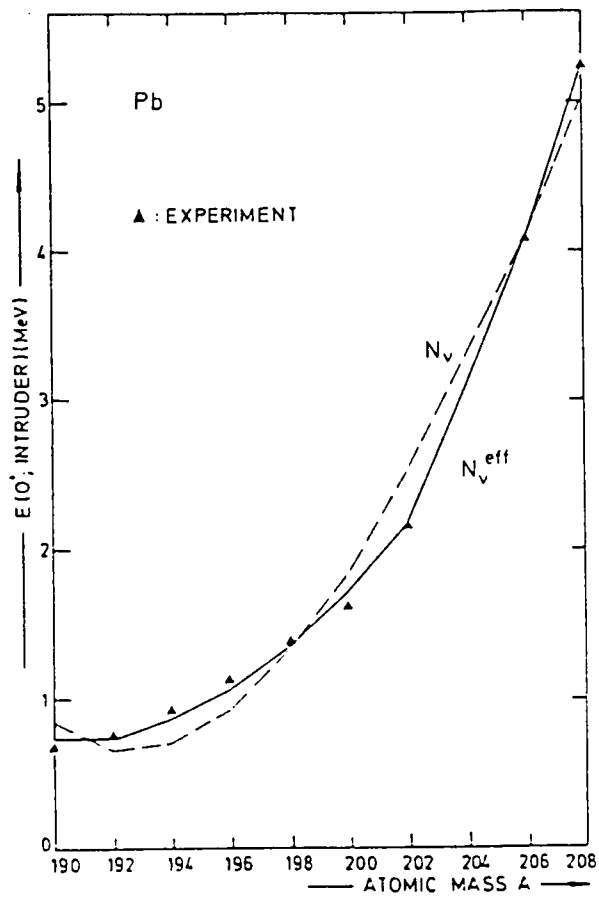

Figure 2.8: The energy fitted with the experimental 0^+ intruder states in the Pb nuclei. The dashed line is calculated up to the double-closed $Z = 82, N = 126$ shell. The full line is fitted including an $N = 114$ subshell closure with the effected neutron pair number correction. (from [Hey87])

quickly as deformation $\mid \beta_2 \mid$ is increased. Most shell gaps are created by the energy splitting of high-j states as mentioned in section 2.1. When the intruder valence particle occupies these single-particle orbitals, the nucleus will be easily deformed energetically and the occupation of these orbitals is a deformation driving effect.

The structure of odd-mass nuclei basically can be set up as a single particle coupling with an even-even "core". This coupling is divided into three limits in the extreme situation (Ref. [Hey83]). It is shown in Fig. 2.9.

Case A. Near spherical symmetry ($\beta = 0$), the excitation spectrum consists of multiplets built on core-excited states. The coupling is weak.

Case B. For prolate shape ($\gamma = 0°$), particle states(small Ω) result in a decoupled or rotation-aligned spectrum, hole states (large Ω) give a strongly-coupled spectrum.

Case C. For oblate shapes ($\gamma = 60°$), the reversed situation occurs: a strongly-coupled spectrum arises when coupling a particle state (large Ω), and a decoupled (or rotation-aligned) spectrum results when coupling a hole state.

In fact, the particle-"core" coupling lies between these limits for most situations. The triaxial deformation ($0° < \gamma < 60°$) is needed to fully account for the observed energy spectra.

2.5 Beta Decay

As β decay is involved in the experimental part of this work, it will be discussed briefly in this section. In β decay the parent nucleus does not change its mass number while its atomic number changes by one unit. The β decay include three modes: electron emission (β^-), positron emission (β^+) and electron capture(EC). After the continuous energy and momentum spectra of β decay was explained by the Pauli neutrino hypothesis in 1933 and confirmed in experiment later, the three

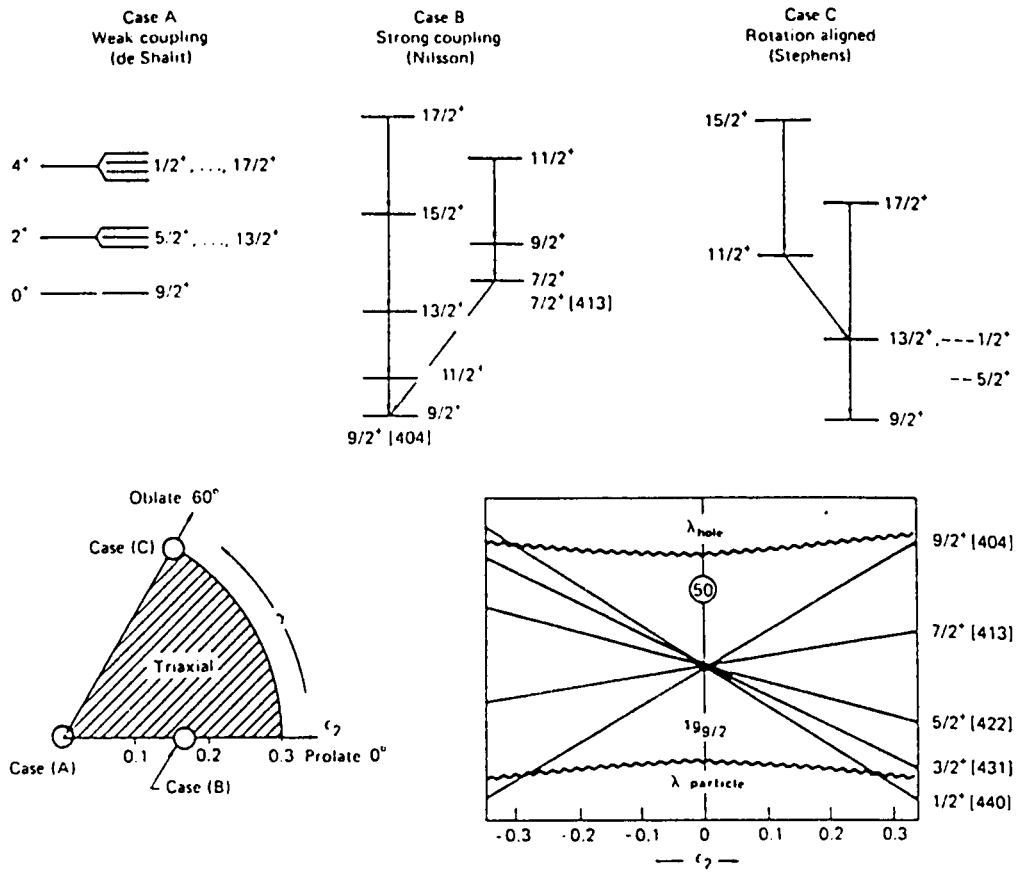

Figure 2.9: The three important limiting cases of particle-core coupling(from [Hey83]). The level schemes illustrate the band structure of hole states. For particle states the schemes of case B and C are exchanged.

decay modes are written as

$$\left.\begin{array}{lrcl} \beta^-: & {}^A_Z X & \rightarrow & {}^A_{Z+1}Y + e^- + \overline{\nu} \\ \beta^+: & {}^A_Z X & \rightarrow & {}^A_{Z-1}Y + e^+ + \nu \\ EC: & {}^A_Z X + e^- & \rightarrow & {}^A_{Z-1}Y + \nu \end{array}\right\} \tag{2.30}$$

Where ν and $\overline{\nu}$ represent the neutrino and antineutrino. In the nucleus, it also can be written as

$$\left.\begin{array}{lrcl} \beta^-: & n & \rightarrow & p + e^- + \overline{\nu} \\ \beta^+: & p & \rightarrow & n + e^+ + \nu \\ EC: & p + e^- & \rightarrow & n + \nu \end{array}\right\} \tag{2.31}$$

When the spins of emitted electron and neutrino are anti-parallel, the decay is labeled as a vector Fermi transition; when the spins are parallel, it is called an axial-vector Gamow-Teller transition.

Probability of β-decay. From the basic Fermi theory(1934), the probability of an electron emission per unit time with momentum between p and $p + dp$ is

$$I(p)dp = \frac{2\pi}{\hbar}\left|\int \Psi_f^* H \Psi_i d\tau\right|^2 \frac{dn}{dE} \tag{2.32}$$

Where $\frac{dn}{dE}$ is the number of final states per unit decay energy. Since the interactions among the produced nucleus, electron and neutrino are very weak, the wave function of the final state is the product of the wave functions for the individual parts

$$\Psi_f = u_f \phi_\beta \phi_\nu \tag{2.33}$$

Under the free particle approximation, the non-relativistic wave functions of the electron and neutrino are

$$\begin{aligned} \phi_\beta &= V^{-1/2} exp(i\mathbf{k}_\beta \cdot \mathbf{r}) \\ \phi_\nu &= V^{-1/2} exp(i\mathbf{k}_\nu \cdot \mathbf{r}) \end{aligned} \tag{2.34}$$

Finally considering the effect of the electrostatic field of the nucleus, the Coulomb correction factor $F(Z, E)$ (called the Fermi function) is added. The probability is

$$I(p)dp = \frac{g^2 \mid M_{if} \mid^2}{2\pi^3 c^3 \hbar^7} F(Z, E)(E_{max} - E)^2 p^2 dp \tag{2.35}$$

where $M_{if} = \int u_f^* u_i exp[-i(\mathbf{k}_\beta + \mathbf{k}_\nu) \cdot \mathbf{r}] d\tau$ is transition matrix element and g is the strength constant of the *weak* interaction. The total probability of all β particle emission is the decay constant λ given by integrating over the momentum distribution as

$$\lambda = \int_0^{p_{max}} I(p)dp \approx \frac{m_e^5 c^4 g^2 \mid M_{if} \mid^2}{2\pi^3 \hbar^7} f(Z, E_{max}) \tag{2.36}$$

$$f(Z, E_{max}) = \int_0^{p_{max}} F(Z, E) \left(\frac{E_{max} - E}{m_e c^2}\right)^2 \left(\frac{p}{m_e c}\right)^2 \frac{dp}{m_e c} \tag{2.37}$$

The plane wave part in the transition matrix element can be expanded by the Bessel function

$$exp(i\mathbf{q} \cdot \mathbf{r}) = \sum_l Y_{l0}(\theta) B_l(qr) \tag{2.38}$$

The transition probability therefore can be expressed in terms of orbital angular momentum $< l >$ eigenstates. Transitions with $l = 0$ are called allowed β-decay; those with $l = n$ are called nth-forbidden transition. The practical calculation of the transition probability gives 2-3 orders of magnitude difference in rates for the neighboring nth transitions.

Probability of K-electron capture: The interaction between the nucleus and the electron in the K-orbit is stronger than for electrons in the other orbits. Relatively the capture probability of the K electron is bigger than others. But when the mass energy difference of the initial and final nuclei is too low ($E_K > (M_i - M_f)c^2 > E_L$), the K-electron capture is impossible and the L-electron capture will be the most probable process. Only the probability of K electron capture is discussed here. The wave function of the electron in the K shell is given by

$$\phi_K = \frac{1}{\pi^{1/2}} \left(\frac{Z m_e e^2}{\hbar^2}\right)^{3/2} exp\left(-\frac{Z m_e e^2}{\hbar^2} r\right) \tag{2.39}$$

Considering that there are two electrons in the K shell, the total probability of K

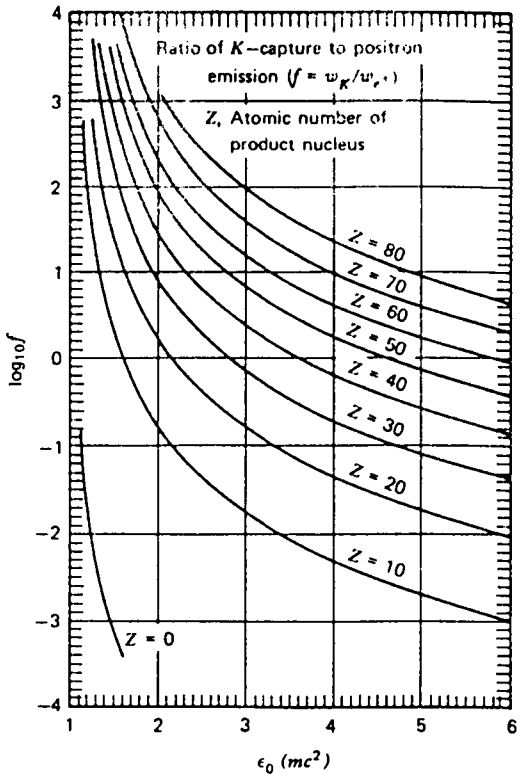

Figure 2.10: Ratio of K-capture to positron emission

electron capture is

$$\lambda_K = \frac{2m_e^5 c^4 g^2}{\pi^2 \hbar^7} \left(\frac{Ze^2}{\hbar c}\right)^3 \mid M_{if} \mid^2 E_\nu^2 \tag{2.40}$$

The energy of neutrino E_ν is a single value because there is only neutrino emission in this process.

If the mass energy difference of initial and final nuclei is bigger than $2m_e c^2$ and the atomic number(Z) of the final nucleus is one more than initial nucleus, it is possible in principle that the β- decay and electron capture occur simultaneously. The ratio of $\frac{\lambda_K}{\lambda_{\beta+}}$ can be used to check the β decay theory. For an allowed transition, comparing Eq. 2.36 and Eq. 2.40

$$\frac{\lambda_K}{\lambda_{\beta+}} = 4\pi \left(\frac{Ze^2}{\hbar c}\right)^3 \frac{E_\nu^2}{f(Z, E_{max})} \tag{2.41}$$

which is not a function of the transition matrix. This ratio for different Z is shown in Fig. 2.10. The transition energy for a heavy nucleus is small, so K capture is a

more dominant decay mode than β^+-decay in the heavy mass region.

2.6 Gamma Decay

The produced nuclei from β-decay and other nuclear reactions usually are in excited states. The excited nucleus can be de-excited by the emission of γ rays. Nuclear γ decay results from the electromagnetic(**EM**) interaction in nuclei. The γ spectroscopy has been extensively applied to the study of static and dynamic properties of nuclei, because the EM interaction is considered to be a well known one. The long-range nature of the EM force makes it quite sensitive to the collective motion and the well-established EM theory provides a test of the fundamental symmetries. The γ transition selection rules, probability and multipole mixing ratio will be discussed in this section, to show their dependence on the basic quantum numbers (eigenvalues) of the nuclear states and how these are used to set up a level scheme with excitation energy (E_x), angular momentum (I) and parity (π).

As a micro system, the nuclear radiation will obey quantum mechanics. The nuclear excitation energy (E) and angular momentum (I) are both quantized. The transition energy (E_γ), angular momentum (L) and parity (π_γ) of a photon are

$$E_\gamma = E_i - E_f \tag{2.42}$$

$$\mathbf{L} = \mathbf{I_i} - \mathbf{I_f} \tag{2.43}$$

$$\pi_\gamma = \pi_i/\pi_f \tag{2.44}$$

As the nuclear charge distribution generates both electric and magnetic moments and each can generate electromagnetic radiation, the transitions are correspondingly classified as electric (E) and magnetic (M) transitions. The multipole character of transition determines the orbital angular momentum L and parity according to these

simple reactions

$$\left.\begin{array}{ll} \textit{Electric multipole radiation}: & \pi_\gamma = (-1)^L \\ \textit{Magnetic multipole radiation}: & \pi_\gamma = (-1)^{L+1} \end{array}\right\} \tag{2.45}$$

From quantum electromagnetic theory, the probabilities of electric and magnetic multipole transitions are [Eji89]

$$\lambda_{E(M)}(L) = \frac{8\pi(L+1)}{L[(2L+1)!!]^2}\frac{k^{2L+1}}{\hbar}B\{E(M),L\} \tag{2.46}$$

where $B\{E,L\}$ and $B\{M,L\}$ are called electric and magnetic reduced transition probabilities. After averaging on the initial states and summing over the final states

$$B\{E(M),L\} = \sum_{M_f,M,M_i}\frac{1}{2I_i+1}\mid \mathrm{M}\{E(M),LM\}\mid^2 \tag{2.47}$$

where the multipole transition operator M is written as

$$\mathrm{M}\{E,LM\} = e\sum_{k=1}^{Z}\int r_k^L Y_{LM}^*(\theta_k,\phi_k)\psi_f^*\psi_i d\tau \tag{2.48}$$

$$\mathrm{M}\{M,LM\} = -\frac{1}{L+1}\frac{e\hbar}{2m_pc}\sum_{k=1}^{Z}\int r_k^L Y_{LM}^*(\theta_k,\phi_k)\nabla\cdot(\psi_f^*\hat{L}_k\psi_i)d\tau \tag{2.49}$$

The theoretical evaluation of the transition operator is involved with the nuclear initial and final wave functions. It may be calculated only for the specific nuclear models.

In the single-particle shell model, the nucleus is spherical and the γ emission is the result of a single proton transferring from one state to another state, the upper limit of the transition probabilities are

$$\lambda_E(L) = \frac{4.4(L+1)}{L[(2L+1)!!]^2}\left(\frac{3}{L+3}\right)^2\left(\frac{E_\gamma}{197}\right)^{2L+1}R^{2L}\times 10^{21}sec^{-1} \tag{2.50}$$

$$\lambda_M(L) = \frac{1.9(L+1)}{L[(2L+1)!!]^2}\left(\frac{3}{L+3}\right)^2\left(\frac{E_\gamma}{197}\right)^{2L+1}R^{2L-2}\times 10^{21}sec^{-1} \tag{2.51}$$

The contribution of each multipole to the total transition probability is related by a power series $(R/\lambda)^{2L}$, where R is the radius of nucleus and λ is the wavelength of

the 2^L-pole radiation. From the last two equations, two conclusions are reached:

a). The higher the multipolarity of transition, the lower the transition probability will be. For heavy nuclei, if the γ energy is about 1 MeV,

$\lambda_{E(M)}(L+1)/\lambda_{E(M)}(L) \approx 10^{-3}$.

b). For a given multipolarity L, an electric transition is faster than a magnetic transition. Usually $\lambda_M(L) \approx \lambda_E(L+1)$.

This is the reason that the *E2* transition frequently competes favorably with the *M1* transition. Usually the experimental value of the multipole transition probability is lower than the theoretical value, because Eq. 2.50 and 2.51 are the upper-limit of transition. But for deformed nuclei, some *E2* transition probabilities are much higher than the shell model theory value which must be explained by the collective model.

Electromagnetic theory indicates that there is a particular angular distribution for a given multipole electromagnetic transition. If the nuclei are polarized, the angular distribution of the γ transitions can be observed. But producing a polarized target or ion beam is difficult experimentally. Frequently the γ angular correlation is used to determine the multipolarity of radiation. In the next section, another method will be introduced which is used in this work to determined the multipolarity of the transition.

2.7 Internal Conversion

The excited nucleus de-excites with the ejection of an atomic electron in a process called internal conversion. The nuclear excitation energy $E\gamma$ is transmitted internally to the ejected orbital electron. The energy of the ejected electron is

$$E_i^e = E_\gamma - B_i \tag{2.52}$$

where B_i is the electron binding energy of the ith shell. Internal conversion competes with γ emission. Then, the total probability of an EM transition is given by

$$\begin{aligned} \lambda &= \lambda_\gamma + \sum \lambda_i \\ &= \lambda_\gamma (1 + \sum \alpha_i) \end{aligned} \tag{2.53}$$

where λ_i is the i-shell electron conversion probability and α_i is the i-shell internal conversion coefficient. Practically, only three inner-shell ($i = K, L, M$) electrons are considered because the probabilities of emitting other outer-shell electrons is small.

For an electric transition, the Coulomb interaction is considered, and the transition operator for the K-shell electron is

$$M(EL) \propto \sum_{i=1}^{Z} \int \int exp(-i\mathbf{k}_e \cdot \mathbf{r}_e) \psi_f^* \frac{e^2}{|\mathbf{r}_e - \mathbf{r}_i|} \psi_i \frac{1}{a^{3/2}} exp\left(\frac{-r_e}{a}\right) d^3 r_i d^3 r_e \tag{2.54}$$

where $\mathbf{k}_e$ is the final electron wavevector, ψ is the nuclear state and a is the Bohr radius of the K-shell electron. When $1/|\mathbf{r}_e - \mathbf{r}_i|$ is expanded by the orbital angular momentum, the multipole transition operator is written as

$$M(EL) \propto \frac{e k_e^{L-2}}{a^{3/2}} \int exp(-i\mathbf{k}_e \cdot \mathbf{r}_e) \left(\frac{1}{k_e r_e}\right)^{L+1} exp\left(\frac{-r_e}{a}\right) d^3(k_e r_e) \cdot [B\{EL\}]^{1/2} \tag{2.55}$$

where $B\{EL\}$ is mentioned in Eq. 2.47. Comparing Eq. 2.47 and Eq. 2.55 for K-shell electrons, the internal conversion coefficient α_K is

$$\alpha_{K_L} \propto Z^3 k_e^{2L-3} / k_\gamma^{2L+1} \propto Z^3 k_\gamma^{-L-5/2} \tag{2.56}$$

since $k_e \propto k_\gamma^{1/2}$ for non-relativistic electrons. The conversion coefficient for magnetic transitions is similar.

The conversion coefficient is independent of the nuclear matrix element. It only depends on the γ and electron momenta and electron wave function which are expressed as E_γ, J, k, Z and $\sim exp(-i\mathbf{k}_e \cdot \mathbf{r}_e)$. The conversion coefficient and

ratios (as α_K/α_L) are used to determine the multipolarity of the transitions. The numerical values of conversion coefficients have been given in several *Nucl. Data Tables* [Tru72]. The experimental conversion coefficients are compared with the theoretical value in this work to set limits on multipolarities of the transitions.

$0^+ \rightarrow 0^+$ *transition*: It will be specially mentioned here because it is often taken as the indication of shape coexistence. The intrinsic spin and parity of a γ ray is 1^-. From the γ decay selection rules, the γ transition is impossible for a $0^+ \rightarrow 0^+$ decay; only internal conversion is allowed (At higher energy $\Delta E > 2m_e c^2$, the creation of an electron-positron pair is possible and its probability increases with transition energy to become the main decay mode). The electric monopole operator of internal conversion in the shell model is defined as

$$\mathrm{M}(E0) = \sum_{i=1}^{Z} e r_i^2 \tag{2.57}$$

And the reduced transition probability is

$$\begin{aligned} B\{E0\} &= \mid \langle f \mid \mathrm{M}(E0) \mid i \rangle / eR^2 \mid^2 \\ &= \left| \frac{\langle \phi_f | \sum e_j r_j^2 | \phi_{ij} \rangle}{eR^2} \right|^2 \end{aligned} \tag{2.58}$$

where R denotes the nuclear average radius. From the last equation, $E0$ internal conversion radiation has a strength proportional to the difference in their nuclear radii; a transition between the deformed 0^+ state to spherical 0^+ state will result with an enhanced electric monopole transition. For any transition between the same J^π, the *E0* internal conversion component is possible and will be enhanced between bands built on two different shapes. An α_K value larger than the theoretical value for a M1 transition is taken as a sure indicator of an *E0* component and a possible indicator of shape coexistence.

CHAPTER 3

Experimental Arrangment

3.1 Experimental Set-Up

The mass-separated, radioactive sources were produced at the University Isotope Separator at Oak Ridge (UNISOR) which is on-line to the Holifield Heavy-Ion Research Facility (HHIRF) at the Oak Ridge National Laboratory. The layout of the experimental area is shown in Figure 3.1. Heavy-ion projectiles, accelerated with the HHIRF Tandem Accelerator, were incident on the solid target placed in the FEBIAD ion source. Radioactive isotopes were produced by fusion evaporation reactions (HI, xn). The cross-section of the selected reaction channel is connected with the probability of forming a compound nucleus and the decay pattern of the compound nucleus, which change with the incident energy and different projectile-target combinations. Usually a statistical reaction model is used to calculate the forming and decaying processes of a compound nucleus and the cross-section of a given channel. In this experiment, a 53mg/cm^2 stack of Re foils was used as a target. The natural Re is constituted of 37.4% ^{185}Re and 62.6% of ^{187}Re. For the best productivity, an ^{16}O ion beam was accelerated to 155-MeV to produce ^{199}Bi mainly through the ${}^{187}_{75}Re({}^{16}O, 4n){}^{199}_{83}Bi$ reaction; and an acceleration energy of 170-MeV was used to produce ^{193}Bi by the channel ${}^{185}_{75}Re({}^{16}O, 8n){}^{193}_{83}Bi$.

The radioactive nuclides produced by (^{16}O, xn) reactions would either recoil or diffuse into the FEBIAD ion chamber. The high temperature inside the ion source chamber caused the produced nuclides to ionize. The ionized nuclei were extracted

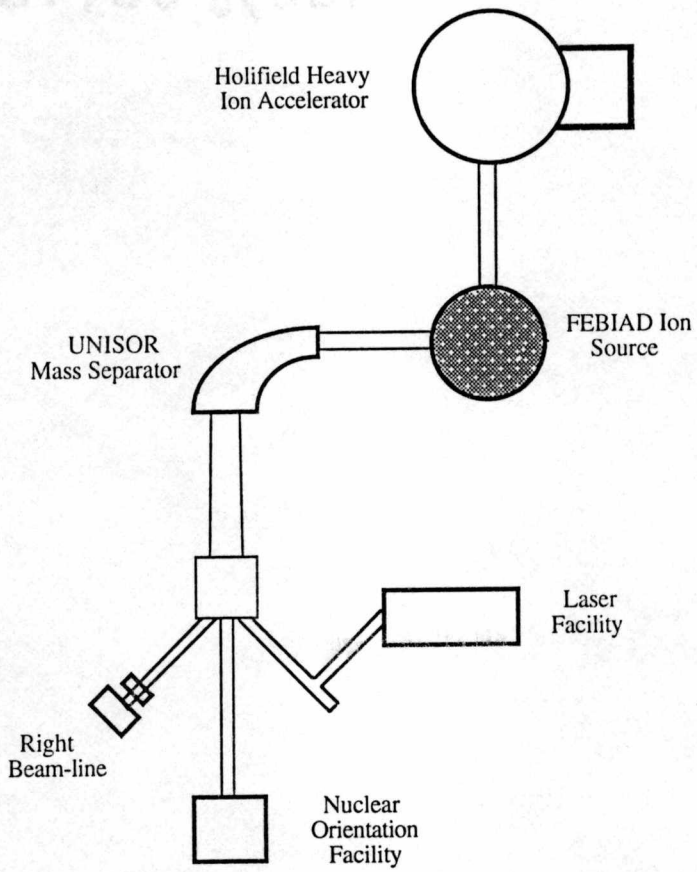

Figure 3.1: Layout of the UNISOR area of the HHIRF

through an aperture at the end of the chamber and accelarated by a 50-keV potential into the UNISOR mass separator. The singly-ionized atoms were separated spatially by the 90° bending magnet according to mass and the desired mass was guided into the right-beam-line and deposited on a stationary mylar tape.

There was a measurement station at the end of right beam line which is shown in Figure 3.2. Three N-type hyper-pure Ge γ detectors (Up, Down and Left) and one Si(Li) electron detector (Right) were used in this experiment. One computer controlled the tape-transport system by use of a stepping motor which moved the atoms deposited on the mylar tape to the measurement point periodically. The tape moving direction was arranged so that the radioactive isotopes were on the electron detector side of the mylar tape, because of the poor transmission capacity for electrons through the tape.

3.2 Data Acquisition

Two computers were utilized to acquire γ and e^- singles and coincidence data. A micro-VAX II was used to control and record the singles spectra. The energy signals from the γ and electron detectors passed a preamplifier and were amplified by spectroscopy amplifiers. The amplified pulse heights were transferred to Analog-Digital-Converters (ADCs) which produced digital numbers proportional to the pulse heights. These numbers were transmitted to the computer which incremented the count in that channel of the spectrum being stored. For each collection cycle six spectra taken from equal time segments were accumulated. γ and electron spectra were stored in the corresponding six sections of a Nuclear Data Interface memory. The data of the next cycle was added on the last one; after many cycles the spectra were dumped to data files on disk. A view of these six spectra together gives the decay behavior of the peaks over time, as will be discussed in detail in the

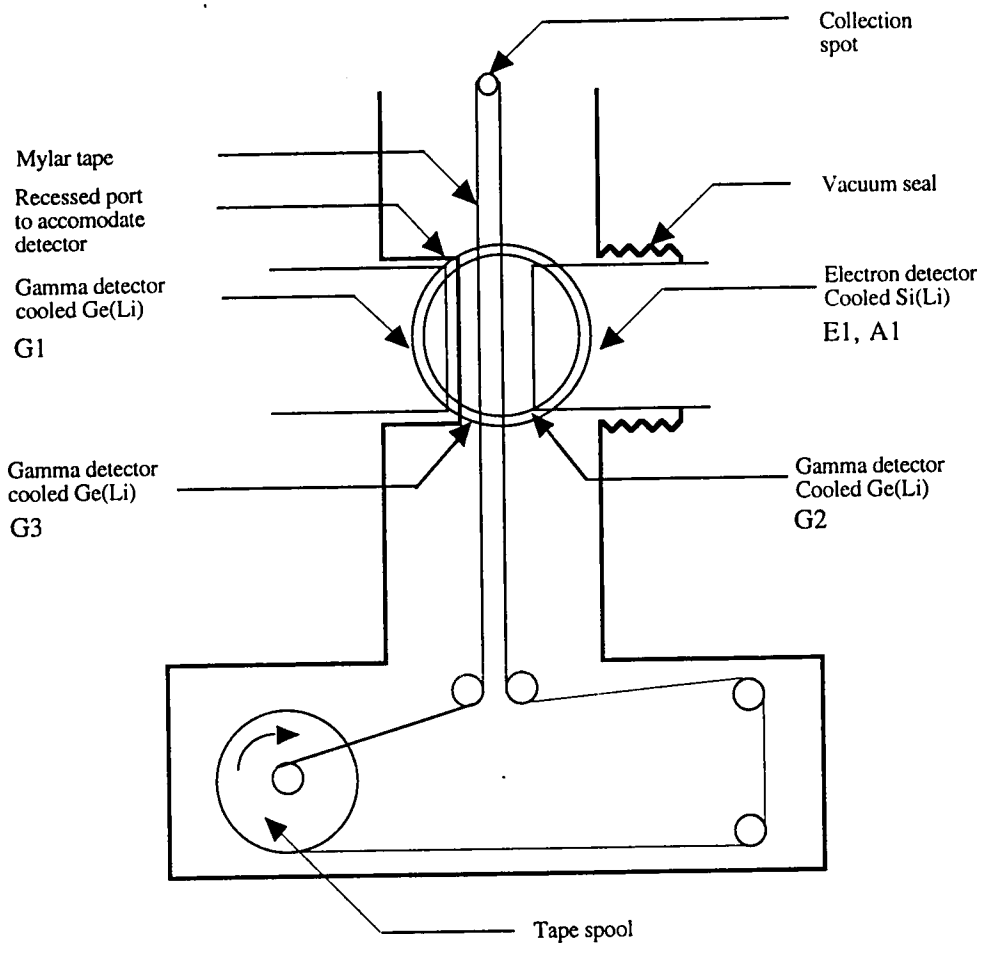

Figure 3.2: Diagram of the measurement station of the right-beam-line

next section.

A Concurrent computer was used for the coincidence data collection. The coincidence circuit is shown in Figure 3.3. The energy signals were sent to gated ADCs. The pulse from the preamplifier through the Timing- Filter-Amplifier (TFA) and Constant-Fraction-Discriminator (CFD) gave out the precise time signal. In a timing range, the time difference between neighboring signals is converted to the related pulse amplitude by a Time-Amplitude-Converter(TAC) first and then to a digital signal by an ADC. The coincidence level was set as 2, so any more than two pulses from different detectors occurring in a pre-set timing window ($\sim$ 200 ns) was taken as one coincidence event.

The data acquisition is monitored and managed by the Event Handler, which is a programmable CAMAC-based controller. The program was written in assembly language for this experiment, it would control opening the gate of all ADCs and let the energy and time- relationship signals pass through when a coincidence event occurred and then closed the gates until the computer finished the recording process of this event and reset. This data collection method is called event-by-event mode. Data were accumulated in the memory unit from which some histograms could be viewed to monitor the experiment. Data were also recorded onto the magnetic tape. After the experiment, the tapes can be scanned at will to change the timing window on the TAC channel or other parameters to get the best coincidence matrix files (.his). This is the advantage of the event-by-event recording format. The experiment can be repeated with different gating conditions any time when the tape is scanned, such flexibility is difficult or impossible by using hardware gates in the experiment.

Coincidence Circuit

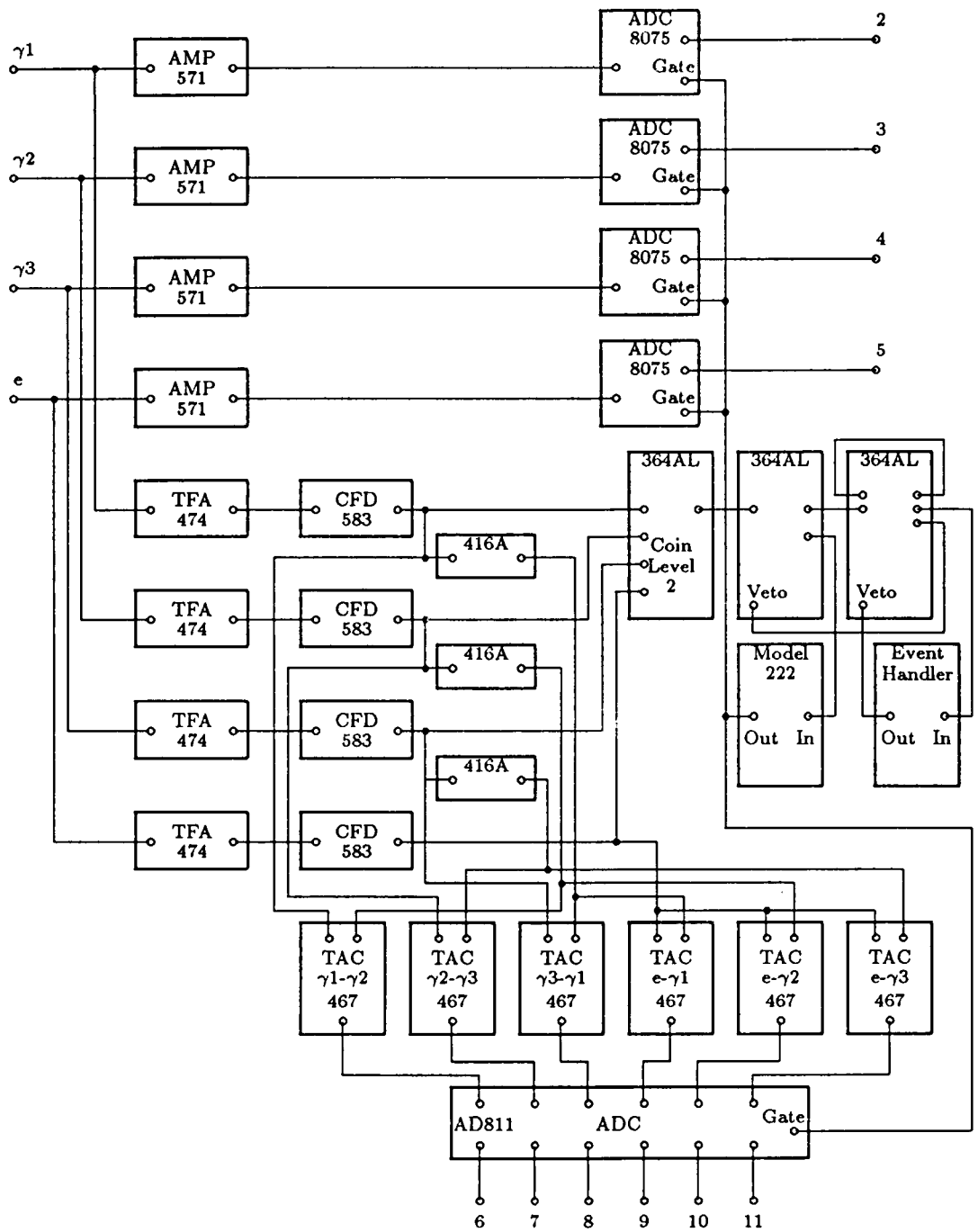

Figure 3.3: Experiment coincidence circuit scheme

3.3 Data Analysis

3.3.1 Detector calibration

Before the on-line experiment, all detectors were calibrated using a National Bureau of Standards "Mixed-Radionuclide Point Source" with γ-rays energies ranging from 27.4 keV to 1596.0 keV. The standard source was put into the beamline with the same geometrical position as the on-line experimental source. The energy and efficiency calibrations were facilitated by a computer code and calibration data file for the standard source used. The gains of the amplifers were adjusted to the desired levels before the experiment and checked after the experiment. But because of the very high counts in the experiment, there was a small energy shift of the on-line data relative to peaks from the standard sources. In fact the energies of known γ-rays of ^{199}Pb from NDS [Sch88] proved to be a more reliable energy calibration. It was checked self-consistently by the level scheme. The energy calibration of the electron detector was given by matching the K-shell electron energy with the corresponding γ-ray energy. The electron detector was thick enough to stop electrons between 50 keV and 1500 keV. No useful electron peak intensity was found out of this range, so the relative efficiency of the electron detector was taken as a constant.

3.3.2 Singles Spectra

The energy signals from the γ-ray and electron detectors were amplified and collected by computer directly in histograms called singles spectra. The singles spectra were analyzed to obtain energies, γ-ray intensities and internal-conversion coefficients. The peak position and area were fitted by use of the spectrum analysis code, SAM written by W. Milner at HHIRF. The electron and γ-ray peaks were fit

with a Gaussian function plus low- and high-energy tails.

$$F(x_0, H, a, A_{s,low}, A_{s,high}) = H \cdot \begin{cases} exp\left[-\frac{(x-x_0)^2}{a^2(1+A_{s,low}\cdot(x_0-x)/a)}\right] & x < x_0 \\ exp\left[-\frac{(x-x_0)^2}{a^2(1+A_{s,high}\cdot(x-x_0)/a)}\right] & x > x_0 \end{cases} \quad (3.1)$$

Where x_0 is peak position, H is the peak height, a is the Gaussian function width at $1/e$ max and $A_{s,low}/A_{s,high}$ are parameters of low-/high-energy tails. Near the central position, the fitting function is a pure Gaussian function and far from the peak it follows an exponential fall-off, ($exp[-|x-x_0|/(a \cdot A_s)]$). The high- energy tail of the γ-peaks was very small; only low-side asymmetry was used. At first, about ten single strong peaks distributed through the whole energy range were selected to fit the parameters $A_{s,low}, A_{s,high}$ as constant and a as a straight line. Then these parameters were used for the all peaks in the spectra, so only two parameters x_0, H per peak were varied in the final fitting.

The decay-time tendency was used to identify the transitions from each isotope of the decay chain. One of the actual decay chains in the experiment was

$$^{199}Bi \rightarrow ^{199}Pb \rightarrow ^{199}Tl \rightarrow ....$$

If pure ^{199}Bi ions were extracted from the mass separator, the number of different nuclei present during the deposit cycle ($0 < t < \tau$) is

$$N^{Bi}(t) = \frac{I}{\lambda_{Bi}}(1 - e^{-\lambda_{Bi}t}) \quad (3.2)$$

$$N^{Pb}(t) = \frac{I\lambda_{Bi}}{\lambda_{Bi}-\lambda_{Pb}}\left[\frac{1}{\lambda_{Pb}}(1 - e^{-\lambda_{Pb}t}) - \frac{1}{\lambda_{Bi}}(1 - e^{-\lambda_{Bi}t})\right] \quad (3.3)$$

and during the measurement cycle ($0 < t < \tau$):

$$N^{Bi}(t) = \frac{I}{\lambda_{Bi}}(1 - e^{-\lambda_{Bi}\tau})e^{-\lambda_{Bi}t} \quad (3.4)$$

$$N^{Pb}(t) = \frac{I\lambda_{Bi}}{\lambda_{Bi}-\lambda_{Pb}}\left[\frac{1}{\lambda_{Pb}}(1 - e^{-\lambda_{Pb}\tau})e^{-\lambda_{Pb}t} - \frac{1}{\lambda_{Bi}}(1 - e^{-\lambda_{Bi}\tau})e^{-\lambda_{Bi}t}\right] \quad (3.5)$$

where I is the intensity of beam, τ is the length of the deposit and measurement cycles, λ is the decay constant. The activity measured between t_1 and t_2 is

$\int_{t_1}^{t_2} \varepsilon_{eff}\lambda_A N^A(t)dt$. So

$$C^{Bi}(t_1 \rightarrow t_2) = \varepsilon_{eff}\frac{I}{\lambda_{Bi}} \quad (1-e^{-\lambda_{Bi}\tau})(e^{-\lambda_{Bi}t_1} - e^{-\lambda_{Bi}t_2}) \tag{3.6}$$

$$C^{Pb}(t_1 \rightarrow t_2) = \varepsilon_{eff}\frac{I\lambda_{Bi}\lambda_{Pb}}{\lambda_{Bi}-\lambda_{Pb}} \quad \left[\frac{1}{\lambda_{Pb}^2}(1-e^{-\lambda_{Pb}\tau})(e^{-\lambda_{Pb}t_1} - e^{-\lambda_{Pb}t_2}) - \right.$$
$$\left. \frac{1}{\lambda_{Bi}^2}(1-e^{-\lambda_{Bi}\tau})(e^{-\lambda_{Bi}t_1} - e^{-\lambda_{Bi}t_2})\right] \tag{3.7}$$

For stronger radioactivity and better identification of γ and e^- lines, a 30 minute cycle ($\sim$ 27 min half-life of ^{199}Bi) was selected in the experiment of ^{199}Bi β-decay. The singles spectrum was divided into six equal time sections called multiscaled spectra. According to Eq. 3.6, the transition intensity from Bi decay would decrease as a regular exponential function. The intensity ratio of the 6th group over 1st group ($C^{Bi}(t_5 \rightarrow \tau)/C^{Bi}(t_0 \rightarrow t_1)$) is 0.53. The experimental value of stronger γ-rays from ^{199}Bi decay is fitted with the theoretical value. The half-life of ^{199}Pb is 90 minutes which is longer than ^{199}Bi and the cycle time, for the cycle time used, the intensity would increase with time. From Eq. 3.7, the ratio of $C^{Pb}(t_5 \rightarrow \tau)/C^{Pb}(t_0 \rightarrow t_1)$ is 1.71. But because of the competition of reaction channel $^{187}Re(^{16}O, p3n)^{199}Pb$ and since some of the ^{199}Bi decayed to Pb in the ion source before separation, there were ^{199}Pb nuclei from the mass separator deposited on the tape directly. The experimental value of ^{199}Pb decay ratio is about 1.2. From Eqs. 3.6 and 3.7, the calculation yields a ratio of ^{199}Pb activity of 1.2 when the beam intensity of ^{199}Pb from the mass separator is 50% of ^{199}Bi (Figure 3.4).

The half-life of ^{193}Bi is 67 s, so the cycle time was set at 60 seconds for the experiment of ^{193}Bi β decay. The cross-section of $^{185}Re(^{16}O, 8n)^{193}Bi$ is very small. The competition of reaction channels $^{185}Re(^{16}O, p7n)^{193}Pb$ and $^{185}Re(^{16}O, 2p6n)^{193}Tl$ is more important. The experimental values of decay ratio for different isotopes were closer. For weak transitions, it was difficult to identify the γ-ray and conversion electron lines only by a decay ratio. The problems are increased by doublets in the spectra. The coincidence spectra were used for a further check

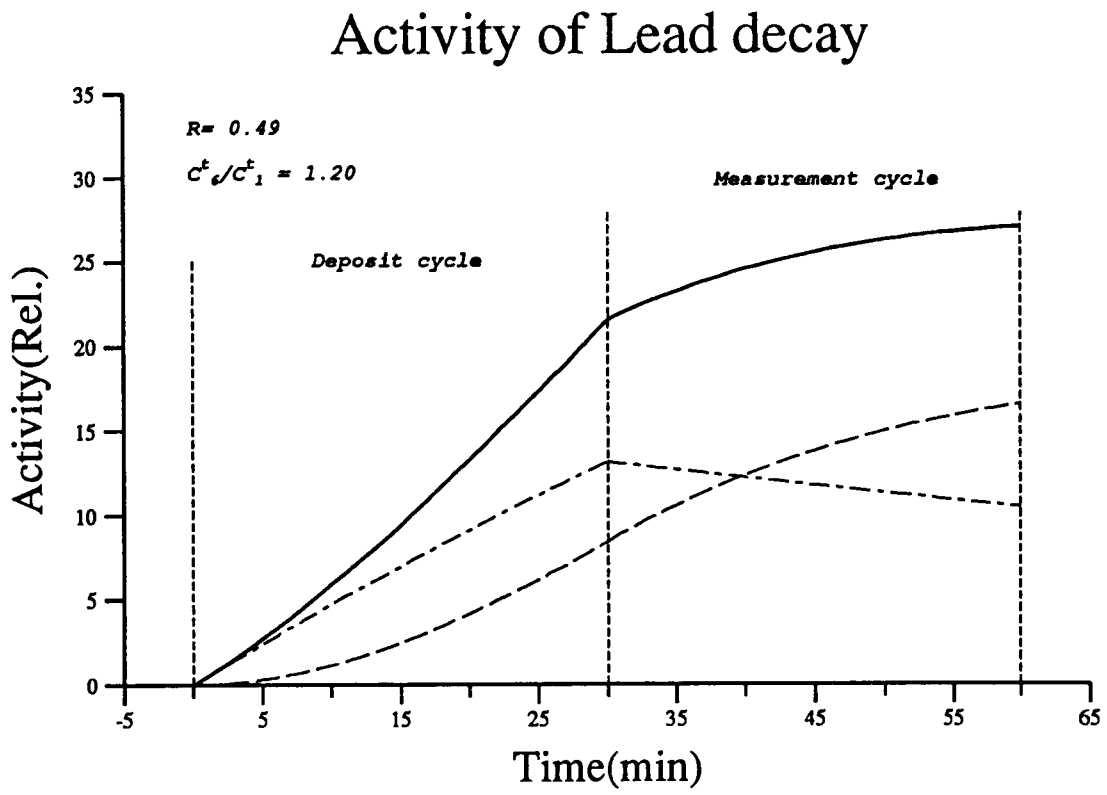

Figure 3.4: Experimental decay tendency of ^{199}Pb. R is the ratio of beam intensity of ^{199}Pb from the mass separator to that of ^{199}Bi. The dashed-line is the activity of ^{199}Pb from ^{199}Bi β-decay. The dot-dashed-line is the activity of ^{199}Pb which came directly from the separator. The solid-line is the total activity of ^{199}Pb. R was adjusted to make $C_6^t/C_1^t = 1.20$.

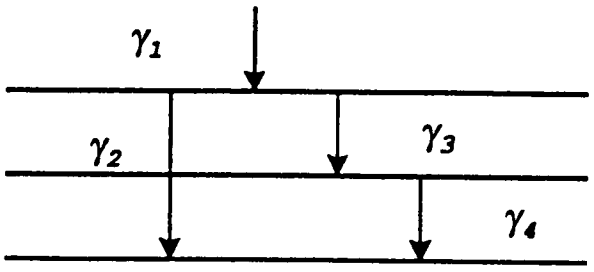

Figure 3.5: Schematic diagram of γ-γ coincidence relationship

of the identifications based on decay tendencies.

3.3.3 Coincidence Spectra

The γ-ray and electron spectra from the decay of heavy isotopes are very complicated, usually containing hundreds of peaks. Some peaks are doublets or even multiplets. To construct a decay scheme, energy sums can suggest some level placements, but more importantly time coincidence relationships establish decay cascades. The 2-dimensional matrix was set up by scanning the event tape after the experiment. A coincidence between two γ photons at energies $E_{\gamma 1}, E_{\gamma 2}$ would add a count at cross point $(E_{\gamma 1}, E_{\gamma 2})$ in the matrix. To illustrate the technique, a schematic diagram is shown in Figure 3.5. γ_1 is time coincident with all other three γ transitions. γ_3 is coincident with γ_4, but γ_2 is not time related with γ_3 and γ_4. From the 2-dimensional coincidence matrix, there is only the γ_1 peak in the γ_2 gated spectrum. A spectrum gated by γ_3 will contain both γ_1 and γ_4. The presence or absence of coincident lines, energy, multipolarity and intensity of each transition are four factors to establish the location of transitions in a level scheme.

In the last section it was pointed out that for any double coincidence event, *ie.* for a γ-ray and electron or two γ-rays within 200ns of each other, e^- and γ-ray energies and several TAC signals were written on the record tape. From a preview

scan, the six related timing spectra (TAC) from four detectors were checked. Because of the fluctuation of the electric pulses and shift, 50-100 ns wide coincidence peaks appeared in the TAC spectra. Different timing windows were set by utilizing gates on TACs in the second scan to decrease the random accidental coincidence in the γ-γ and e^--γ. A two dimensional matrix with directions corresponding to the two energies of the coincident rays was constructed with the program SCAN developed by W.T. Milner. The program is controlled by informtion input through a ⟨.chl⟩ file.

The energy calibrations of the energy axes of the 2-dimension matrices were determined by a few strong known coincidence peaks. After gain shift corrections three γ-γ and three e^--γ matrixes were added to yield one sum γ-γ matrix and one e^--γ matrix by program DAM which was written by W.T. Milner. All coincidence peaks from total projections of the sum matrixes were picked out to select a series of gates to study the coincidence relationships among the transitions. Sometimes a 'walking gate' method was used to identify the doublets and different coincidence relationships for different doublet components. The X-ray peaks in a gated spectrum identifies the element that the gating transition belongs to.

From TAC spectra and the total projected spectra it was shown that background exists in the coincidence matrix. It includes the contribution of random accidental coincidence and compton scattering. For background subtraction, a gate is set on the neighboring channels close to the gated peak and the resulting background spectrum is subtracted from the peak gated spectrum. The result of subtraction is shown in Figure 3.6. The first spectrum ($ID = 1$) is a spectrum gated by the 841 keV (from ^{199}Bi β-decay), which shows strong background and accidental coincidence peaks at 354 keV and 367 keV (both from ^{199}Pb β-decay). The second spectrum ($ID = 2$) has the neighboring background spectrum subtracted; the resulting spectrum has a lower background, the intensity of the 367 keV peak is

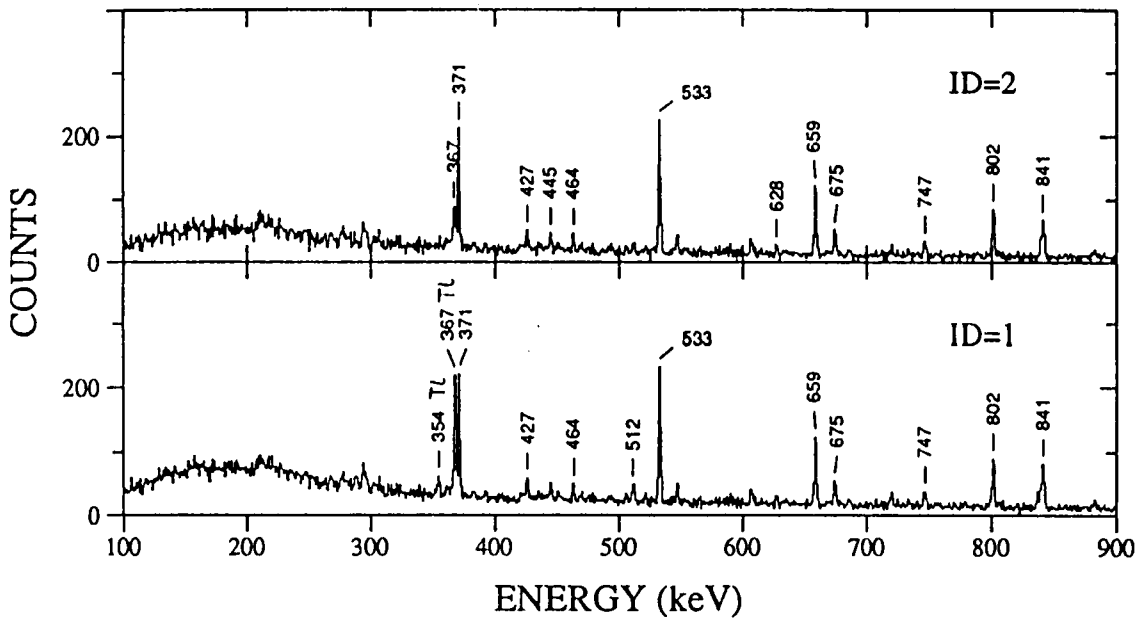

Figure 3.6: Gated spectra before and after background subtraction

much weaker, and the 354 keV peak has disappeared.

3.3.4 Multipolarity

The conversion coefficients for different multipole transitions from the theoretical model were discussed in the last chapter. Experimentally the relative intensities of the γ transitions and the corresponding conversion electrons were obtained from the peak fitting of singles spectra and efficiency correction. In ^{199}Bi decay, the 1034 keV transition is a pure E2 transition ($7/2^- \rightarrow 3/2^-$) and it was used to normalize the relative intensities of γ and e^- to obtain the theoretical value at this energy. The conversion coefficients of other transitions had values between M1 and E2 theoretical values and were called M1/E2 or E2/M1 mixed transitions depending on which part is stronger. Most experimental points were in this range as expected by the general decay theory. Several conversion coefficients higher than

the M1 value were interpreted to result from E0+M1+E2 transitions because higher multipole transitions seldom compete with E2 or M1 decay. No pure E0 transition was found in this work.

Coincidence spectra were used to obtain the conversion coefficients where doublets made it difficult to extract reliable intensities from the singles data. One γ-ray transition results in three electron peaks from K, L, M shell electron emission, which creates more doublets in electron spectra, especially in the lower energy range. Sometimes two separated peaks in the γ-spectrum would result in a doublet in the electron spectrum because of the different electron binding energy for different elements, or vice versa. Conversion electrons are not only in coincidence with X-rays from the parent nuclide ε-decay, but also with the X-ray from after the K-shell electron is ejected, and the outer shell electron has jumped to the lower vacant position. The probability of a conversion e^- being coincident with a X-ray is higher than for the corresponding γ-ray. So X-ray gated spectra can not be used to calculate the conversion coefficient.

CHAPTER 4

Experimental Results

This Chapter is devoted to the experimental results and is divided into three sections for ^{199}Pb, ^{193}Pb and ^{193}Tl, respectively. ^{193}Tl spectra are the by-product of the experiment of ^{193}Bi β-decay.

4.1 ^{199}Bi β-decay and ^{199}Pb Level Scheme

4.1.1 Spectra Analysis

Singles γ and e multiscaled spectra and γ-γ, γ-e, X-γ and X-e spectra from decay of ^{199}Bi (which has a half life of 27 minutes) were analysed. γ and e singles spectra are shown in Figures 4.1 and 4.2. Time multiscaled spectra, electron energy shift and coincidence spectra were used to identify the transitions. The energy shown in the singles electron spectrum is the energy of the electron plus the K-shell electron binding energy of Pb which is the same as the γ-ray energy for the same transition. Since the K-shell binding energy is 2.5 keV less for Tl than Pb, comparing of γ and e^- spectra provides elemental identification. Thus, several strong γ-lines at energies 354, 367, 1383, 1659 keV belong to Tl. 720 and 1136 γ peaks are doublets since appropriate e^- lines apears for both Pb and Tl.

The γ-ray and internal conversion data from the β-decay of ^{199}Bi are given in Table 4.1. Coincidence relationships between transitions are given in Table 4.2. Energy uncertainties of most transitions are about 0.2 keV mainly from energy calibration. Some weak peaks and doublets have a bigger fitting error, uncertainties

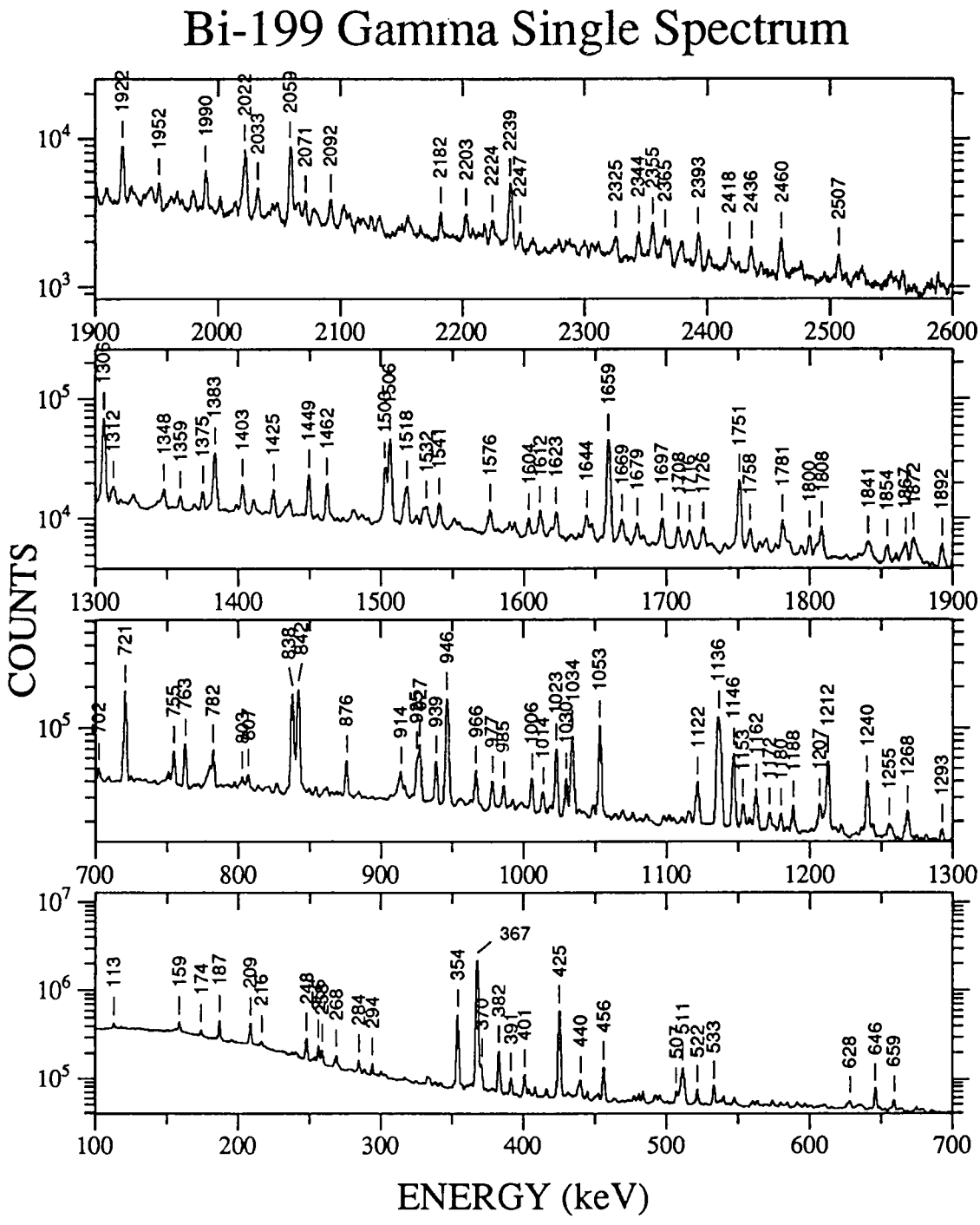

Figure 4.1: ^{199}Bi β-decay singles γ spectrum

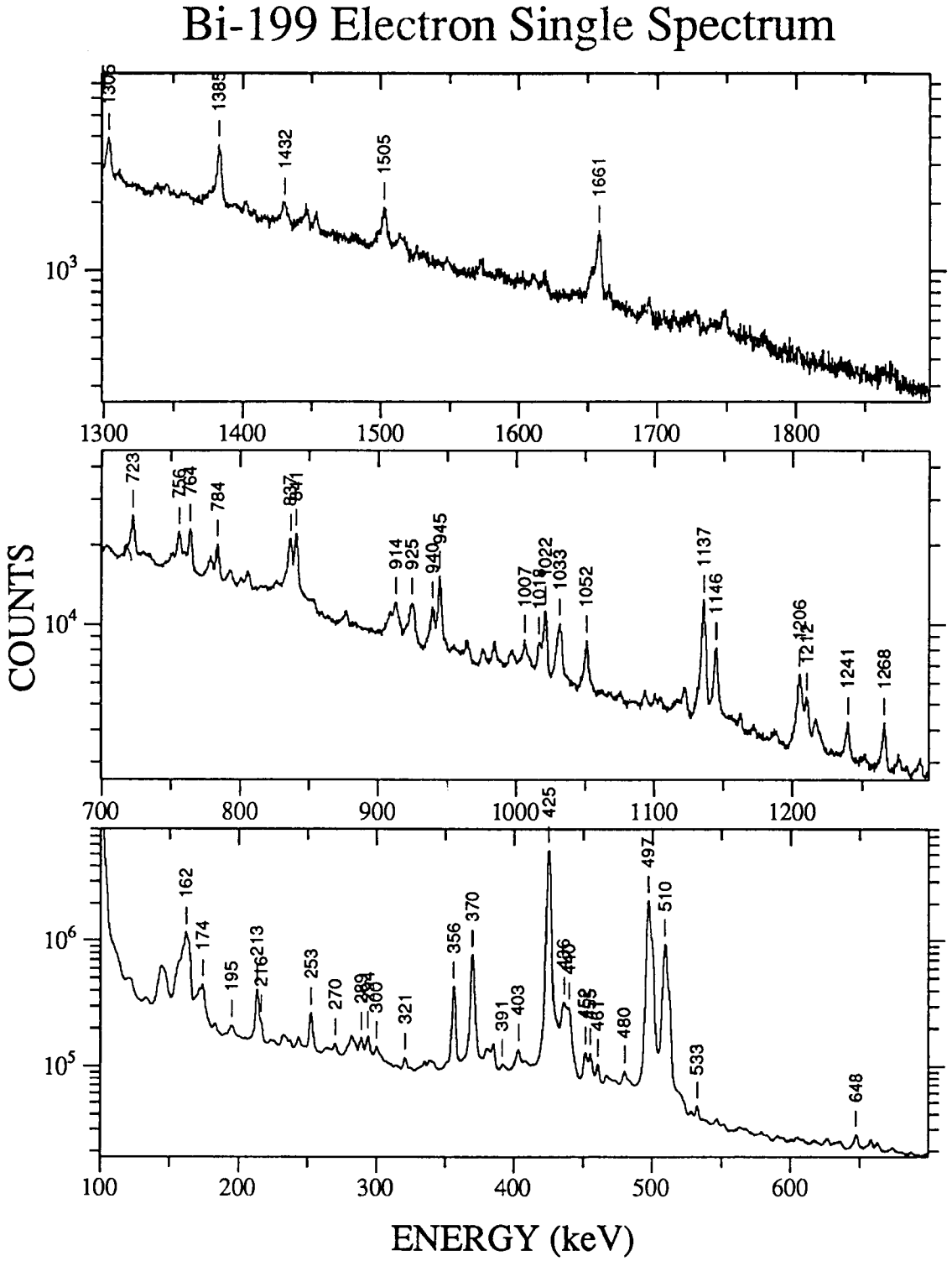

Figure 4.2: ^{199}Bi β-decay singles electron spectrum

Table 4.1 Transitions from ^{199}Bi β^+/ε Deccay

Transition Energy (keV)	γ-ray Intensity (Relative)	Assignment in ^{199}Pb Initial → Final	α_k	Multi-polarity
126.4(2)	0.6(1)	1937 → 1811		
156.3(2)	1.7(1)			
162.6(2)	0.9(1)	1811 → 1648		
183.2(2)	1.0(2)	1937 → 1754	1.6(3)	M1
194.9(3)	1.9(1)	1937 → 1742	1.24(8)	M1
197.1(5)		2278 → 2080		
216.3(2)	4.3(3)	216 → 0	0.97(7)	M1
237.0(5)		1825 → 1648		
237.8(2)	2.4(2)	1811 → 1574	0.59(5)	M1+E2
240.1(2)	2.9(4)	1274 → 1034		
248.4(5)	1.5(9)	1953 → 1705	0.38[a]	M1+E2 ?
253.2(2)	3.6(7)	1317 → 1064	0.29(15)	M1+E2
270.3(6)	1.1(5)		0.9(4)	E0+M1+E2
277.9(3)	1.6(3)	2358 → 2080		
279.1(5)	1.5(4)	2360 → 2080		
279.2(3)	0.5(2)	1643 → 1363	0.8(3)	E0+M1+E2
284.4(2)	9.1(5)	1348 → 1064	0.24(2)	E2+M1
288.3(3)	1.5(3)	1213 → 925		
288.4(3)	1.7(3)	1937 → 1648	1.7(4)	E0+M1+E2
294.0(2)	7.7(5)	1811 → 1517	0.55(4)	M1
300.1(2)	2.9(3)	1574 → 1274	0.70(7)	E0+M1+E2
303.3(2)	1.6(3)	2495 → 2193	0.50(7)	M1
307.5(2)	0.5(1)	1655 → 1348 ?		
314.2(2)	0.8(2)		0.37(9)	M1
317.1(2)	2.3(2)	1274 → 957		
319.4(2)	1.1(2)			
325.1(2)	1.3(1)			
338.2(2)	2.4(2)	2080 → 1742	0.49(5)	E0+M1+E2
341.3(3)	0.9(2)	1705 → 1363	0.9(3)[a]	E0+M1+E2
341.9(3)	1.4(2)	1690 → 1348		
350.9(4)	2.4(4)	2093 → 1742	0.5(1)[a]	E0+M1+E2
359.5(5)	3. (1)	1317 → 957		

[a] From gated coincidence spectra.

[b] Intensity of doublet.

? Unconfirmed transition position

Table 4.1 (Continued)

Transition Energy (keV)	γ-ray Intensity (Relative)	Assignment in ^{199}Pb Initial → Final	α_k	Multi-polarity
360.2(5)	2. (1)	1517 → 1157		
362.8(2)	3.1(5)	1937 → 1574		
370.2(3)	6. (2)	1648 → 1278		
379.1(5)	1.5(5)	1742 → 1363	0.19(6)[a]	M1
391.0(3)	8.(1)	1348 → 957	0.07(1)	E2+M1
391.0(3)	2.(1)	1754 → 1363	0.05(2)	E2+M1
406.1(5)		1754 → 1348		
414.8(6)		2495 → 2080		
415.9(3)	4.3(3)	1574 → 1158		
425.3(2)	156. (8)	436 → 11	2.39(12)	M4
426.5(5)	1.5(5)	1704 → 1278		
431.5(2)	2.0(3)	2080 → 1648		
444.6(2)	3.9(3)	2093 → 1648		
451.9(4)	1.1(5)	2389 → 1937		
452.1(4)	3.1(6)	2026 → 1574	0.10(5)[a]	M1+E2
463.2(2)	1.4(1)	1742 → 1278		
473.0(2)	1.3(2)	2358 → 1885		
480.4(2)	4.8(3)	1754 → 1274	0.31(2)	E0+M1+E2
483.5(2)	6.0(3)	1517 → 1034		
491.2(2)	1.4(1)	1648 → 1158		
497.0(3)	0.9(2)	1655 → 1158		
507.0(2)	6.9(5)	2080 → 1574		
509.6(5)	2.3(8)	1574 → 1064		
521.4(3)	5.9(4)	2458 → 1937		
522.1(5)	2.5(3)	1885 → 1363	0.062(4)[a]	E2+M1
533.1(2)	12.1(7)	1811 → 1278		
537.2(2)	2.5(3)	1811 → 1274	0.047(7)	E2+M1
539.7(2)	5.2(4)	1573 → 1034	0.022(4)	E2+M1
547.1(2)	4.1(3)	2358 → 1811	0.079(6)	M1
560.1(2)	2.5(2)	1517 → 957		
563.3(2)	2.9(2)	2080 → 1517	0.064(5)	M1+E2
579.1(3)	1.0(5)	1643 → 1064		
579.8(2)	2.0(3)	2797 → 2217	0.086(14)	M1
584.1(2)	2.0(2)	1648 → 1064	0.058(7)	M1+E2
590.8(2)	2.5(2)	1655 → 1064	0.064(6)	M1
592.7(2)	1.4(1)			
596.6(2)	2.0(2)	1754 → 1158		
600.5(2)	1.1(1)	2797 → 2197		

Table 4.1 (Continued)

Transition Energy (keV)	γ-ray Intensity (Relative)	Assignment in ^{199}Pb Initial → Final	α_k	Multi-polarity
607.3(2)	1.0(1)	1885 → 1278		
610.1(2)	1.7(2)	2495 → 1885	0.069(8)	M1?
626.3(5)	2.5(5)	1690 → 1064		
628.0(2)	5.0(4)	2276 → 1648	0.050(4)	M1+E2
648.8(2)	2.2(2)	2166 → 1517	0.221(20)	E0 ?
656.4(2)	2.1(2)	1690 → 1034		
658.9(2)	6.9(4)	1937 → 1278	0.042(3)	M1+E2
662.3(5)	1.2(2)	2026 → 1363		
663.3(4)	0.5(1)	1937 → 1274	0.12(3)	E0+M1+E2
664.7(2)	1.8(2)	2942 → 2278		
674.6(2)	2.8(3)	1953 → 1278	0.048(5)	M1
679.0(2)	1.9(2)	1953 → 1274		
697.6(2)	0.8(1)	1655 → 957		
704.1(2)	1.1(1)	2278 → 1574	0.120(13)	E0?
708.9(2)	2.4(2)	925 → 216		
715.1(2)	0.8(1)			
720.6(3)	12.(1)	1754 → 1034	0.011[a]	E2+M1
730.0(5)	1.6(5)	2093 → 1363		
735.0(2)	1.2(2)			
741.1(2)	1.3(2)			
747.0(3)	2.5(5)	2026 → 1278		
750.8(3)	4.5(3) ?			
751.8(3)	1.0(1)	2026 → 1274		
768.4(2)	1.9(2)			
771.4(2)	2.1(2)			
777.1(6)	1.0(5)	1811 → 1034		
779.4(2)	9.1(6)	1937 → 1158	0.025(2)	M1+E2
797.0(2)	2.9(4)	1754 → 957		
800.8(3)	2.0(4)			
802.5(2)	5.0(5)	2080 → 1278	0.011(2)	E2+M1
805.1(3)	1.5(2)			
806.7(2)	6.4(4)	2080 → 1274	0.024(2)	M1+E2
818.8(2)	1.9(2)	2093 → 1274	0.012(3)	E2+M1
821.0(2)	2.3(2)	1885 → 1064		
826.5(3)	3.5(3)			
827.9(3)	1.5(1)		0.053(7)	E0+M1+E2
837.6(2)	96. (5)	1274 → 436	.0064(4)	E2
841.0(5)	3.1(3)	2119 → 1278		

Table 4.1 (Continued)

Transition Energy (keV)	γ-ray Intensity (Relative)	Assignment in ^{199}Pb Initial → Final	α_k	Multi-polarity
841.7(2)	101. (6)	1278 → 436	.0067(4)	E2
845.0(5)	2.2(11)	2119 → 1274		
849.0(2)	2.0(2)	2197 → 1348		
854.0(6)	¡ 0.5	1811 → 957		
859.4(2)	2.3(2)	2797 → 1937		
865.0(2)	1.6(2)		0.020(4)	M1+E2
868.3(2)	1.7(2)	2026 → 1158		
870.9(2)	1.2(2)			
884.0(2)	2.1(2)	2458 → 1574	0.011(2)	E2+M1
906.9(3)	1.4(4)			
909.7(3)	1.5(4)		0.049(13)	E0?
911.9(2)	5.9(5)	2616 → 1705 ?		
913.8(2)	12.6(8)	925 → 11	0.011(1)	E2+M1
916.6(2)	5.7(5)	2942 → 2026 ?	0.021(2)	M1
921.6(2)	2.1(3)	2495 → 1574		
925.1(2)	18.3(10)	925 → 0	0.010(1)	E2+M1
927.1(2)	33.1(20)	1363 → 436	.0062(4)	E2+M1
946.0(2)	105. (6)	957 → 11	.0055(3)	E2
956.1(2)	1.8(3)		0.029(5)	E0+M1+E2
961.8(5)	0.6(3)	1996 → 1034		
962.3(4)	1.6(5)	2480 → 1517		
966.0(2)	17.3(10)	977 → 11	.0058(4)	E2+M1
977.2(2)	12.7(8)	977 → 0	.0061(4)	E2+M1
983.2(3)	1.6(3)			
985.3(2)	9.9(6)	2797 → 1811	0.009(1)	M1+E2
989.3(6)	1.6(8)			
991.8(2)	4.0(5)	2026 → 1034		
997.3(3)	1.2(5)	1213 → 216		
998.4(2)	3.4(4)	2276 → 1278	0.011(2)	M1+E2
1001.3(2)	2.0(3)	2276 → 1274		
1013.4(2)	8.7(6)	3106 → 2093		
1018.6(2)	3.1(3)	1996 → 977	0.019(3)	M1?
1022.8(2)	40.2(21)	1034 → 11	.0095(5)	E2+M1
1034.0(2)	55.2(28)	1034 → 0	.0050(3)	E2
1038.6(2)	3.0(3)	1996 → 957		
1041.9(2)	2.5(4)	2358 → 1317		
1048.2(2)	4.7(3)	2026 → 977		
1052.8(2)	71. (4)	1064 → 11	.0034(3)	E2?

Table 4.1 (Continued)

Transition Energy (keV)	γ-ray Intensity (Relative)	Assignment in ^{199}Pb Initial → Final	α_k	Multi-polarity
1063.7(2)	1.8(2)	1064 → 0 ?	0.010(3)	M1+E2
1068.8(2)	3.0(3)	2026 → 957		
1076.0(2)	2.2(2)	2033 → 957		
1085.8(2)	2.5(2)	2120 → 1034		
1097.7(2)	2.7(2)			
1101.4(2)	3.0(2)	2166 → 1064		
1104.7(2)	1.7(2)	2082 → 977		
1110.5(2)	2.1(3)	1327 → 216 ?		
1119.5(5)	1.0(5)	2278 → 1158		
1121.3(2)	20. (2)	3059 → 1937		
1135.7(4)	10. (3)	2093 → 957		
1137.1(3)	40. (5)	1574 → 436		
1146.4(2)	44. (3)	1158 → 11	.0068(5)	E2+M1
1152.2(5)	8. (3)	1369 → 216		
1152.9(3)	3. (1)	2217 → 1064		
1157.5(2)	3.7(3)	1158 → 0		
1162.1(2)	17.2(9)	2120 → 957		
1171.4(2)	6.1(4)			
1174.4(2)	1.7(2)		.016(2)	M1?
1179.3(3)	4.0(4)	2213 → 1034		
1177.6(5)	1.8(2)	2921 → 1742		
1183.7(2)	1.1(2)			
1187.9(3)		2942 → 1754		
1188.7(3)	9.6(6)	2166 → 977		
1206.5(3)	10.8(8)	1643 → 436		
1209.2(4)	4.6(4)	2166 → 957		
1212.2(2)	42. (4)	1648 → 436	.0040(3)	E2+M1
1217.1(4)	2.2(6)			
1221.6(3)	3.0(6)	2495 → 1274	0.011(2)	M1?
1235.7(2)	2.3(2)	2193 → 957		
1239.9(3)	14. (2)	2197 → 957		
1240.5(5)	13. (2)	2166 → 925		
1243.5(2)	3.8(3)	2278 → 1034		
1254.9(3)	4.0(3)	2829 → 1574	.0043(6)	E2+M1
1256.0(4)	2.5(2)	2213 → 957		
1267.1(5)	8. (1)	2193 → 925		
1268.2(3)	2.0(4)	1705 → 436	0.05(2)	E0+M1+E2
1274.4(3)	1.0(2)			

Table 4.1 (Continued)

Transition Energy (keV)	γ-ray Intensity (Relative)	Assignment in ^{199}Pb Initial → Final	α_k	Multi-polarity
1281.2(3)	1.2(2)	3093 → 1811		
1305.6(2)	64. (4)	1742 → 436		
		1317 → 11 ?	.0019(2)	E1?
1311.5(5)	2. (1)	2829 → 1517		
1312.4(4)	5. (2)	2237 → 925	.0034(3)	E2+M1
1317.6(3)	1.1(3)	1754 → 436		
1326.3(2)	3.7(4)	2360 → 1034		
1343.9(3)	2.3(3)			
1347.5(2)	6.7(4)	2921 → 1574		
1368.8(2)	2.0(3)	2942 → 1574		
1374.5(2)	6.1(4)	1811 → 436		
1379.7(3)	1.8(2)		0.003(2)	E2
1398.3(2)	2.0(2)	2672 → 1274	0.005(1)	E2+M1
1402.4(3)	1.3(6)	2360 → 957		
1410.3(2)	4.4(3)	3059 → 1648	.0019(4)	E1?
1413.3(3)	1.2(2)			
1419.1(2)	1.2(2)			
1424.0(3)	7.1(5)	2458 → 1034		
1424.4(5)	2.0(2)	3235 → 1811		
1432.7(3)	2.3(3)	2389 → 957	0.015(2)	E0?
1435.4(2)	5.0(4)	2360 → 925		
1448.1(5)		2797 → 1348		
1448.5(4)	16.4(9)[b]	1885 → 436	.0018(2)	E1?
1461.5(2)	12.5(7)	2495 → 1034		
1464.6(3)	0.8(1)	2389 → 925		
1479.6(5)	3.3(3)[b]	2797 → 1317		
1480.3(5)		2829 → 1348		
1485.9(2)	1.4(2)	3297 → 1811		
1505.9(2)	48. (3)	1517 → 11	.0011(1)	E1
1506.2(6)	3.0(3)	3023 → 1517		
1517.4(2)	12.9(8)	1517 → 0 ?		
1529.5(2)	4.3(3)	3105 → 1574		
1540.5(2)	6.9(5)			
1550.8(2)	2.5(2)	2829 → 1278 ?	0.003(1)	E2+M1
1554.3(2)	1.6(2)			
1575.5(2)	6.1(4)	3093 → 1517	.0019(2)	E2
1586.0(4)	2.4(5)	3105 → 1517		
1589.1(3)	2.4(3)			

Table 4.1 (Continued)

Transition Energy (keV)	γ-ray Intensity (Relative)	Assignment in ^{199}Pb Initial → Final	α_k	Multi-polarity
1613.2(2)	1.0(1)			
1618.9(2)	2.2(2)			
1622.5(2)	6.7(4)		.0019(3)	E2
1633.0(10)	1.1(5)			
1638.1(3)	1.1(2)			
1641.8(4)	1.3(2)			
1644.3(4)	5.9(5)[b]	2080 → 436		
1643.4(5)		2921 → 1278		
1647.1(2)	4.0(3)	2921 → 1274		
1658.8(4)	(2.8)	2616 → 957		
1667.9(2)	5.6(4)	2942 → 1274	.012(1)	E0?
1678.7(2)	4.6(3)	1690 → 11 ?		
1683.0(3)	1.8(2)			
1695.8(3)	4.9(3)			
1707.6(2)	4.6(3)			
1715.7(2)	4.7(5)			
1725.0(2)	4.7(3)	3480 → 1754 ?		
1740.3(3)	1.2(2)			
1757.5(2)	5.0(4)	2193 → 436 ?		
1764.6(3)	1.8(3)			
1775.5(3)	1.3(2)	3054 → 1278		
1780.3(5)	7.4(5)[b]	2217 → 436		
1780.8(4)		3059 → 1278		
1784.3(2)	2.4(2)	3059 → 1274 ?		
1799.1(2)	3.9(3)			
1804.1(3)	2.2(2)			
1807.6(2)	6.9(4)			
1839.0(3)	2.4(2)			
1841.2(3)	2.6(2)			
1853.4(2)	3.0(2)			
1864.0(3)	1.7(2)			
1866.4(3)	3.4(3)	3023 → 1158		
1871.7(3)	4.8(3)	2829 → 957		
1874.3(3)	2.3(2)	1885 → 11 ?		
1899.8(3)	1.9(2)			
1908.0(3)	1.9(3)			
1921.6(2)	9.8(6)	2358 → 436		
1928.5(3)	2.0(2)			

Table 4.1 (Continued)

Transition Energy (keV)	γ-ray Intensity (Relative)	Assignment in ^{199}Pb Initial → Final	α_k	Multi-polarity
1939.3(3)	1.1(2)			
1945.6(3)	2.4(2)			
1951.3(3)	3.3(3)			
1961.2(3)	1.5(2)			
1965.7(3)	1.9(2)			
1989.2(2)	5.4(4)	3023 → 1034		
2012.9(3)	1.3(2)			
2018.5(3)	2.1(2)	3297 → 1278		
2021.5(3)[b]	11.1(6)[b]	2033 → 11		
		2458 → 436 ?		
2047.6(3)	1.8(2)			
2058.7(2)	12.7(7)	2495 → 436 ?		
2064.4(3)	2.5(3)			
2070.0(3)	2.2(3)	3105 → 1034		
2077.0(3)	1.4(2)			
2101.7(3)	2.4(2)	3059 → 957		
2106.2(3)	1.4(1)			
2113.7(3)	1.0(2)			
2117.9(3)	1.1(2)			
2124.4(3)	1.4(3)			
2154.3(3)	1.6(2)	2166 → 11 ?		
2165.1(3)	0.6(1)	2166 → 0 ?		
2181.5(3)	1.9(2)	2193 → 11 ?		
2201.4(6)	2.1(2)[b]	3235 → 1034 ?		
2202.6(6)		3480 → 1278		
2223.3(3)	1.7(2)	3257 → 1034		
2246.2(3)	1.1(1)			
2309.9(3)	0.8(1)	3235 → 925 ?		
2324.2(3)	1.4(2)			
2342.7(3)	1.8(2)			
2354.4(3)	2.9(2)			
2363.7(3)	1.8(2)			
2378.1(5)	1.3(2)			
2391.7(3)	2.3(2)			
2416.6(3)	1.3(1)	3480 → 1064		
2458.9(3)	2.5(2)			
2505.6(3)	1.4(1)			

Table 4.2. Coincidence Relationship of ^{199}Pb γ-Decay

Energy	Coinsidence Line (keV) (S: Strong, W: Weak)
126.4	294 533 1121 1374
162.6	370 547 985S 1212S 1281 1424W
183.2	351W 391W 444 452 480S 521 596 720S 797 837 859 927 946S 1023S 1034S 1121 1135 1146 1212 1305 1317W
195.3	379 401 416 451 507 521 563W 802 806 827 837 841 859 927 1052W 1122 1305S 1505W 1643W
216.3	709S 997 1111 1152S
237.0	300 416 539 547 821 985 1022W 1034W 1137S 1212 1424
240.1	300 481 1022 1034 1221W
248.4	334 341 427 762 841 875 926 985 1212 1268 1435
253.2	1052
270.3	783 1034W 1305W
277.9	378 507 563W 802 806 837 841
279.7	559W 667W 741W 927S 958 972 1026 1644
284.4	849W 927W 1053S 1480
288.5	371 452 521 584W 841 859W 925 1122 1212S
294.0	483 547 560 945 985S 1424W 1506S
300.1	237 240 452 507 837S 1212 1348 1369 1529
303.3	370 641 728W 925 1135 1268 1446W 1505 1659W 2077W 2180
307.5	284 709 725 985 1505
317.1	414W 946
319.4	920W 984
329.7	183 781W
338.2	195 253 277W 379 414 927 1052W 1238 1305S
341.5	248 284 391 414 761 763 927S 1052 1305
360.0	945 1146
362.8	300 521 540 838 1022 1034 1121 1137S 1212 1239 1505 1517 1589
370.2	163 288 444 452 457 628W 749 827 842S 946 1410
379.1	195 338W 927S 1146 1212W
391.2	342 522W 875 926 945S 1448
416.5	237 362W 645 704 741 827 884 1146 1157 1256 1347
431.5	370 1212
444.6	183 370 841 1212S
451.9	183 195 288 363W 659 781W 837 853 917 1137S 1212W
463.2	195 842
469.0	253 837 841 946 1644
473.0	247 607W 926 946 1022 1136 1187 1304 1448 1505

Table 4.2. Continued

Energy	Coinsidence Line (keV) (S: Strong, W: Weak)
480 4	183S 240 837S 913W 1023 1034 1188
483.5	294S 564 1023S 1034S 1505 1575 1586
491.2	1136 1146
497.0	720 1146
500.6	1137W 1537W
507.0	195 278 300 1023 1034 1137
521.7	288 658W 841 927 1137 1211W
533.1	547 566 841S 985S 1424 1485W
537.2	837 986W 1211W 1505
539.7	238 1023 1034 1242 1256 1347 1448W
547.1	163 237 294 533 841 1137 1374 1505
560.1	294 946 1505W
563.3	195 288 278W 280W 1505
579.8	925 1052 1152 1305 1505W 1780
584.0	163 288 946 1052 1528 1540
590.8	163 946 1052S
592.7	1135
600.5	849W
607.3	473W 646W 841 995 1161W
610.1	837W 842W 1448
626.0	1053 1305
628.0	370 1212
646.0	196 416 432W 543 649 661 741 758 813 854 1306
648.8	646 925 1505
656.4	841 1023 1034
658.9	451 521 841S 1121
662.8	241 451 521 837S
664.7	927 1242
674.7	841
679.0	837S 841 1052 1162
697.6	946 1380
704.1	300W 1137
709.0	216S 288
715.1	926 1022W
720.6	183 521 913 1023 1034 1188
735.0	1305 1448
741.1	416W 646

Table 4.2. Continued

Energy	Coinsidence Line (keV) (S: Strong, W: Weak)
751.8	216 837 946
771.4	838 1305
777.0	1034
779.5	927 1146 1505
787.2	318 465W 469W 1305
797.0	183 946
800.8	252 1136 1305
802.5	195 278 841S
806.7	195 278 837S
813.7	646 1206 1305
818.9	826 837
821.2	231 1053
826.5	370 1013W
837.6	216 300S 480S 537 662 679 725 752 806 818 845 1002 1221 1398 1541 1647 1668 1784 1834 1899 2009 2201
841.7	195 288 294 370S 427 445 464 533S 547 607 628 659 675 747 802 842 927 985 1097 1121 1410 1423 1449 1643 1775 1780 1872 2201
845.0	837
849.0	284 391 1033 1052W 1305
853.6	646 927
859.3	183 195 288 658 780W
865.0	1022
868.3	1146
882.1	720W 842 977 1022
884.0	841 1137
893.4	1053
898.9	916W 1023W 1267W
906.9	805W 853W 976 1307
909.7	416W 1306
911.9	1268 1305
913.8	1041 1053 1268 1311
916.6	720W 837W 991 1023
921.6	300 838W 946 980 1137
925.1	288 946 952 1229 1239 1267 1312 1325 1435 1464
927.1	280 341 379 391 522 662 715 730 754 779 842
946.0	294 317 329 360 370 391S 560 697W 733W 750 797 854W 921 944 983 1013 1038W 1068 1075 1135S 1162S 1209 1239S 1256 1402 1658 1803 1871 2101

Table 4.2. Continued

Energy	Coinsidence Line (keV) (S: Strong, W: Weak)
954.	913 925 1505W
956.1	256 1023W
962.4	962 1022 1034 1505
966.0	730 837 841 966 980 1018 1023 1048 1104 1187 1212 1216 1345 1424 2029
977.2	636W 857W 1047 1104 1188 1243 1505 1560
983.2	946
985.3	162 237 294 533 537W 842 1374 1505
989.3	1034 1135
991.8	1023 1034 1052
998.4	842
1001.3	837
1013.4	946 1136
1018.6	946 966
1022.8	183 240 483 507 540 720 992 1085W 1179 1243 1424 1461 1989 2222
1034.0	183 240 483 507 540 720 927 992 1085 1179 1243 1326 1424 1461 1989 2222
1038.6	837 946
1041.9	1305
1048.2	966 977
1052.8	253S 284S 584 591 626 820 946 992 1152 1212 1281W
1068.8	946
1076.0	946 1505
1085.8	946W 1023W 1034
1097.7	841
1101.4	946 1052 1505
1104.7	927 966 977
1110.5	216 1212
1120.0	1146 1157
1121.3	183 195 288 658 841
1135.7	946
1137.1	238 363 452 507 884 922 1075 1254 1346 1447 1484 1808
1146.4	360 416 497 596 779 838 868 1120 1179
1152.5	216S 1052
1157.5	416 596 841 868 1121
1162.1	946

Table 4.2. Continued

Energy	Coinsidence Line (keV) (S: Strong, W: Weak)
1171.4	1052 1212W 1228W
1174.4	1052W
1179.4	195W 1023 1034 1146 1305W
1183.7	533
1188.0	391 406 480 720 966 977
1206.5	634 837W 946 1052W
1209.2	946
1212.2	163 237 289 294 431 444 628 1004 1111 1120 1410
1217.1	1146
1221.6	837
1235.7	303 946
1239.7	946
1254.9	300 539 1137
1268.1	248 303 913 917 925 1312W
1274.4	965W
1281.2	237 294 841 1052
1305.6	195 338 351 709 1040 1179 1480
1312.1	913 925 945W 1505
1326.3	1023 1034
1347.5	300 416 539 1137
1374.4	547 985 1424
1402.4	946
1410.3	370 1212
1424.2	238 294 533 777 837 841 1023 1034 1374
1435.4	925
1448.6	392 473 610 1137W
1461.5	1023 1034
1480.3	253 284 391 1305
1505.9	294 547 563 595W 648 778 871 962 977 985 1312 1505 1586
1517.4	
1529.5	1137
1540.5	
1575.5	483 927W
1643.7	195 278 841 946
1658.8	946
1667.9	240 837
1678.7	244W 253W 280W 926W

Table 4.2. Continued

Energy	Coinsidence Line (keV) (S: Strong, W: Weak)
1725.0	
1757.5	
1780.4	580 841
1807.6	284 841 945W 1305
1871.7	946
1921.6	
1989.2	1023 1034
2021.5	
2058.7	301
2070.0	689 1023W 1034W
2201.8	841
2223.3	1023 1034

are as big as to 0.6 keV. Relative intensities of γ-rays were deduced from the singles spectrum except for the weak lines and doublets. The 1034 keV transition from $7/2^-$ state to $3/2^-$ was taken as a pure E2 transition to normalize the relative intensities between γ and e spectra. Using this parameter in the low energy region, the 425 keV $M4$ transition was checked. The theoretical value of α_K is 2.41 and the fixed experimental value is 2.39(12). Experimental α_K/α_L and $\alpha_{L1+L2}/\alpha_{L3}$ ratios are 1.89(2), 2.7(2) compared with theoretical values 1.96 and 2.81. The γ intensity of the 425 keV transition in Table 4.1 is not important here, because part of it is from atoms in the 436 keV isomeric state which were extracted from the mass separator directly. It would be different under different experimental conditions.

As was discussed in Chapter 2, the probability of lower multipole transitions is much bigger than higher ones. If it is possible, excited states will decay to neighboring spin states. For the first $13/2^+$ state of ^{199}Pb, the nearest spin state in the lower excited energy region is $5/2^-$, the lowest possible multipolarity is $M4$. So this isomeric state has a very long half life (12.2 min) and competitive $\varepsilon + \beta^+(7\%)$ decay.

Several other transitions with conversion coefficients much larger than the

M1 transition theoritical value are interpreted as *E0+M1+E2* transitions. In the 927 keV gated electron and γ spectra (Fig. 4.3), the 379 keV transition is *M1* and 391 kev is *E2+M1*. The 342-keV transition having a stronger relative electron intensity yielding an α_k (0.9(3)) which is about 3.5 times the *M1* theoretical value must be an $E0 + M1 + E2$ transition. The 352- and 441-keV peaks in the electron spectrum are the L-lines of 280- and 367(Tl)-keV transitions. The 371- and 426-keV peaks are the accidental coincidence peaks or incompleted background subtraction of two huge K-line electron peaks of transition energies at 367(Tl)- and 425(Pb,M4)-keV. Another important *E0+M1+E2* transition is the 1268 keV line. In expanded singles spectra (Fig. 4.4), the ratio of electron to a γ-ray counts for the 1268 keV transition is clearly shown to be bigger than neighboring peaks. Considering it is a doublet (coincident with 248 and 925 keV at different locations in the scheme), the γ counts in the 248 keV peak in the 1268 keV electron gate is about half as large as in the 1268 keV γ gate; but no 925 keV peak was found in 1268 keV electron gate. It can be concluded that less than one tenth of the electrons from the 1268 keV transition energy is through in the coincidence with 925 keV. The corrected α_k for the 1268-keV transition between 1705 and 436 keV is 0.05(2), about 6 times the *M1* transition theoretical value.

4.1.2 Level Scheme of ^{199}Pb

The level scheme of ^{199}Pb presented in Figs. 4.5-4.7 is constructed with the γ-rays and conversion electrons attributed to the β-decay of ^{199g}Bi. The figure is separated into three parts for clarity. It is based primarily on the coincidence relations. Energy sums and differences were also used in conjuction with coincidence data to place levels. Strong γ-lines observed without coincidence peaks are assumed to decay to the ground state, first excited state, or the isomeric level (1st positive parity state), if its energy is equal to the energy of an excited state, these are

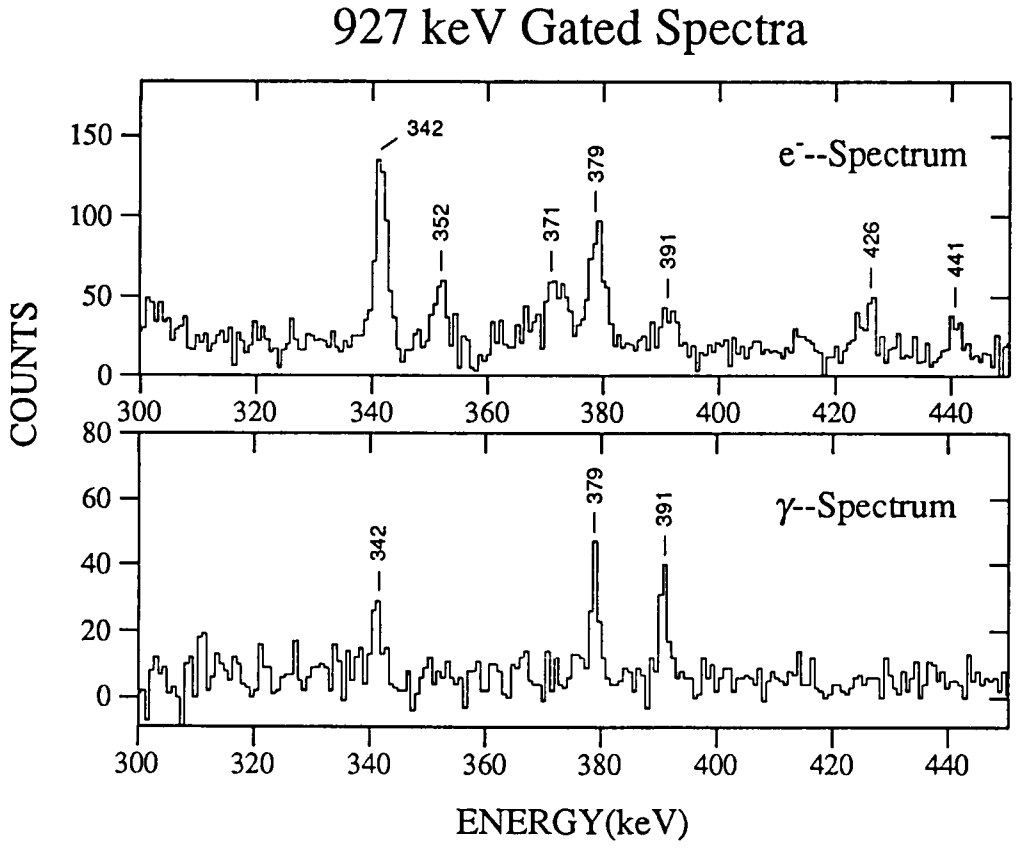

Figure 4.3: The e and γ spectra in coincidence with the 927-keV γ ray.

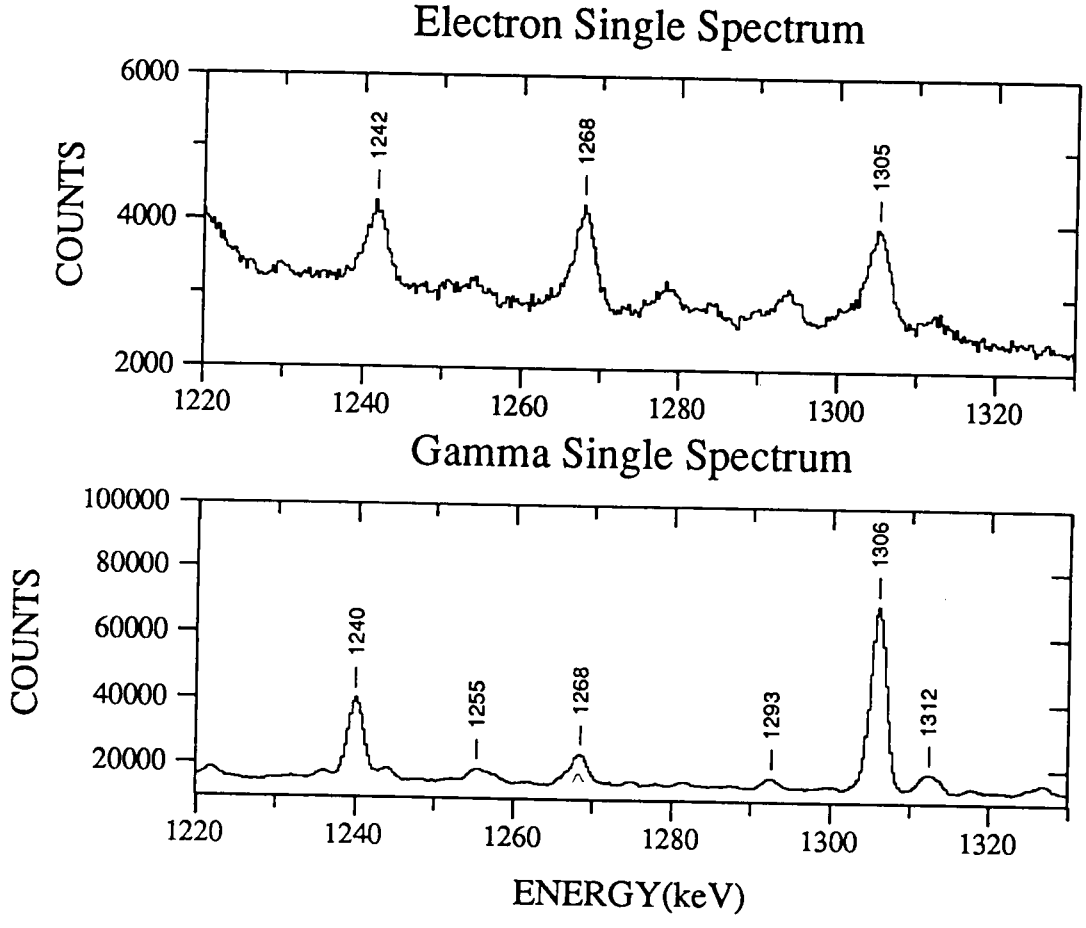

Figure 4.4: Singles e and γ spectra at 1268 keV energy region

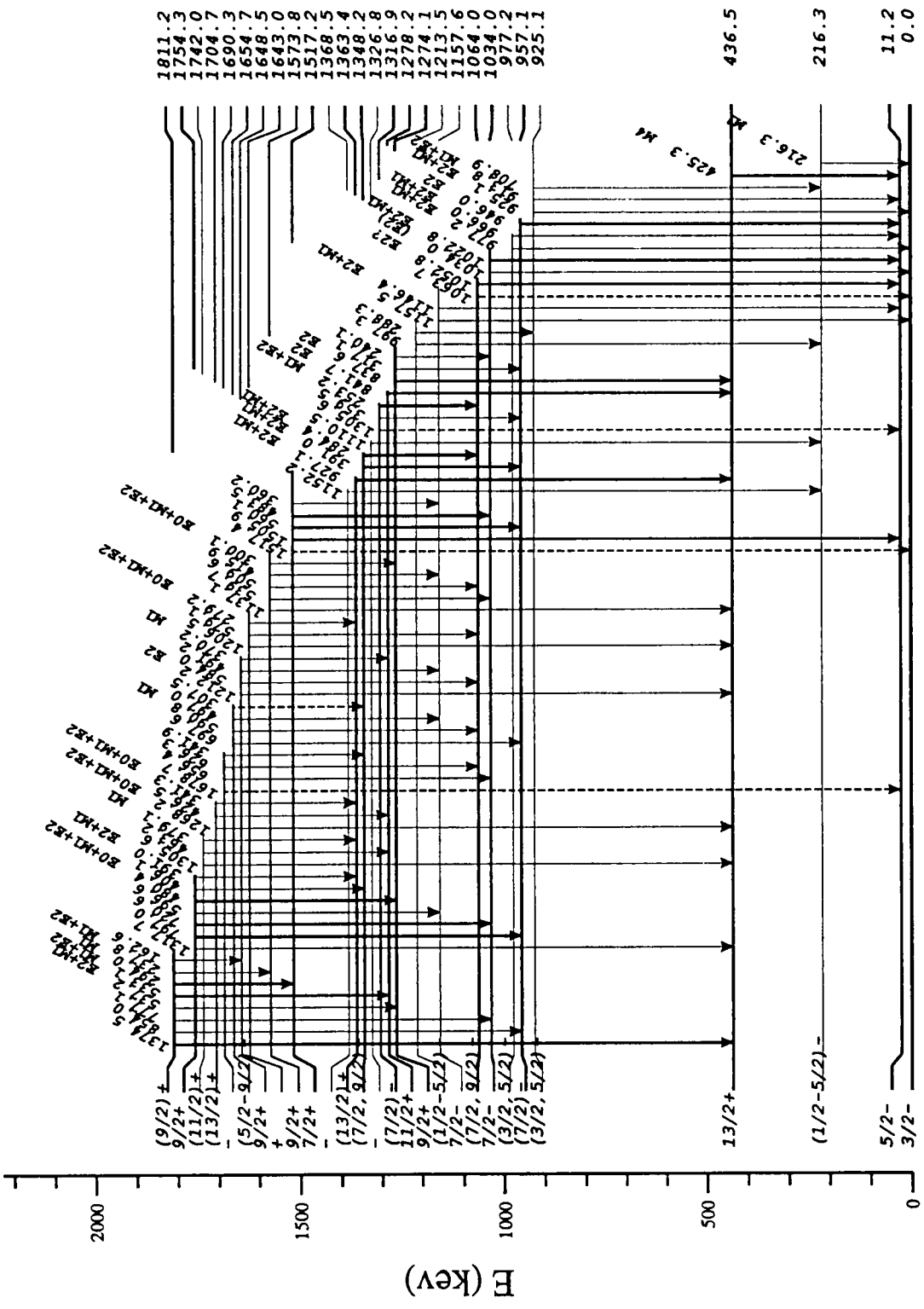

Figure 4.5: ^{199}Pb level scheme (part I).

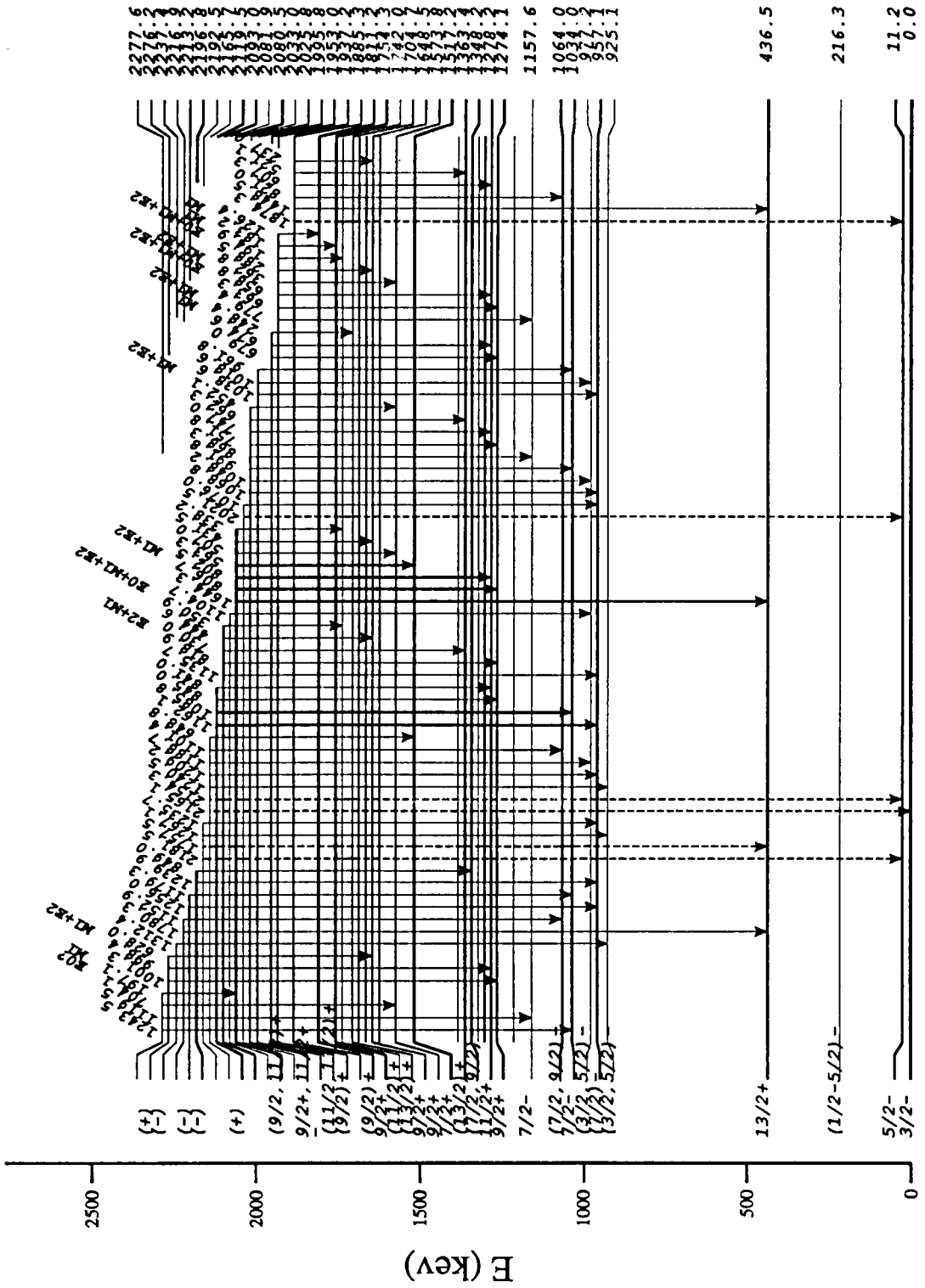

Figure 4.6: ^{191}Pb level scheme (part II).

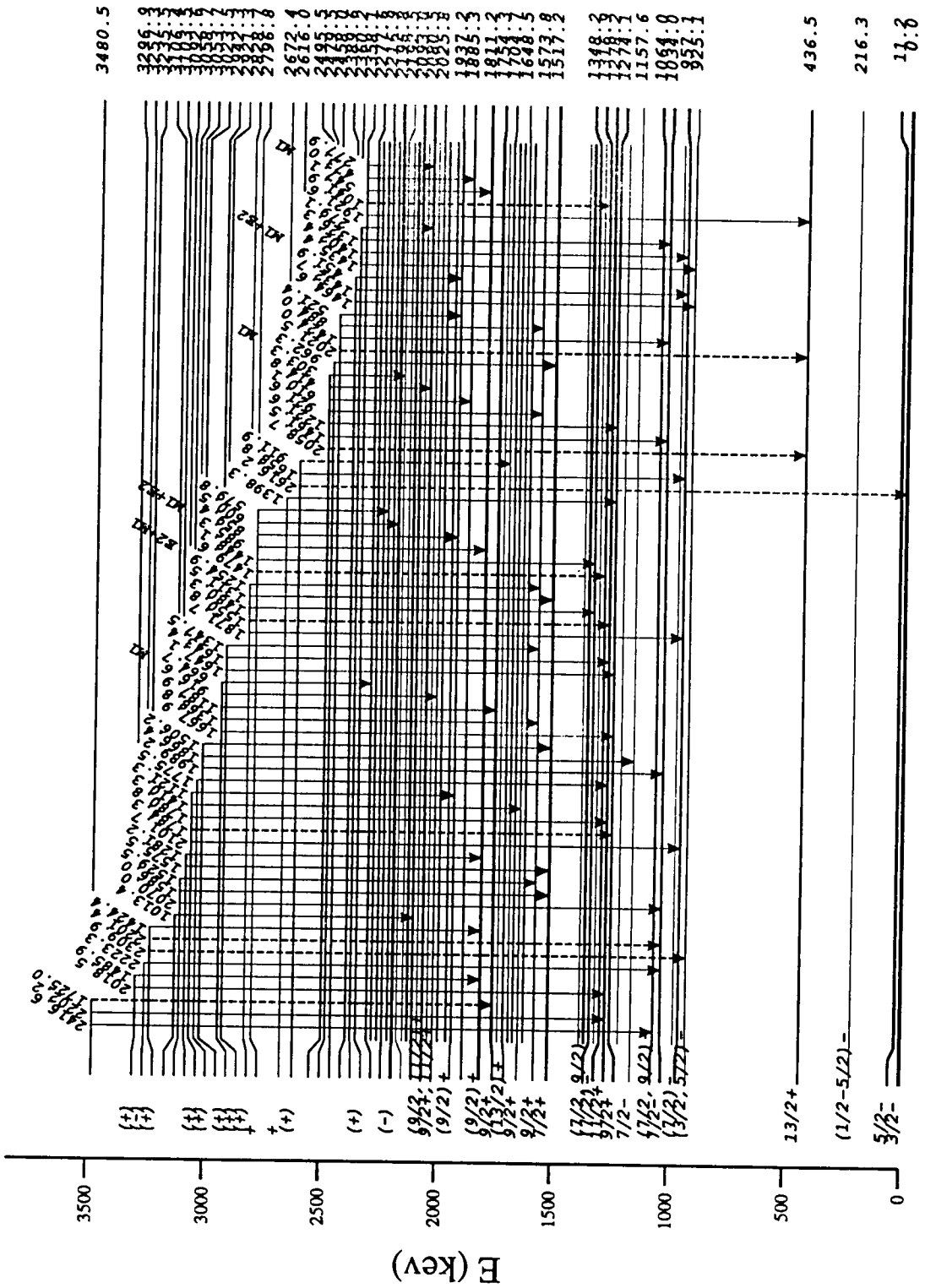

Figure 4.7: ^{199}Pb level scheme (part III). Only the levels related with the transitions from the higher states which spin, parity and energy are marked in the scheme.

indicated by dashed lines in Figure 4.5. The present scheme of ^{199}Pb has 67 levels compared with the 16 previously known levels[Sch88]. A total of 216 γ-lines from the 296 observed transitions in the range from 100 to 2500 keV attributed to the decay of ^{199g}Bi have been placed in the level scheme.

The present work is based on the several known levels [Ri78]. The ground-state spin and parity of ^{199}Pb has been assigned $3/2^-$ from the hyperfine structure and its magnetic and quadrupole moments, μ and Q [Tho83]. Some other levels will be discussed in detail if different from the previous work.

The excitation energies of all states were determined by fitting to the energy of transitions which connected them to the scheme. The minimum χ-square method is used in the fitting.

$$\chi^2 = \sum_{k=1}^{n} \frac{1}{[\Delta E_\gamma(k; i \rightarrow f)]^2} [E_\gamma(k; i \rightarrow f) - (E_L(i) - E_L(f))]^2 \qquad (4.1)$$

where $E_\gamma(i \rightarrow f)$ and $\Delta E_\gamma(i \rightarrow f)$ are the energy and energy uncertainty of the γ-ray from the i state to the f state. $E_L(i)$ is the excitation energy of state i and n is the number of transitions put into the scheme. The energies of levels are the variables in the fitting process to make χ^2 minimum. An alterative method includes an additional weight factor of $\frac{1}{E_L(i)}$ to account for a larger uncertainty in the higher energy levels.

$$\chi'^2 = \sum_{k=1}^{n} \frac{1}{E_L(i) \cdot [\Delta E_\gamma(k; i \rightarrow f)]^2} [E_\gamma(k; i \rightarrow f) - (E_L(i) - E_L(f))]^2 \qquad (4.2)$$

The level energies deduced were the same with these methods to within 0.1 to 0.2 keV.

First Excited state: The spin and parity has been assigned $5/2^-$ for it is a favored state from α-decay of ^{203}Po and the 425 keV $M4$ transition from the $13/2^+$ state [Sch88]. The previous work set its energy as 5(4) keV from IT decay because the measurement low-limit was 9.3 keV. But in this work the 1023 and 1034 keV

gated spectra were found to have the same 14 γ-lines in coincidence (Fig. 4.8). Being strong transitions they must decay to low-lying states and having the same coincidence relationships they must decay from the same level. The 1023 keV transition has been put into the scheme above the 1st excited state and the 1034 keV transition above the ground state. Thus, the energy of the 1st excited state is 11.2 keV. Three other twin γ gated spectra with a gate energy difference of about 11 keV (914-925, 966-977, 1146-1157) are used to establish three new levels.

No transition directly to the ground state was found in previous work. All other states were connected to the 1st excited state. So the excitation energies in this work are higher than the corresponding previously known levels by about 6 keV. The second level at 19.5 keV in the previous decay scheme is not supported by the present work since all three transitions (926, 1034, 1780 keV) connected with this state have been moved to other positions in the new decay scheme in order to satisfy coincidence requirements.

216.2 keV State: The 216 keV and 1052 keV transitions are both coincident with the 1152 keV transition; this was an early problem in this work before it was found that the 1152 kev is a doublet. Otherwise, from the known position of the 1052 keV transition, the 216 keV would be placed at an excitation energy higher than 2 MeV and would necessarily be in coincidence with the 1052-keV transition as well. Since the 216-keV transition is of $M1$ character, the 216.2-keV state has a negative parity and a spin between 1/2 and 5/2. By comparing the systematic trend of higher A Pb nuclei, (see section 5.1), it is likely a $1/2^-$ state. The 216-keV gated spectrum contains four coincidence lines (709, 997, 1111, 1152 keV) which are not in coincidence with each other, hence establishing four new levels. The spins of the four new levels should be equal to or lower than 5/2.

436.5 keV State: The well known $13/2^+$ state of ^{199}Pb is isomeric with a half-life of 12.2 minute. The 425 $M4$ transition decays to the first excited $5/2^-$ state

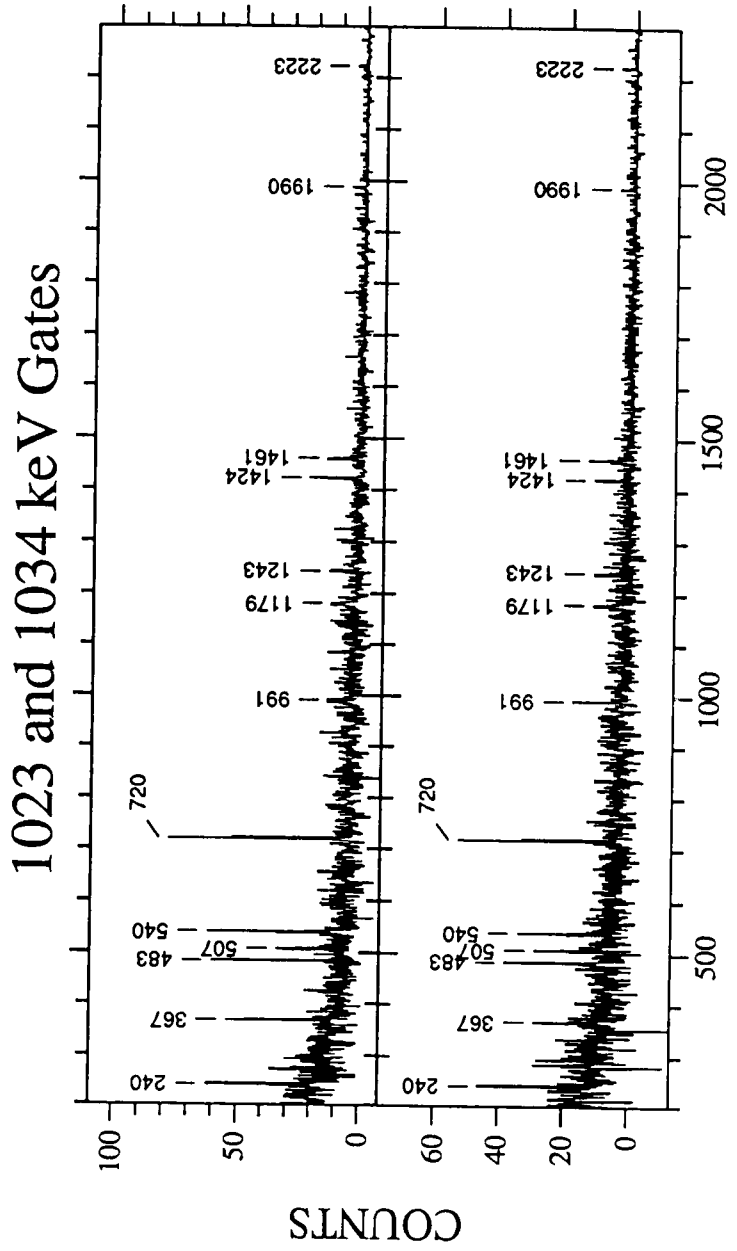

Figure 4.8: γ-ray spectra in coincidence with 1023 keV and 1034 keV γ-ray transitions.

since it is the lowest multipolarity transition possible. The only difference is its excited energy is 6 keV higher than the previous result and more transitions were found which decay to this state.

925.0 keV State: There are three transitions from this state to the three lowest levels. The 709 keV is coincident with 216 keV transition and the 709 and 925 keV transitions both are coincident with a 288 keV transition. The energy difference of the 914 and 925 keV transitions is 11.3 keV, both are *M1+E2* transitions and coincident with 1268 and 1312 keV transitions. So the 925 and 914 keV transitions to the ground and first excited state permits an assignment of $(3/2, 5/2)^-$ for the 925-keV level.

977.2 keV State: The 966 and 977 keV transitions have an energy difference of 11.2 keV and both are coincident with 1048-, 1105- and 1188-keV transitions. The spin and parity of this new level is $(3/2, 5/2)^-$ because the 966- and 977-keV have a mixed E2/M1 multipolarities and decay to the $5/2^-$ first excited state and the $3/2^-$ ground state separately.

1034.0 and 1064.0 keV States: These two levels were from previous work, the 1034 keV transition is moved to a decay from the 1034 keV state. As it decays from $7/2^-$ to the $3/2^-$ ground state, the 1034 keV is a pure E2 transition and it is comfirmed by comparing the α_k value with 425 keV *M4* decay. It was used to normalize the α_K measurement. The 1052 keV transition in the previous work was assigned an *E2(+M1)*. In this work, its experimental conversion coefficient is 0.0034(3) lower than the theoretical value of 0.0048 for an *E2* transition. But a $7/2^+$ state is impossible at such low excitation either as a single particle state or collective state; the 1052 keV is still taken as an *E2* transition. On the basis of its energy the 1064 keV transition was put into the scheme from the 1064 state to the ground state. No coincidence line was found for this weak transition.

1157.6 keV State: This is the last level decaying to the two lowest levels

with the energy difference of 11.1 keV. The 1146- and 1157- keV transitions are both coincident with 416, 596, 868 and 1120 keV transitions. The 1146-keV is an *E2+M1* transition to the $5/2^-$ state. Also, there are possible *E*1 transitions from $9/2^+$ states to the 1157.6 state. Thus, an assignment of $7/2^-$ is given to this state.

1213.5 keV State: A 997-keV transition coincident with 216-keV transition and 288-keV transition coincident with 709- and 925-keV transitions leads to the placement of this new level. The transition between this state and the 216-keV state ($1/2^-$, systematically) implies a spin change of 2 or less, which results in a spin and parity of this state of $(1/2\text{–}5/2)^-$.

1274.1 and 1278.2 keV States: Both 837 keV and 841 keV are *E2* transitions to the $13/2^+$ state. By systematics one is $9/2^+$, the other is a $11/2^+$ state. From the 1274-keV state, two transitions (240, 317 keV) decayed to $7/2^-$ states. These were treated as candidates of *E1* decay since the conversion electron intensities were too weak to be measured in this experiment. So 1274-keV level is assigned as $9/2^+$ and the 1278-keV level is assigned as $11/2^+$ state.

1316.9 keV State: This is a known $(7/2)^-$ state, but the main 1305-keV transition is moved to another place because of coincidence data and a 360-keV transition is added which decays from this state to the 957 keV state.

1326.8 and 1368.5 keV States: These two new levels were added to the scheme because of 1110-keV and 1152-keV transitions coincident with 216-keV transition. Both should be low spin ($\leq 5/2$) negative parity states.

1363.5 keV State: This is the second $13/2^+$ state seen in high spin work [Pau88]. A single 927-keV transition is to the first $13/2^+$ state.

1704.7 keV State: There are one transition (248 keV) in and three transitions (341, 427 and 1268 keV) out of this state. The 248 keV is coincident with three other transitions. the 341-keV is coincident with 927-keV and the 427-keV coincident with the 842 keV transition. This state is placed because of these coincidence

relations. The 1268-keV and 341-keV transitions with admixtures of *E0+M1+E2* decay to the first and second $13/2^+$ states, thus the 1704.7-keV level is another $13/2^+$ state and is considered as the deformed state. This is the most important new level with regard to shape coexistence which was found in this nuclide and will be discussed in the next chapter.

1754.3 keV State: The 480-keV *E0+M1+E2* ($\alpha_{k,exp} \sim 3\alpha_{k,th}(M1)$) transition is strongly coincident with the 837 keV which decays from a $9/2^+$ state. Thus, the spin and parity of this state is $9/2^+$. Four transitions (406, 597, 721 and 797 keV) decayed to $(7/2, 9/2)^-$ states and should be *E1* transitions which were too weak to be confirmed in this experiment. The 391 keV is a doublet, so the uncertainty of conversion coefficient is big ($\alpha_k = .05(2)$). In the spectroscopic analysis, this transition is set as an *E2(+M1)* transition because theoretical value for *E2* is 0.03. Since it decayed to the second $13/2^+$ state (1363.2 keV), this transition should be a pure *E2* decay from the difference in spins of two. It is just tenable in the experimental uncertainty.

Spins of some positive parity states: There are *M1(+E2)* transitions from the 1811.2 keV state to $9/2^+$ and $11/2^+$ states, thus, it should be $(9/2, 11/2)^+$ itself. The 1517-keV state is connected to 1811-keV state by *M1* transition (294 keV), and hence the 1517-keV level has a positive parity and spin of $(7/2 \rightarrow 13/2)$. The 1505 keV transition decays from 1517 keV level to the $5/2^-$ state. The experimental α_K is consistant only with an *E*1 assignment. So the 1517-keV level is a $7/2^+$ state and the 1811-keV level is a $9/2^+$ state.

Other New Levels: Most new levels are connected with more than one transition and confirmed by coincidence data. Several new states, which are connected with only one transition, were added to the scheme because they are supported by clear coincidence evidence. Since a 2223-keV transition is coincident with both 1023- and 1034-keV transitions, a new level was added at 3257 keV. Also since a 1312-keV

transition was coincident with both 913- and 925-keV transitions a level was added at 2237.2 keV and since the 1424-keV transition was coincident with 238-, 294-, 533-, 777-, 854-, 1374-keV and some strong cascade transitions (837, 841-keV), a level was added at 3235.5 keV.

4.2 ^{193}Bi β-decay and ^{193}Pb Level Scheme

4.2.1 Spectra Analysis of ^{193}Bi β-decay

As was discussed in the last chapter, the cross-section of the $^{185}Re(^{16}O, 8n)$ ^{193}Bi reaction channel used in this experiment is small. In the singles spectra, the γ-rays from ^{193}Bi, ^{193}Pb and ^{193}Tl β-decays are mixed together. The strongest, the 365-keV γ-line, from the first excited state to the ground state of ^{193}Tl, is at least 20 times stronger than any other γ-ray in the singles spectrum. Thus, it was necessary to rely on coincidence spectra to assign transitions and accidental coincidences had to be appropriately recognized.

The cleaner γ and e^- spectra for ^{193}Bi decay were obtained by gating on the Pb X_{K_α}-line as shown in Figures 4.9 and 4.10. The accidental 365-keV line is still among the biggest coincidence peaks. Because of the complexity of γ and electron spectra, only the transitions which have been placed in the decay scheme are listed in the Table 4.3. Most γ-ray intensities are determined by gated coincidence spectra. The relative intensity is normalized to the 175 keV γ-line which is the strongest line from the ^{193}Bi decay and decays to the ground state directly. The γ-ray transitions in coincidence with known ^{193}Bi lines are shown in Table 4.4. Because there are accidental coincidence peaks from some stronger transitions, every gated coincidence spectrum was compared with the total projected spectrum; only the peaks having a significantly bigger ratio than that of the 366-keV transition were considered as the real coincidence peaks. The strong coincidence peaks of 515 keV

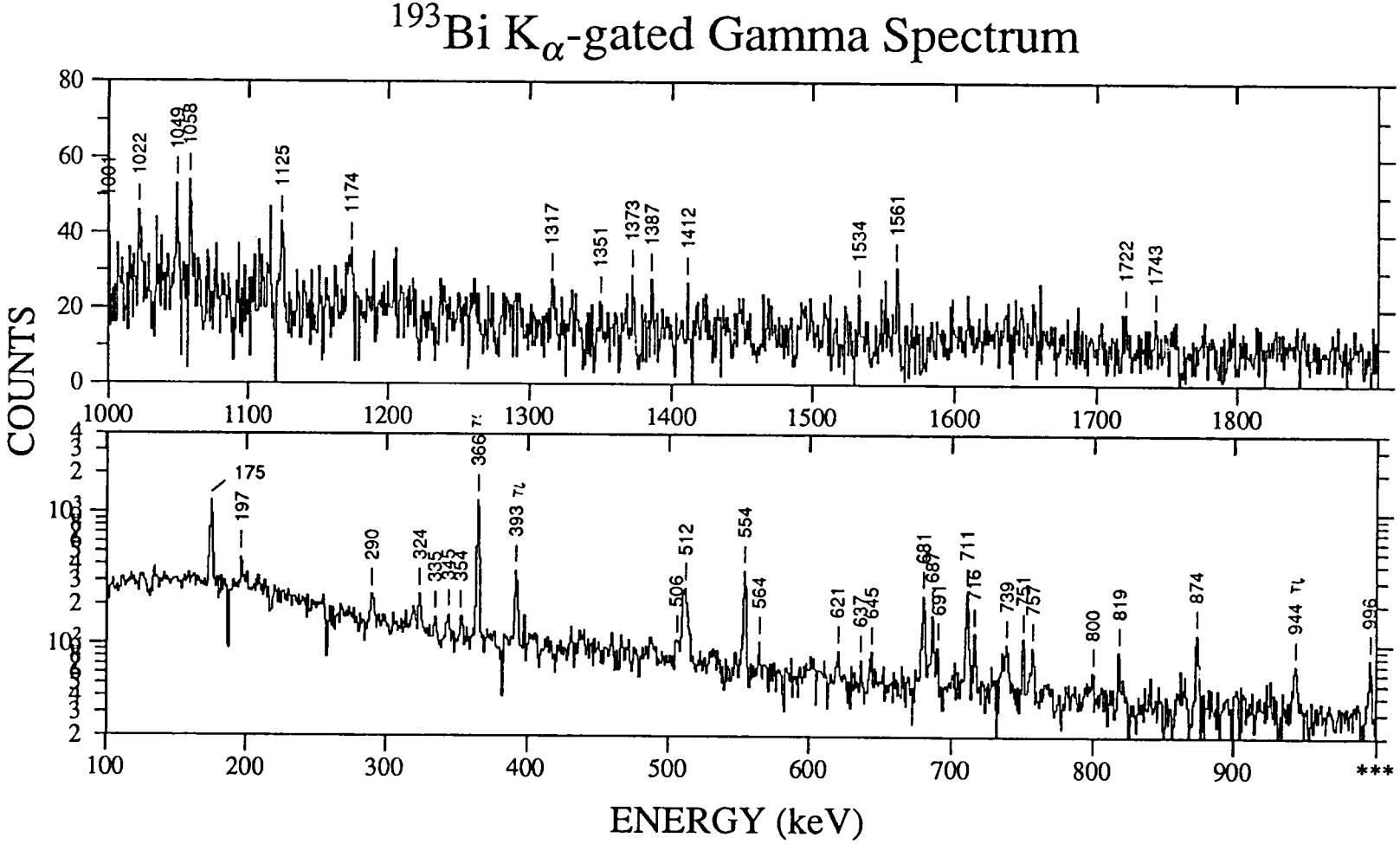

Figure 4.9: The ^{193}Bi Gamma spectrum obtained by gating on the $K_{\alpha 1}$ X-ray from Pb.

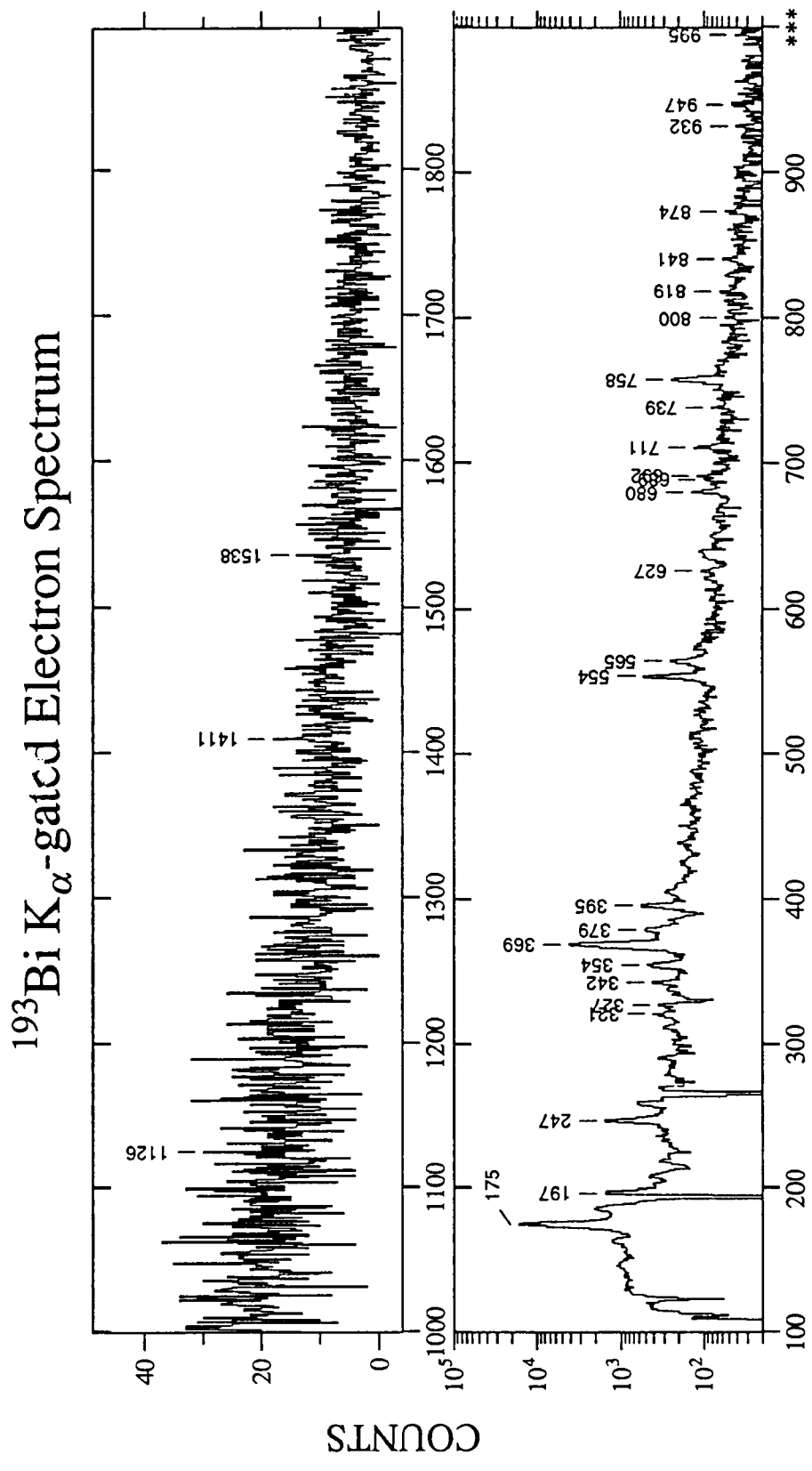

Figure 4.10: The ^{193}Bi electron spectrum obtained by gating on the $K\alpha 1$ X-ray from Pb.

Table 4.3 Transitions from ^{193}Bi β^+/ε Deccay

Transition Energy (keV)	γ-ray Intensity (Relative)	Assignment in ^{193}Pb Initial → Final			α_k	Multi-polarity
174.7(2)	100.	175 →	0		0.90(5)	M1+E2
194.6(5)		1195 →	1000	+X		
196.6(2)	13.(1)	925 →	729		0.5(1)[a]	M1+E2
265.5(5)		1023 →	757	+X		
289.6(2)	13.(1)	1000 →	711	+X		
311.7(4)	4.9(5)	1023 →	711	+X		
319.6(3)	9.(1)	1000 →	681	+X		
335.4(4)	1.0(5)[a]	1197 →	862			
342.0(4)	< 1.[a]	1023 →	681	+X	> 1.1[a]	E0+M1+E2
343.8(3)	4.(1)[a]	1055 →	711	+X		
354.2(2)	9.(1)	354 →	0		0.20(5)[a]	M1
380.6(4)	3.(1)[a]	1091 →	711	+X		
437.5(5)		1195 →	757	+X		
505.8(4)	2.(1)	1368 →	862		0.05(2)[a]	M1+E2
514.2(4)	8.(2)[a]	1195 →	681	+X		
554.0(2)	54.(4)	729 →	175		0.05(1)	M1+E2
557.5(6)		1606 →	1049			
564.5(4)	4.8(8)	739 →	175		0.18(4)[a]	E0+M1+E2
576.3(5)		1333 →	757	+X		
620.0(4)	10.(3)[a]	1348 →	729			
620.8(4)	8.(3)[a]	975 →	354			
622.6(4)	3.(1)[a]	1333 →	711	+X		
636.7(4)	10.(3)[a]	1365 →	729			
644.0(4)	5.(1)[a]	819 →	175			
680.8(2)	82.(5)	681 →	0	+X	.013(2)[a]	E2
687.5(2)	27.(3)	862 →	175			
710.8(2)	74.(5)	711 →	0	+X	.013(2)	E2
738.7(3)	20.(4)	739 →	0			
750.4(2)	20.(2)	925 →	175			
757.4(3)	20.(5)[a]	757 →	0	+X	.13(3)[a]	E0+M1+E2

[a] From gated coincidence spectra.

+X: Levels set up on the 1st $13/2^+$ state which excitation energy is about 100 keV.

Table 4.3 (Continued)

Transition Energy (keV)	γ-ray Intensity (Relative)	Assignment in ^{193}Pb Initial → Final		α_k	Multi-polarity
800.0(4)	6.(1)	975 → 175			
818.7(2)	30.(4)	819 → 0			
821.5(5)	5.(1)[a]	996 → 175			
861.9(5)		862 → 0			
874.0(2)	43.(4)	1049 → 175			
995.9(4)	15.(5)	996 → 0			
997.5(4)	5.(2)[a]	1172 → 175			
1000.3(6)		1000 → 0	+X		
1022.2(5)	2.(1)[a]	1198 → 175			
1022.7(2)	20.(3)	1023 → 0	+X		
1049.1(2)	18.(2)	1049 → 0			
1115.8(2)	14.(1)	1291 → 175			
1125.5(2)	16.(1)	1300 → 175			
1142.1(4)	8.(2)[a]	1317 → 175			
1173.7(2)	9.(1)	1348 → 175			
1190.5(3)	3.(1)[a]	1365 → 175			
1217.3(4)	3.(1)[a]	1392 → 175			
1259.0(4)	3.(1)[a]	1434 → 175			
1316.6(4)		1317 → 0	?		
1358.5(4)	2.(1)[a]	1533 → 175			
1411.8(4)	3.(1)[a]	1587 → 175			
1431.4(5)	2.(1)[a]	1606 → 175			
1469.6(4)	3.(1)[a]	1644 → 175			
1534.1(6)		1533 → 0	?		
1561.4(4)	3.(1)[a]	1736 → 175			
1605.2(6)	> 2.[a]	2334 → 729			
1720.9(5)	2.(1)[a]	1896 → 175			
1979.2(5)	2.5(5)	2905 → 925			
2029.2(5)	2.(1)[a]	2204 → 175			
2351.0(5)	2.(1)[a]	2526 → 175			
2656.2(6)	2.(1)[a]	2831 → 175			

? Unconfirmed transition position

+X: Levels set up on the 1st $13/2^+$ state which excitation energy is about 100 keV.

Table 4.4. Coincidence Relationship of ^{193}Pb γ-Decay

Energy	Coinsidence Line (keV) (S: Strong, W: Weak)
175	197 319 385 459 467 506 554S 564 596 620 630W 637 644 687S 750S 787 800 821 874S 998 1022 1116 1126S 1142 1174 1190 1217 1259 1358 1412 1431 1470 1561 1605 1721 2029 2351 2656
197	175S 554S 1377 1979 2107
290	195 711S
320	195 681S
354	621S
506	175 515 687
514	509 681 736 944
554	175S 197S 620 637 1099
564	175 637 648
620	354 553
644	174 736W
681	320S 342 514 1288
687	174S 335 506
711	194 290 312 344 381 623 783
739	
750	175S 320
757	265W 433 437 576 584 931 945 1075
800	175
819	
821	175
866	
874	175S
996	
1000	
1023	
1049	
1116	175
1125	175
1142	175
1174	175
1190	
1605	175 554

in the 506-keV gated spectrum and 509 keV in the 514-keV gated spectrum come from the Doppler shifted annihilation radiation for which the energy sum of two photons is about 1022 keV.

From a high spin work of ^{193}Tl [New74], the 716-keV transition is from $13/2^- \rightarrow 9/2^-$ state and 755-keV is from $15/2^- \rightarrow 11/2^-$ state. Conversion coefficients for the mass-193 experiment were normalized by the theoretical values of these two pure $E2$ transitions. The α_K values of three transitions (175, 554 and 711 keV), which have relative intensities larger than 50, were obtained from singles spectra. Others were deduced from coincidence spectra by comparing with the three mentioned transitions. Three $E0 + M1 + E2$ transitions were found from ^{193}Bi decay. In Figure 4.11, no conversion coefficient was known for any coincidence peaks; if the 320-keV line were a pure $E2$ decay then the α_K value of 342-keV would be at least 5 times the theoretical value of a $M1$ transition. In Figure 4.12, portions of the γ and e^- spectra containing the 554-keV and 564-keV transitions, both of which decay to the 175-keV state, are compared. The 554-keV transition is $M1+E2$ decay ($\alpha_K = 0.05(1)$); the e^-/γ ratios from this spectrum results in an α_K value of 0.18(4) for the 564-keV transition, which is about 3 times the theoretical value of $M1$ decay. The 681-, 711- and 757-keV transitions decay to the first $13/2^+$ state. The 711-keV was found to be an $E2$ from the singles data and since the 681-keV transition has the same e^-/γ ratio in the gated spectra (Fig. 4.12), it also must be an E2 transition. However, the α_K obtained from these coincidence spectra for the 757-keV line is about 10 times as large and 4.5 times the theoretical value for an M1 transition. The very-converted nature of 342-, 564- and 757-keV transitions are interpreted as being due to $E0$ components to their multipolarities.

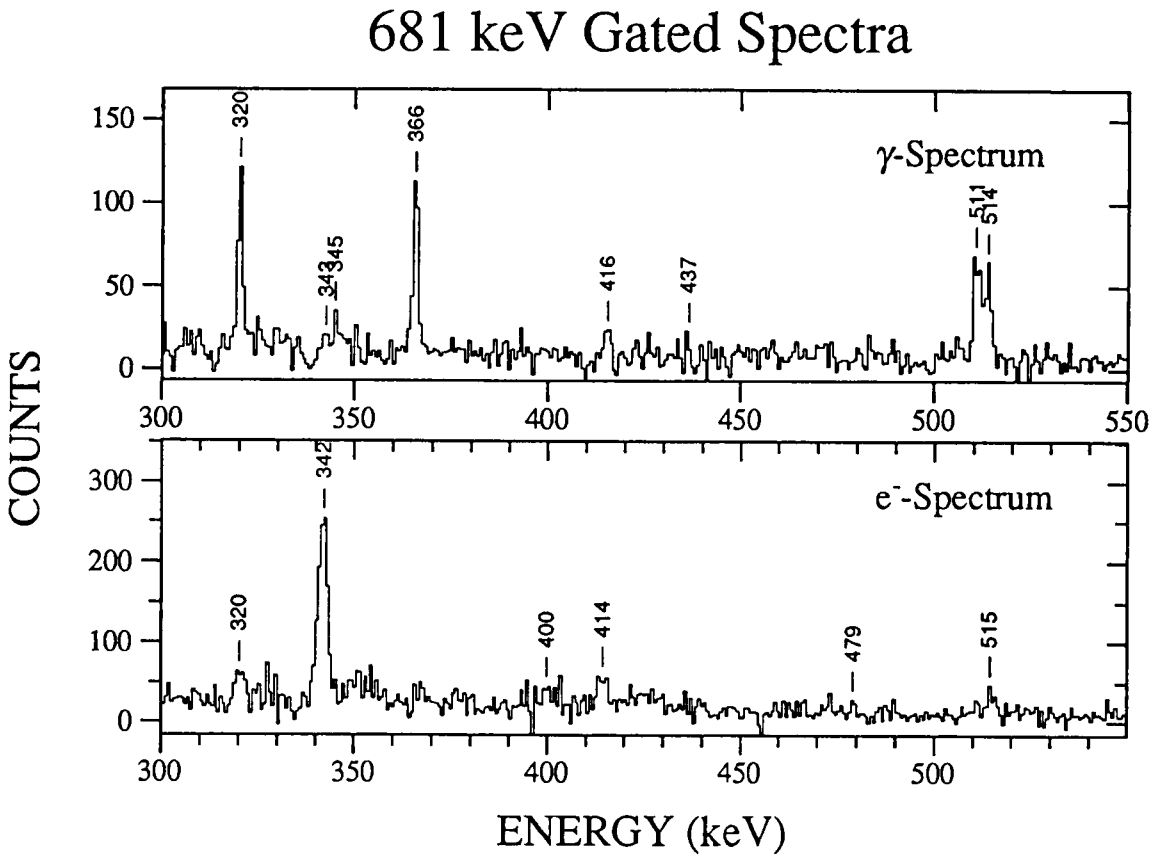

Figure 4.11: γ and electron spectra in coincidence with 681-keV γ transition

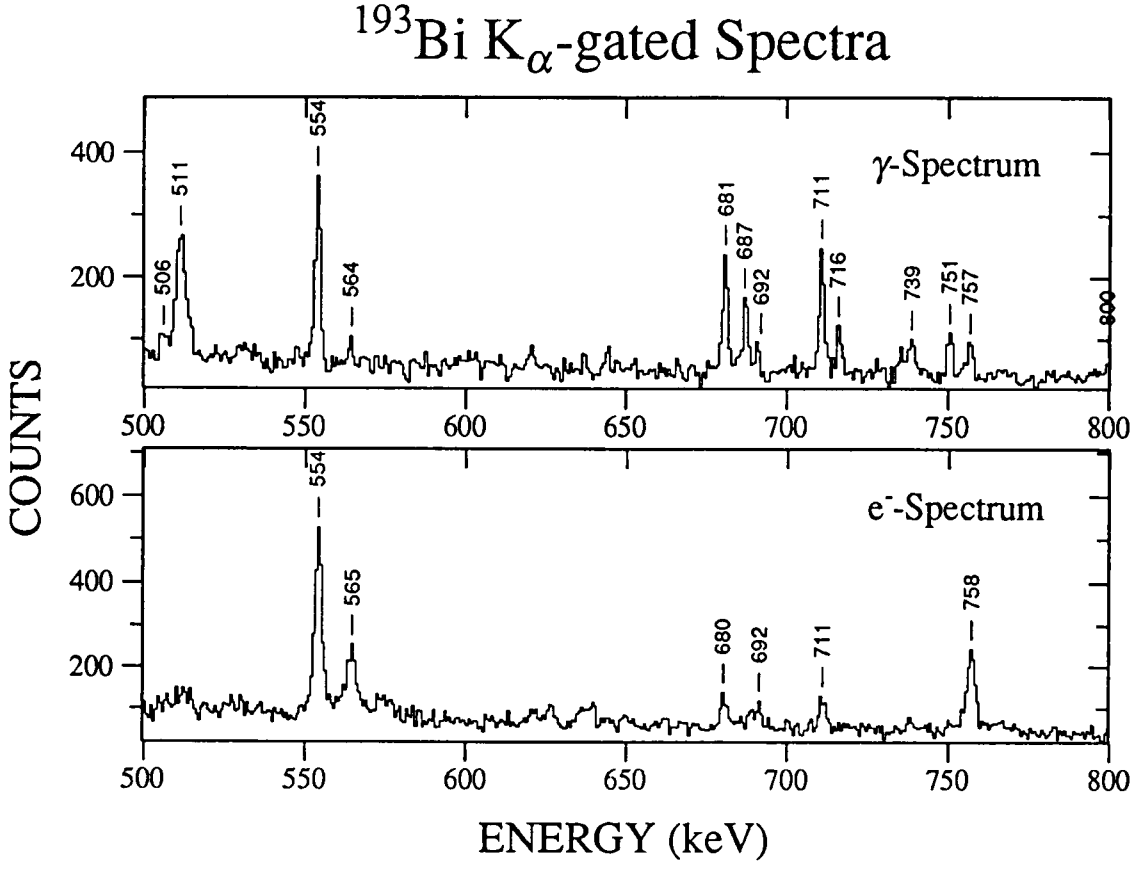

Figure 4.12: Pb $K_{\alpha 1}$ X-rays gated γ and electron spectra for the transition energy range 500-800 keV

4.2.2 Level Scheme of ^{193}Pb

The scheme for the decay of ^{193g}Bi to levels in ^{193}Pb (Fig. 4.13 and 4.14) is based partially on an early work of this group [Bin90b] and depends strongly on the present coincidence data. Transition intensities and energy sums were also considered in placement of levels. Strong γ-rays observed in the Pb $K_{\alpha 1}$-gated spectrum and fitted by energies were placed in the scheme feeding directly to the ground state. Two other γ-rays (1317, 1534 keV) shown in the $K_{\alpha 1}$ gated spectrum and fitted by energies were put into the scheme as possible transitions to the ground state. The excitation energies of states were determined by the same fitting method as used in the last section. In all, 41 excited states have been located and 61 transitions have been assigned to the level scheme.

The ground-state spin and parity of ^{193}Pb has been assigned [Shi90] as $3/2^-$ from systematics of odd-mass Pb nuclei and from the α-decay of ^{197}Po. The 5.8 min isomer of ^{193}Pb has been assigned [Shi90] as $13/2^+$ from the same systematics of odd-mass Pb isotopes, the α-decay of the ^{197}Po isomeric state and consistent with population of high-spin levels in ^{193}Tl from ^{193}Pb β^+/ε decay. No transition was found between the levels placed on the ground state and on the isomer in the previous and present works. The excitation energy of the isomer of about 100 keV is estimated from extrapolation of energy differences of $13/2^+$ and $3/2^-$ states in ^{199}Pb (425 keV), ^{197}Pb (319 keV) and ^{195}Pb (203 keV).

States set up on the ground state

174.7 keV State: The 174.7-keV *M1+E2* transition is the strongest in the ^{193}Bi decay and coincident with most other transitions (Fig. 4.15). The parity of this state is negative and spin is 1/2→5/2. From systematics [Gri91] it is the $5/2^-$ state. This assignment is supported by the fact that the ground state of ^{193}Bi is $9/2^-$; β^+/ec transitions from ^{193}Pb would populate $9/2^-$ states by allowed β-decay

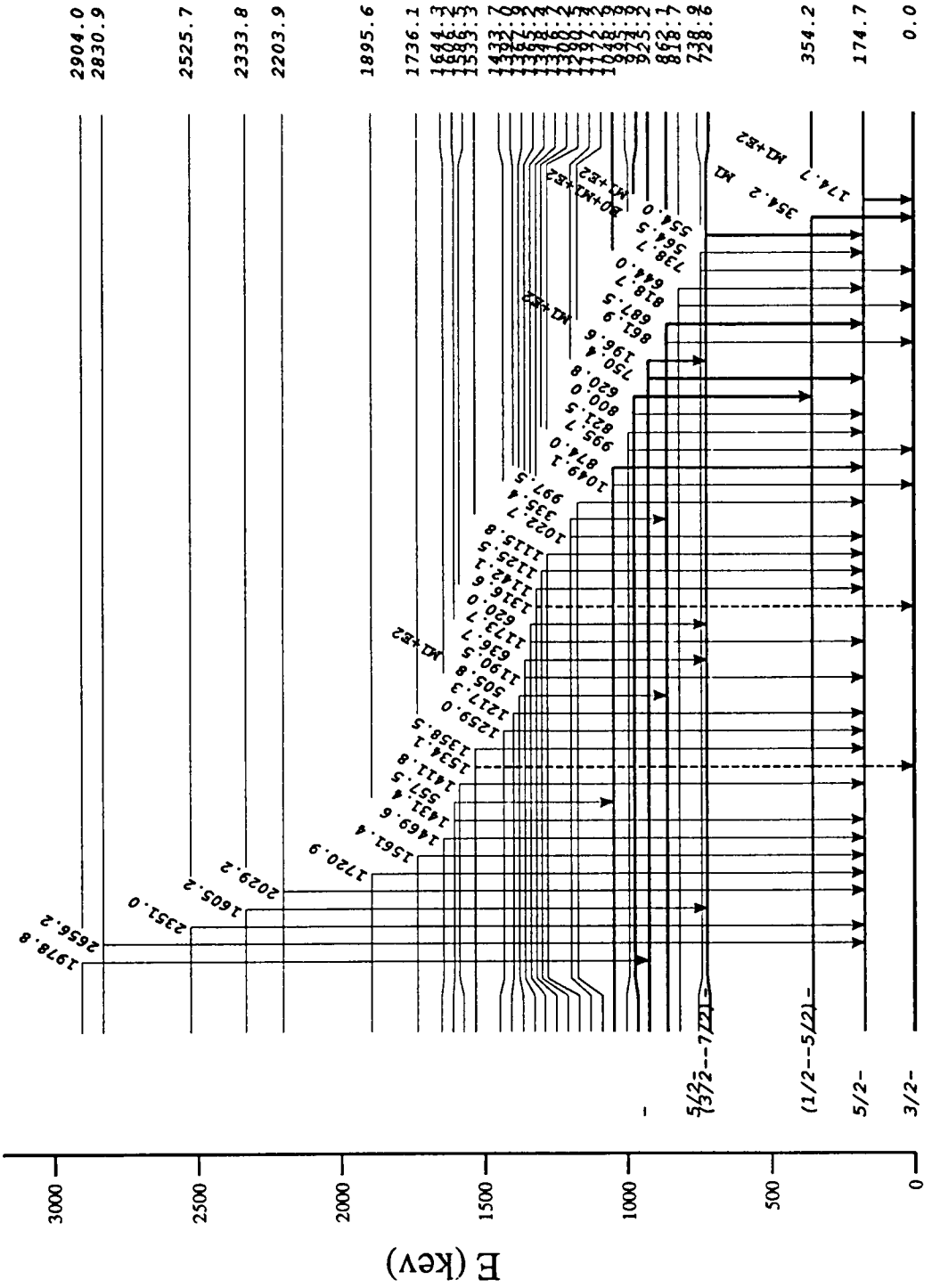

Figure 4.13: Decay scheme set up on the ground state of ^{193}Pb

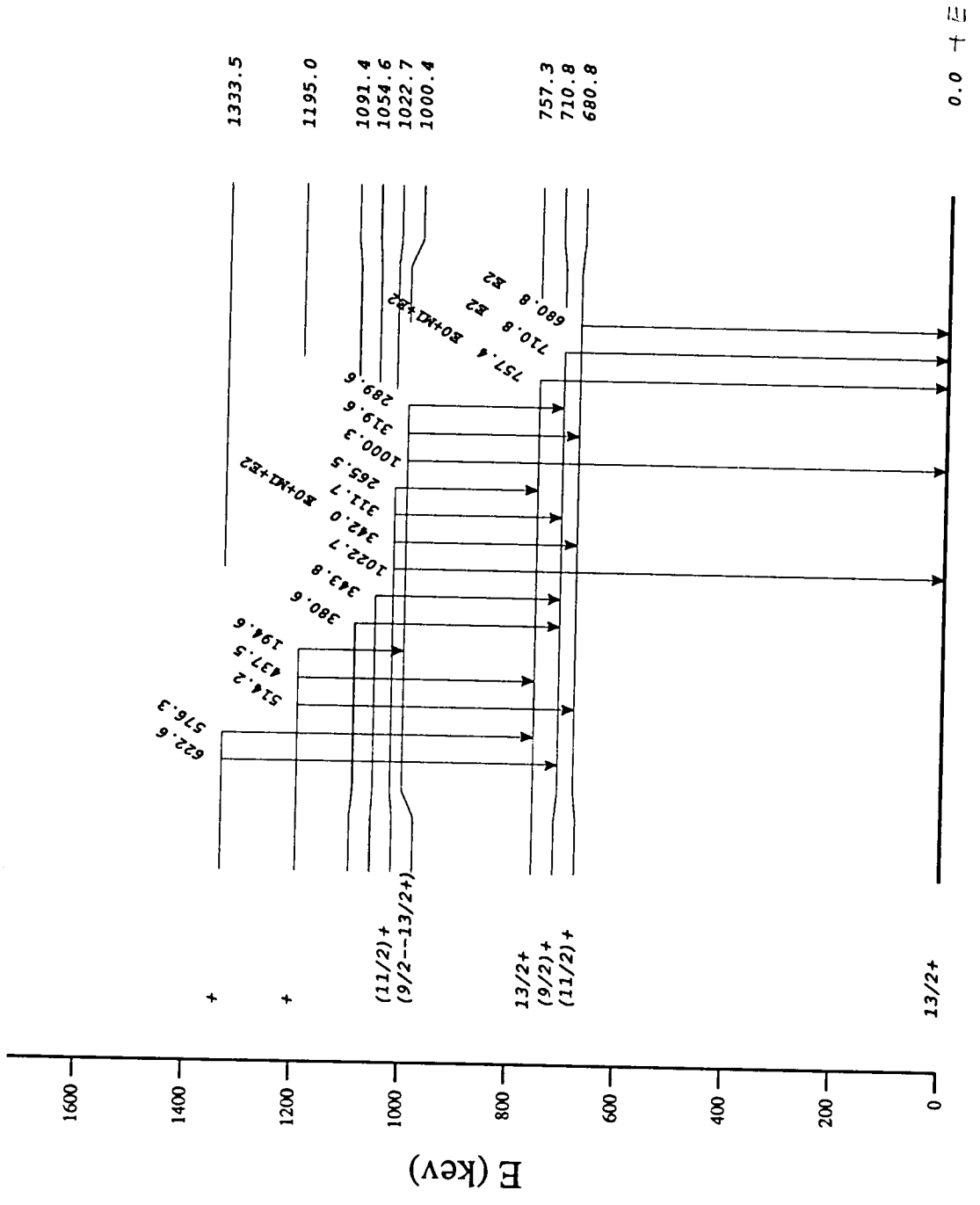

Figure 4.14: Decay scheme set up on the isomer state of ^{193}Pb. The real excitation energies of states should be about 100 keV larger.

and thus, the $5/2^-$ state becomes the preferred final state in the γ decay cascade (see Fig. 4.15).

354.2 keV State: The $M1$ character of the 354-keV transition determined the parity and spin of this state to be negative and $1/2 \rightarrow 5/2$. From systematics [Gri91] it is expected to be the $1/2^-$ state.

738.9 keV State: The 174.7-keV transition is coincident with 564.5-keV *E0+M1+E2* transition. Thus, the parity-spin of this state is $5/2^-$.

Other States: Most states are located by a single transition in coincidence with the 174.7-keV transition (Fig. 4.15). The possibility is large that these states have negative parity and spin values higher than or about equal to 5/2. Coincident peaks in the 506-, 1605- and 1979-keV gated spectra were used to add the 1368.0-, 2333.8- and 2904.0-keV states to the decay scheme.

States set up on the isomeric state

680.8 and 710.8 keV States: Both depopulating transitions (680.8, 710.8 keV) are $E2$ transitions which connect to the isomeric ($13/2^+$) state and are coincident with some decays from upper states. The $13/2^+$ isomer is interpreted as the $i_{13/2}$ neutron coupled to the 0^+ ground state of the core; thus, excitation of the core to the 2^+ state would result is five states from $9/2^+$ to $17/2^+$ in ^{193}Pb. These excited states would decay predominantly by E2 transitions and hence these two states are good candidates. They are populated from β^+/ε-decay of Bi $9/2^-$ state, and hence, the two strong transitions should come from the lower part of the $9/2 \rightarrow 15/2$ spin range. Systematics suggests that the 680.8 keV state is the $11/2^+$ state and the 710.8-keV state is $9/2^+$.

757.3 keV State: There are three transitions (265-, 437- and 576-keV) in and one transition out of this state. The 757.4-keV $E0 + M1 + E2$ transition is coincident with the other three transitions. The very-converted character of 757-

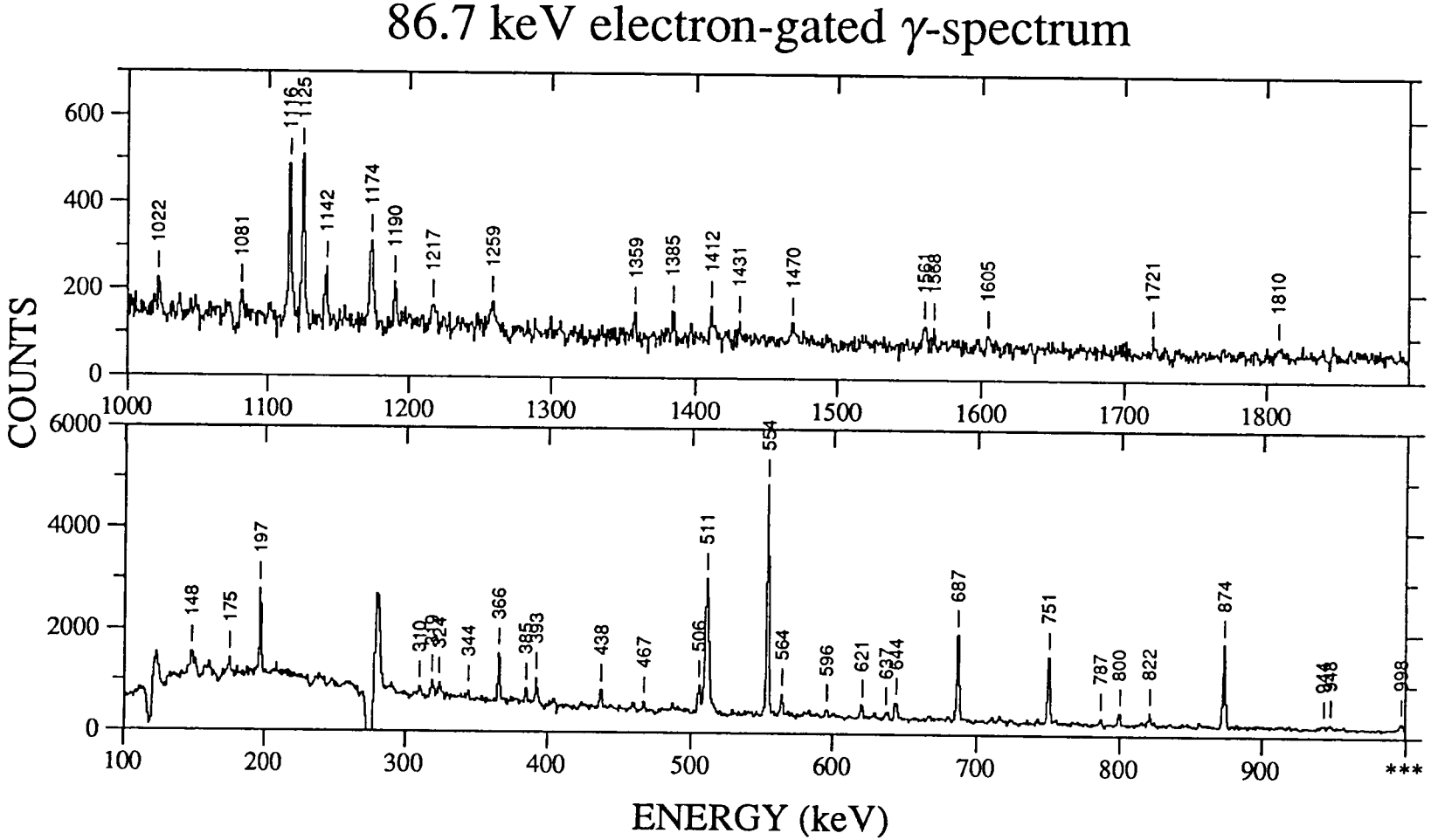

Figure 4.15: Gamma spectrum obtained by gating on the K-shell conversition electron from the 174.7-keV transition.

keV decay indicates it is a deformed $13/2^+$ state.

1000.4 keV State: Three transitions (290-, 320- and 1000-keV) decay to the three positive parity states (9/2, 11/2 and 13/2). It is a possible $(9/2 \rightarrow 13/2)^+$ state. The 290- and 320-keV decays are coincident with a 195-keV transition which decays to this state from the higher level.

1022.7 keV State: Four transitions decay to the first four positive parity states. The 342-keV *E0+M1+E2* transition decays to the $11/2^+$ state, which makes the spin-parity of this state to be $11/2^+$.

1054.6 and 1091.4 keV States: The 343.8- and 380.6-keV transitions are coincident with the 710.8-keV line in a clear manner, thus resulting in the addition of these two states to the decay scheme.

1195.0 and 1333.5 keV States: There are three transitions (195-, 437- and 514-keV) from the 1195-keV state and two transitions (576- and 623-keV) from the 1333-keV state. Both are positive parity states.

4.3 ^{193}Pb β-decay and ^{193}Tl Level Scheme

4.3.1 Spectra analysis of ^{193}Pb β-decay

The purpose of the mass-193 experiment was to study the β-decay of ^{193}Bi, but in practice the intensity of ^{193}Pb β-decay was stronger than ^{193}Bi decay. As the by-product of this experiment, the single γ and e spectra and γ-γ, γ-e, X-γ and X-e coincidence spectra from decay of ^{193}Pb were analysed also. Due to the large number of decay lines, it is difficult to identify the transitions from ^{193}Pb β^+/ε decay by multiscaled singles spectra. The coincident characteristic X-rays and other coincident peaks were used to do it.

The coincident characteristic X-rays of Pb, Tl and Hg obtained by setting gates on the known decay lines are compared with the X-rays in the total projection

in Figure 4.16. The 75.0 keV $X_{K_{\alpha I}}$ line of Pb was used in the last section as a gate energy to get the γ and e^- spectra from ^{193}Bi decay. The $X_{K_{\alpha I}}$ line of Tl at 72.9 keV is mixed with $X_{K_{\alpha II+III}}$ lines of Pb at 72.5 keV. Because $X_{K_{\alpha II+III}}$ lines and $X_{K_{\alpha I}}$ line of Pb have the same coincidence spectra of ^{193}Bi decay, the $X_{K_{\alpha I}}$ line of Tl gated γ and e^- spectra were extracted by subtracting a portion of the $X_{K_{\alpha I}}$ of Pb gated spectrum. The ratio factor was determined by checking a few strong transitions (at 175, 554 681 and 711 keV) from ^{193}Bi decay. It was a little over subtracted to make sure the subtraction of all transitions of ^{193}Bi decay was compelete. The fixed ^{193}Tl X_{K_α} gated γ and electron spectra are shown in Figures 4.17 and 4.18. There are some strong transitions from ^{193}Tl decay shown in the spectra because the high energy tail of Hg $X_{K_{\alpha I}}$ peak is included in the gate. As ^{193}Pb decay, only the transitions having been placed in the decay scheme have γ-ray and internal conversion data are listed in Table 4.5 and coincidence relationships in Table 4.6.

The strongest γ line at 365.5 keV comes from the isomeric state of ^{193}Tl which is a few keV higher than the 365.5 keV state and directly separated from mass separator. The second strongest γ transition at 392.5 keV which decays to the isomeric state was used to normalize the relative intensities of other γ transitions. The α_K values are normalized by the pure $E2$ transition at 716 keV. Several transitions with α_K lying between the theoretical values of E1 and E2 transitions are marked with question.

4.3.2 Level Scheme of ^{193}Tl

The decay scheme of ^{193}Pb is also partially based on the early work of this group [Bin90a] and is primarily constructed by the coincidence spectra. No transition was found between the levels connected with the ground state and the levels connected with the $9/2^-$ isomer. The levels connected with the ground state

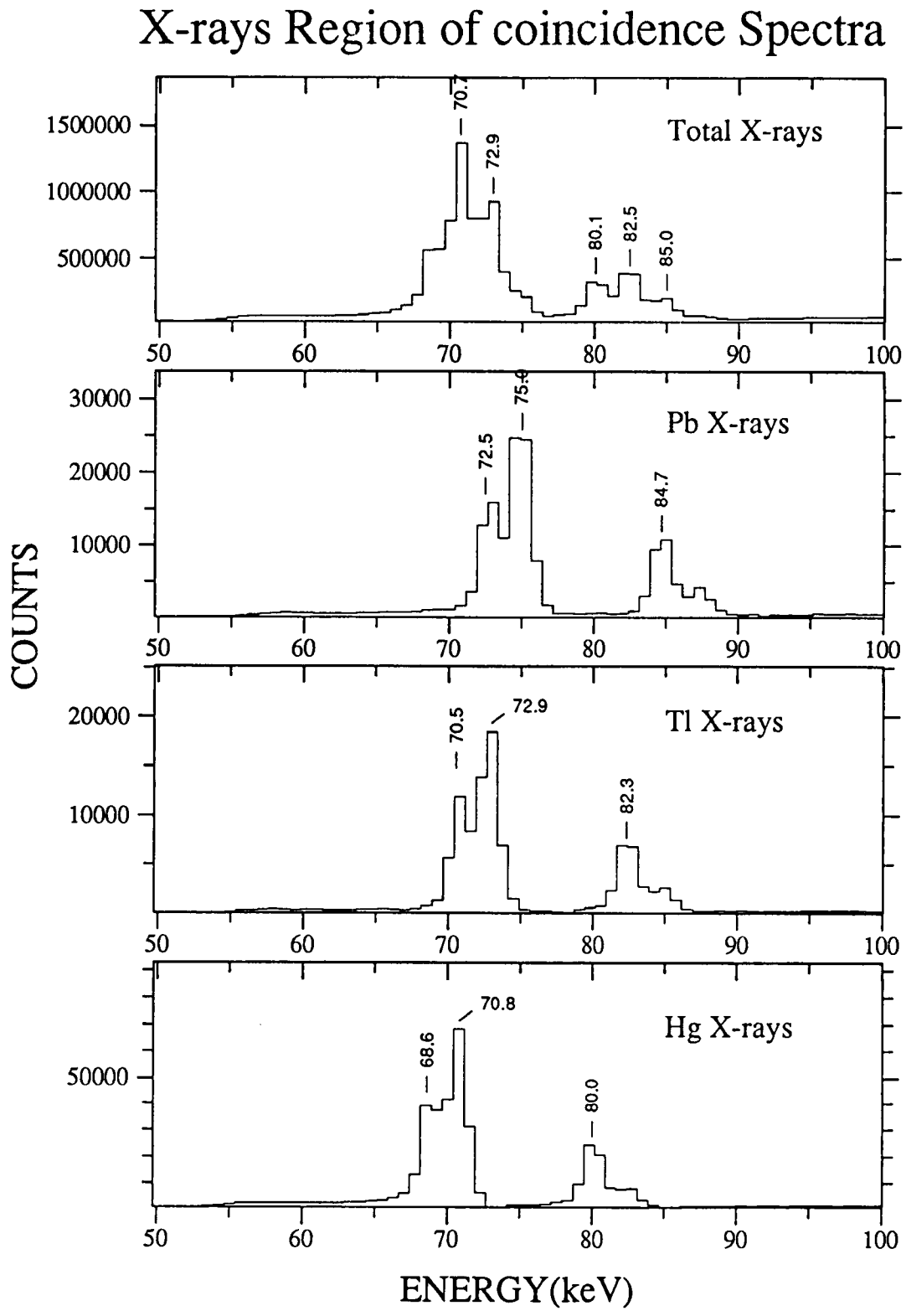

Figure 4.16: Characteristic X-rays of Pb, Tl, Hg and sum X-rays in the experiment.

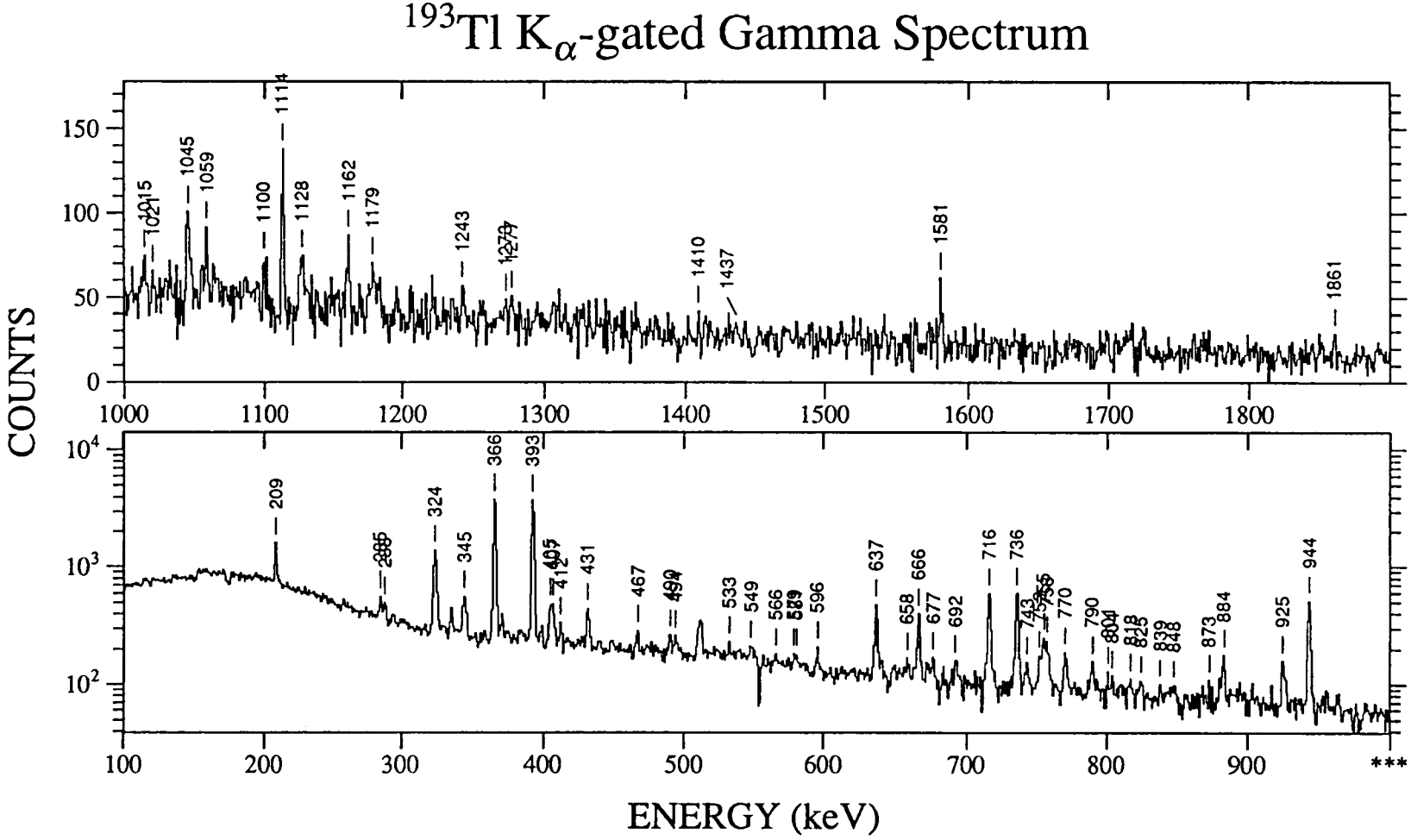

Figure 4.17: The γ spectrum obtained by a gate on $K\alpha 1$ X-rays from ^{193}Tl.

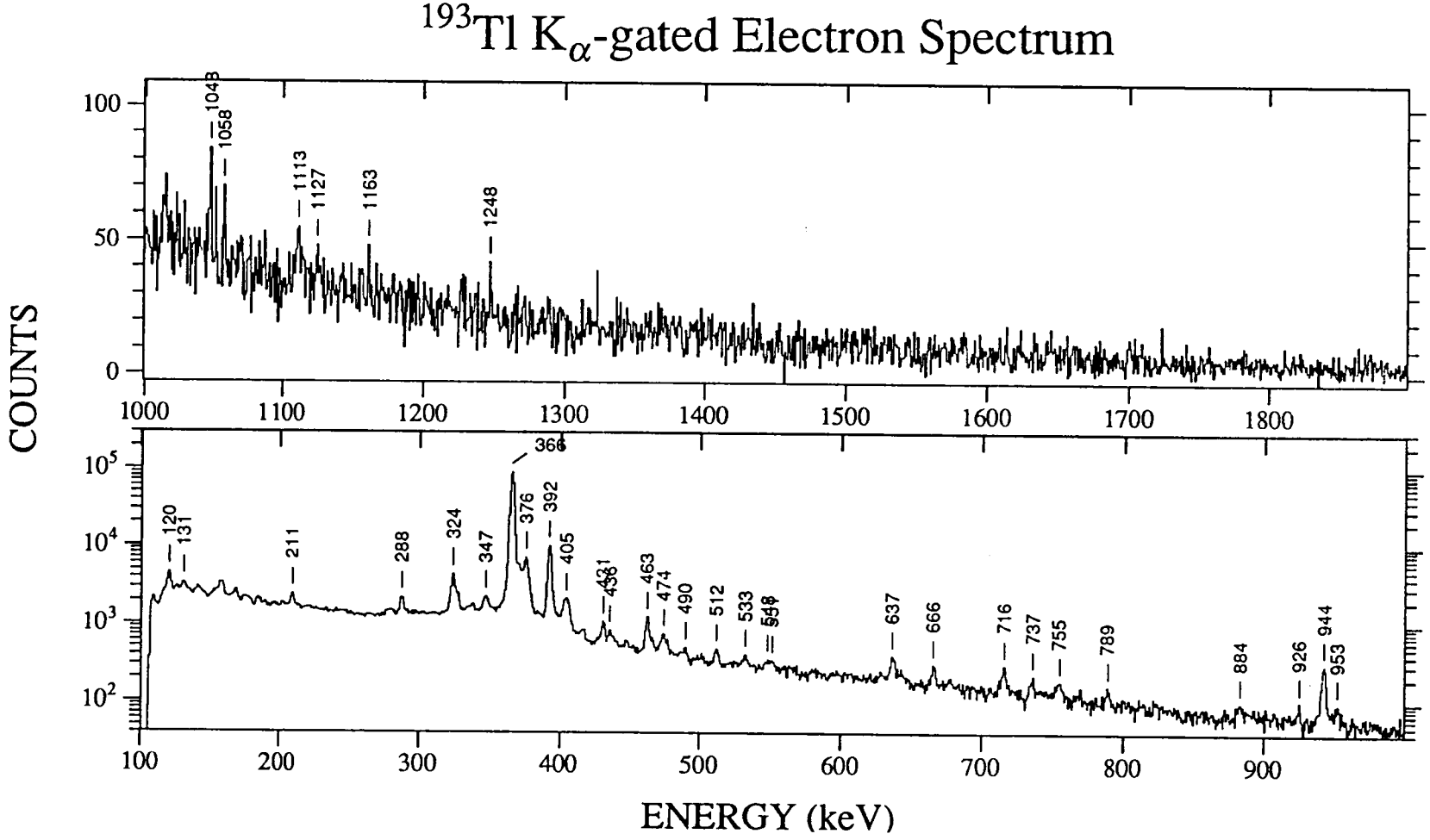

Figure 4.18: The electron spectrum in coincidence with $K\alpha I$ X-rays from ^{193}Tl. The energies shown in the figure are transition energies.

Table 4.5a γ-ray(^{193}Tl) from ^{193}Pb β^+/ε Decay

(Transitions decaying from the levels which are set up on the ground state)

Transition Energy (keV)	γ-ray Intensity (Relative)	Assignment in ^{193}Tl Initial→Final	α_k	Multi-polarity
365.5(2)	2360.	366→0	0.066(4)	E2+M1
395.1(4)	1.2[a]	1644→1249		
404.6(4)	6.7(5)	770→366		
596.1(4)		2123→1527		
756.9(4)	6.(1)[a]	1527→770		
770.1(3)	5.(1)[a]	770→0		
873.6(4)	8.(2)[a]	1644→770		
883.4(3)	7.(1)	1249→366	0.005(1)	E1?
895.2(3)	2.1(2)	2144→1249		
953.7(3)	0.8(2)[a]	2203→1249		
1101.8(5)	1.0(5)[a]	1467→366		
1161.8(3)	4.(1)[a]	1527→366		
1322.1(4)	1.7(4)	1688→366		
1409.0(4)	2.1(2)	1774→366		
1643.3(4)	2.3(3)	1643→0 ?		

[a]) From gated coincidence spectra.

[b]) Doublet peaks.

Table 4.5b γ-ray(^{193}Tl) from ^{193}Pb β^+/ε Decay

(Transitions from the levels set up on the $9/2^-$ isomer state)

Transition Energy (keV)	γ-ray Intensity (Relative)	Assignment in ^{193}Tl[c] Initial→Final	α_k	Multi-polarity
288.1(2)	2.8(3)	1291→1003		
321.8(5)	0.7(2)[a]	1835→1513		
323.8(3)	18.(3)[a]	1082→758	0.19(4)[a]	M1+E2
370.6(3)	11.(3)[a]	1661→1291		
384.4(4)	3.1(5)	2046→1661		
392.5(2)	(100.)	758→366	0.10(1)	M1+E2
406.4(4)	5.3(4)	1901→1494		
412.3(2)	2.6(4)	1494→1082		
416.6(3)	1.1(2)	1930→1513		
427.1(4)	1.1(3)[a]	1921→1494		
431.2(2)	8.9(7)	1513→1082	0.08(2)[a]	M1+E2
466.8(2)	3.1(2)	1961→1494		
490.3(3)	3.0(6)	1493→1003		
512.6(4)	9.(2)[a]	1822→1309	0.03(1)[a]	E2+M1
532.7(3)	1.7(2)	1291→758	0.07(1)	M1
548.5(4)	2.6(3)	1973→1424	0.03(1)	E2+M1
551.4(4)	1.9(2)	1309→758	0.04(1)	M1+E2
579.4(4)	1.7(5)	1661→1082		
580.8(3)	8.(1)	1872→1291		
637.3(2)	31.[b]	1003→366		
658.3(4)	2.6(3)	1661→1003		
666.2(2)	13.(1)	1424→758	0.015(2)	E2+M1
690.4(5)	1.5(5)[a]	2000→1309		
716.4(2)	31.(2)	1082→366	(0.0097)	E2
736.0(2)	22.(2)	1494→758	0.0067(8)	E1?
737.2(3)	2.1(6)[a]	2046→1309		
752.8(4)	5.(1)[a]	1835→1082		
755.1(3)	10.5(11)	1513→758	(0.0087)	E2
755.4(5)	2.7(7)[a]	2046→1291		
757.6(3)	6.(1)[a]	2067→1309		
769.5(5)	7.4(9)[a]	2193→1424?		
789.8(2)	4.(1)[a]	2099→1309		
800.3(4)	1.1(2)[a]	2313→1513		

c) Levels are set up on the isomer state. The excitation energy should add a small value about 10 keV.

Table 4.5b: Continued

Transition Energy (keV)	γ-ray Intensity (Relative)	Assignment in ^{193}Tl[c] Initial→Final	α_k	Multi-polarity
803.9(3)	1.9(2)[a]	2113→1309		
818.7(4)	2.0(5)[a]	1901→1082		
824.4(3)	2.1(2)	2134→1309		
839.2(4)	2.0(2)	1921→1082	0.006(1)	E2?, E1?
847.7(4)	2.2(2)	1930→1082		
878.9(4)	0.8(1)	1961→1082		
883.6(3)	0.9(3)[a]	2193→1309?		
890.9(4)	1.2(2)[a]	1973→1082		
903.0(4)	2.7(2)	1661→758		
925.2(2)	6.7(4)	1291→366	0.0043(4)	E1?
944.0(2)	38.(3)	1309→366	0.0089(9)	E2+M1
957.3(4)	1.6(2)	2267→1309		
965.1(4)	2.5(2)	1723→758		
1020.2(4)	1.2(3)[a]	2330→1309		
1058.9(3)	4.5(4)	1424→366		
1064.0(5)	1.3(4)[a]	1823→758		
1086.7(4)	2.5(3)	2169→1082		
1113.5(2)	7.7(5)	1872→758	0.0041(6)	E2
1127.9(3)	2.0(2)	1493→366		
1140.8(3)	1.2(3)[a]	2450→1309		
1161.7(3)	1.2(3)[a]	2471→1309		
1178.5(3)	2.6(3)	2181→1003		
1182.9(4)	2.7(5)[a]	1941→758		
1196.0(4)	1.5(5)[a]	3068→1872		
1243.6(3)	0.6(2)[a]	2553→1309		
1272.0(4)	0.9(3)[a]	3144→1872		
1296.3(4)	1.7(2)	1661→366		
1379.9(4)	2.3(5)[a]	2462→1082		
1434.8(4)	1.6(3)	2193→758		
1512.7(4)	2.8(6)[a]	2595→1082		
1555.0(5)	2.0(5)[a]	2313→758		
1597.8(5)	4.8(5)	2356→758		
1607.0(4)	4.2(6)	2689→1082		
1644.2(5)	2.3(3)	2726→1082		
1686.8(4)	1.5(3)	2996→1309		
1914.7(5)	1.1(2)	2996→1082		
1968.3(5)	0.6(2)	2726→758		
2406.0(5)		3164→758		

Table 4.6. Coincidence Relationship of ^{193}Tl γ-Decay

Energy	Coinsidence Line (keV) (S: Strong, W: Weak)
288	371 581 637S 755
324	156 393S 412 431 579 753 819 839 848 891 1087 1380 1513 1644 1915
365	405S 756W 874 883S 895 1102W 1162 1322W 1409
393	324S 370 406S 412 427 431 466 533 549 552 666S 736S 753 755S 839 848 903 1064 1114S 1183 1196 1409W 1435 1555 1607 2406
405	366S 756 874
406	324 393S 412 716W 736S 879 933 1243
412	324 393 406 437 466 716 1628
431	324S 393S 417 716S
467	393S 412W 736
490	637S
512	393 552 944
548	393 666 1059
581	288 533 637 925
637	288S 370 490 658
666	393S 549
691	596 944
716	406 412S 431S 753S 789 839 848 879 891 1027 1087 1197 1379 1513
736	393S 406S 427 467 944
753	324 393S 716 1078 1339 1606
755	288 322 393S 716 1078 1339 1606
758	288 365S 393 404 552 596 770W 944S
771	757W 874
790	944
819	324
874	366 405 771
883	366S 395 895 944 954
891	324 375 716 736
895	366 392 716 883
903	392 490
925	371 533W 581

Table 4.6. Continued

Energy	Coinsidence Line (keV) (S: Strong, W: Weak)
944	366 513S 691 737 758 790 804 824 957 1020 1141 1162 1244 1687
1059	548
1114	392S 1196 1273
1141	944
1162	366 392 596
1178	637
1196	288 393 532 581 925 1113
1409	366
1436	393
1555	393
1598	393
1915	324 393
2406	393

$(1/2^+)$ are mainly lower spin states (Fig. 4.19). The levels connected with the isomer $(9/2^-)$ basically are higher spin states (Fig. 4.20 and 4.21). The relative populations of the two level groups were different due to different population of the ground state $(3/2^-)$ and isomer $(13/2^+)$ of ^{193}Pb in the early work [Bin90a]. Prevalent direct β^+/EC feeding from the ground state was also used to determine the spin of some levels. Fifty six excited states were located and 86 transitions assigned to the level scheme of ^{193}Tl.

States set up on the ground state:

The $1/2^+$ spin of the ground state was determined by an atomic beam experiment [Eks76] and α-decay of ^{197}Bi [Coe85]. The parity is from the systematics of odd-mass Tl nuclei. The 365.5-keV E2+M1 transition is the strongest one and determines the energy of the first excited state of ^{193}Tl, this state is fed mostly from the isomeric state of ^{193}Tl which decays to the first excited state. The spin-parity of $3/2^-$ was from the M1 multipolarity of the 365.5-keV transition, the isomeric decay to this state from the $9/2^+$ state, and systematics. The 770.2-keV state is placed by

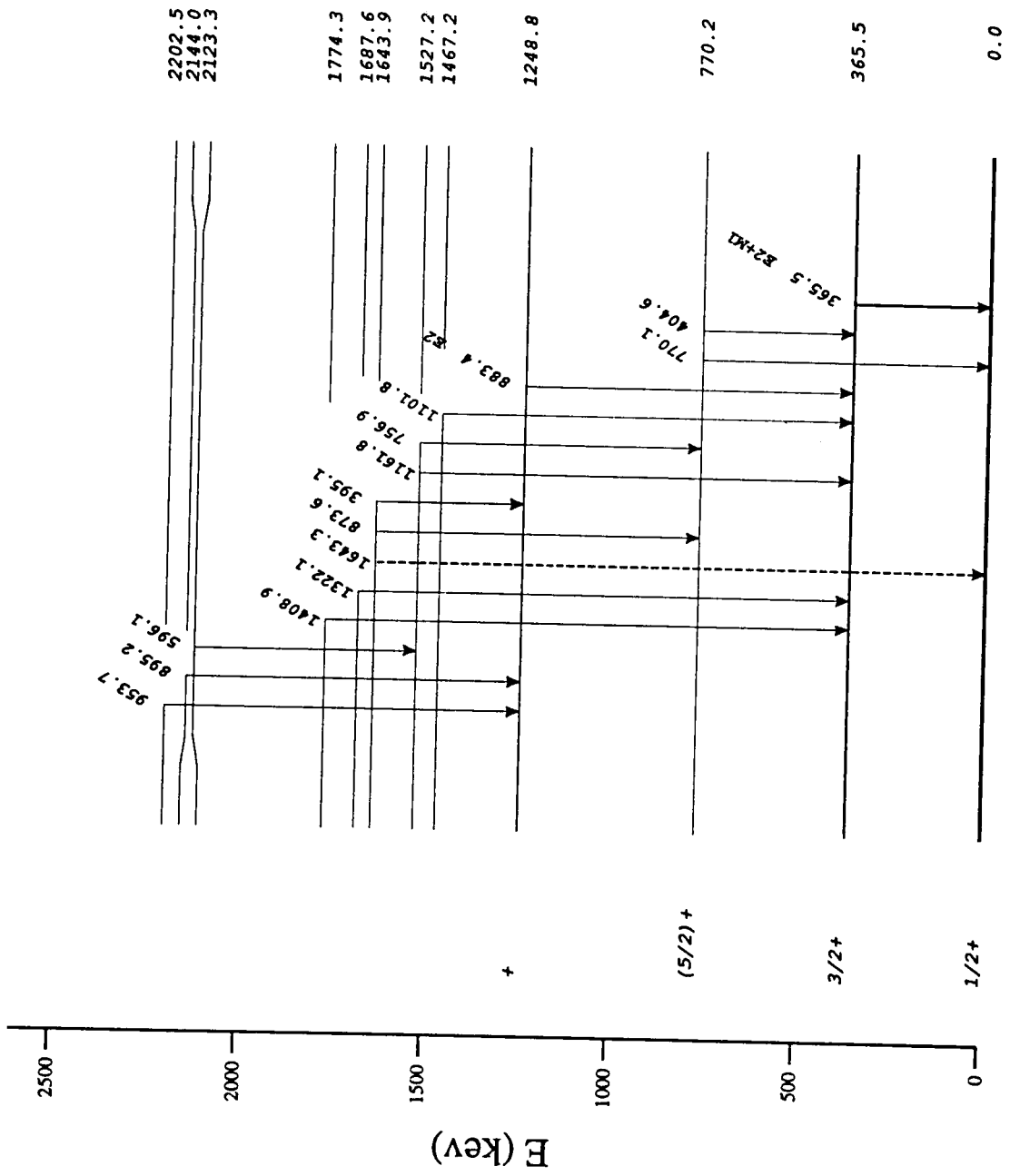

Figure 4.19: The portion of the level scheme of ^{193}Tl which is connected with ground state.

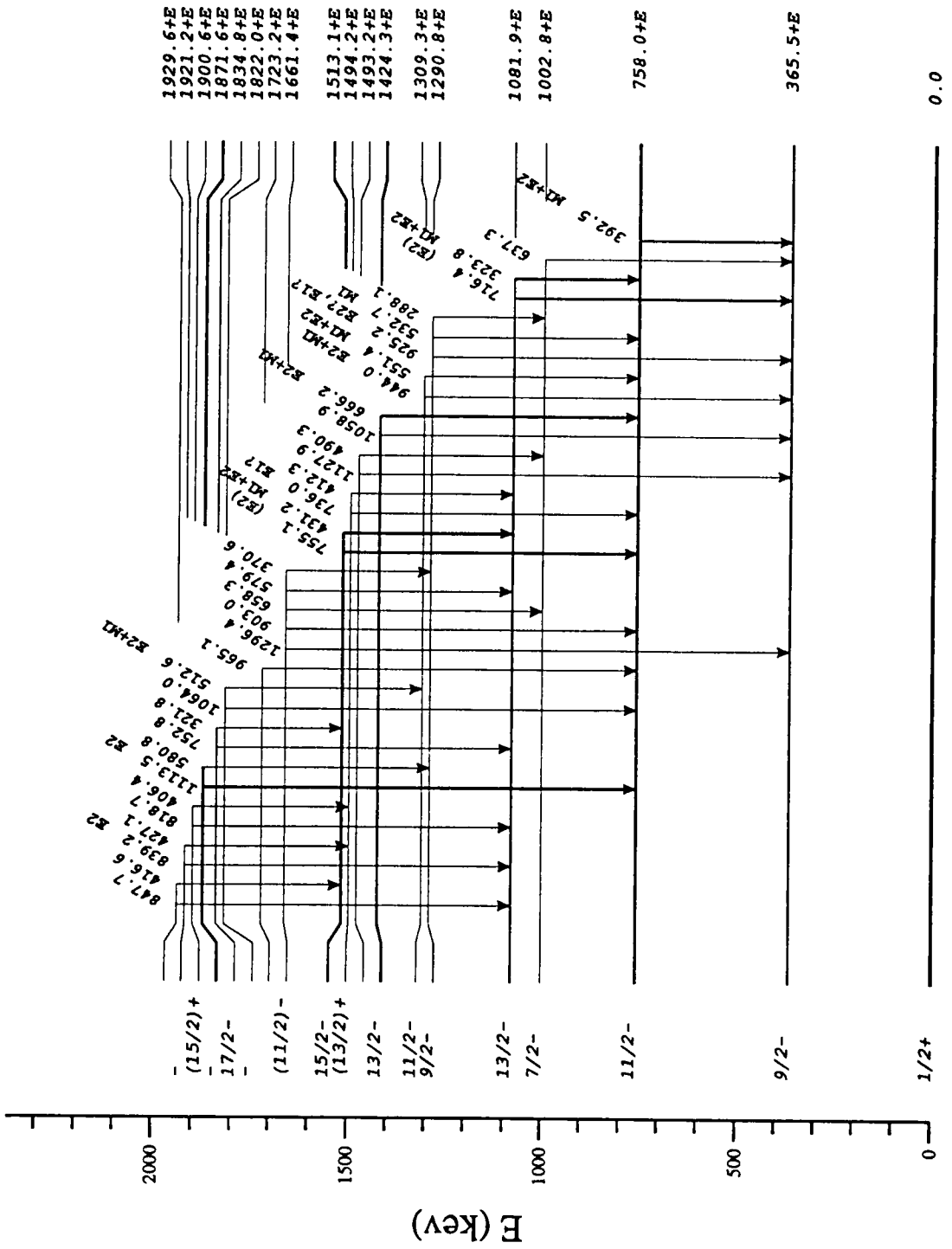

Figure 4.20: Lower part of the portion of the level scheme of ^{193}Tl which is connected with the $9/2^-$ isomeric state.

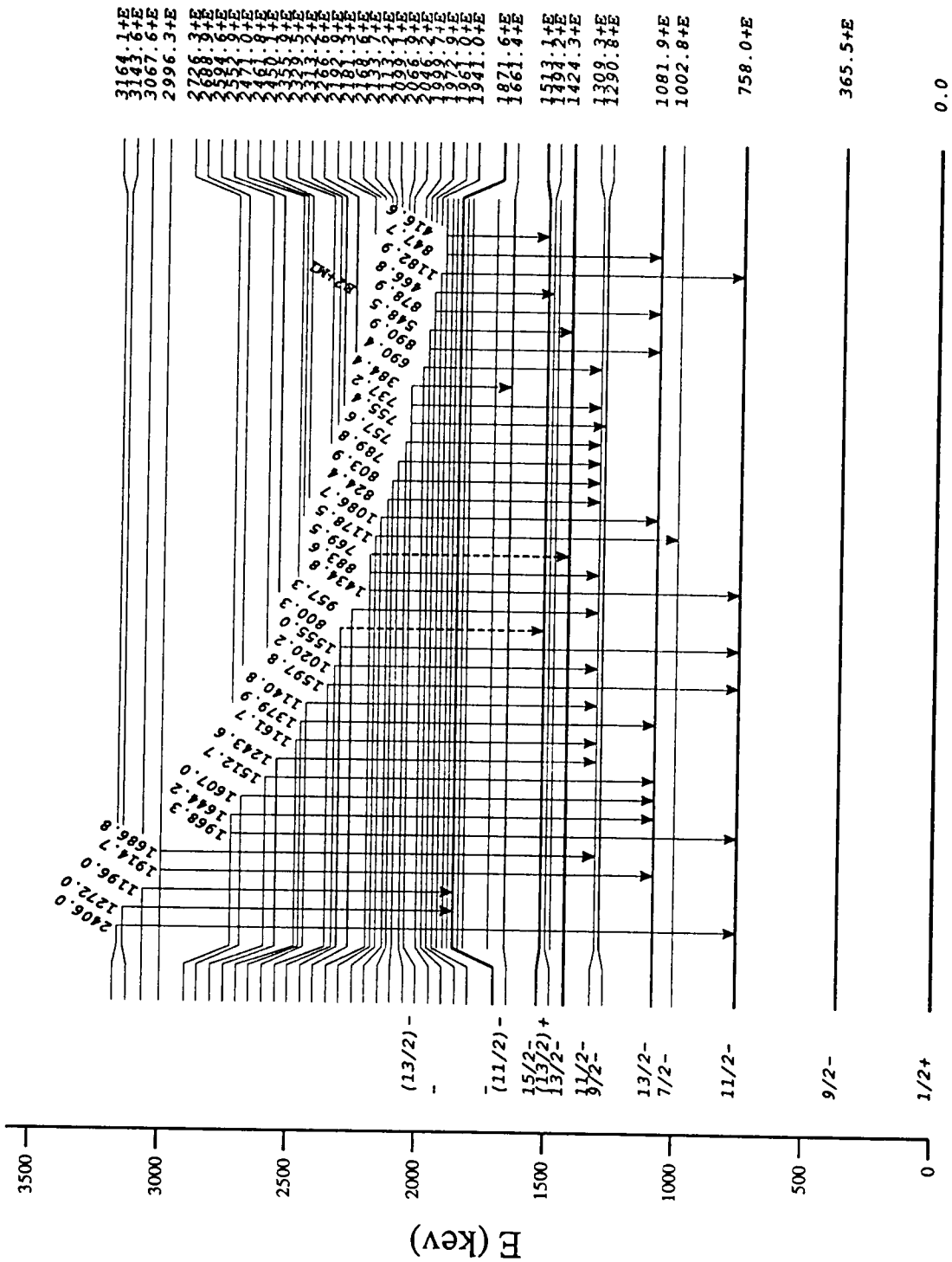

Figure 4.21: Higher part of the portion of the level scheme of ^{193}Tl which is connected with the $9/2^-$ isomeric state.

the coincidence of 405- and 770-keV transitions with 757- and 874-keV transitions and a strong coincidence of the 405-keV transition with the 365-keV transition. The $5/2^+$ assignment is from previous work [Bin90a].

Since the 883.4-keV E2 transition is coincident with 366-, 395-, 895- and 954-keV transitions, the 1248.8-keV state is a positive parity state with a spin $\leq$ 7/2. The 1101.8-, 1322.1- and 1408.9-keV transitions are only coincident with the 365.5-keV transition, so three states at 1467.2-, 1687.6- and 1774.3-keV are added to the decay scheme. From the coincidence relationships of 756.9-keV (v.s. 405-, 366-, 596- and 770-keV) and 1161.8-keV (v.s. 366- and 596-keV) a level at 1527.2-keV and another level at 2123.3-keV were added in the scheme. The 395-keV transition is coincident with the 883-keV transition and the 874-keV transition coincident with 366-, 405- and 770-keV transitions resulting in placement of a level at 1643.9 keV in the scheme. No transition was found in coincidence with 1643.3-keV, from energy considerations it is located as a possible transition from the 1643.9-keV state to the ground state. Both 895- and 954-keV transitions are coincident with the 883-keV transition; thus, 2144.0- and 2202.5-keV levels were added to the scheme.

States set up on the isomer $9/2^-$ state

Excitation energy of the isomer: From the IT decay of this state only the strong 366-keV γ transition was observed and no strong coincidence X_L-line of Tl was found, so its excitation energy is a little higher than 365.5 keV but the difference is not over 13 keV. The real excitation energies of states set up on the isomer should be the energy difference between the state and isomer plus 365.5 keV plus a small value lower than 13 keV. In electron spectrum gated by the $K_{\alpha 1}$ X-ray of Tl, there is a strong electron peak at 375.8 keV which is10.3 keV higher than the strongest 365.5-keV electron peak. It was first suspected to be the M4 transition from the $9/2^-$ isomer to $1/2^+$ ground state which cannot be checked by a coincidence relationship.

But because the same structure appears for the strongest electron line (425-keV) in the ^{199}Bi decay, it is a possible coincidence sum of the conversion electron with the coupling L X-rays which are emitted when an electron moves from the M-shell to the L-shell and detected by the same electron detector. No state was found in the lower excitation energy region which was connected with both the ground state and isomer, because of the big difference of the spin values. But comparing the two separated schemes at higher energy region, the 2113.2-, 2133.7- and 2192.9-keV states set up on the isomer are close to the 2123.3-, 2144.0- and 2202.5-keV states set up on the ground state at the differences of 10.1-, 10.3- and 9.6-keV. No coincidence data from present work can support that they are the same states or that the energy of the E3 transition from isomer ($9/2^-$) to 365.5-keV state ($3/2^+$) is about 10.1 keV. Therefore in the present work the energies of all levels set up on the isomer are still marked with "+E" which is believed to be about 10 keV.

9/2[505] band: The isomeric state has been interpreted as a $h_{9/2}$ proton coupled with the ground state of even-mass Hg. A rotational band is set up on it which has been confirmed by a high spin work [New74]. The 758.0-keV state is an $11/2^-$ which connects with the isomer with a 392.5-keV M1+E2 transition. The 1081.9-keV state is a $13/2^-$ state which decays to the isomer by a 716-keV E2 transition and to the $11/2^-$ state by a 324-keV M1+E2 transition. The 1513.1-keV state is a $15/2^-$ which decays to the $11/2^-$ state by a 755-keV E2 transition and to the $13/2^-$ by a 431.2 M1+E2 transition. The 1834.8-keV state is a $17/2^-$ and connects with the $15/2^-$ and $13/2^-$ states by 753- and 322-keV transitions. The $17/2^-$ is the highest spin state identifed from the β^+/ε-decay of ^{193}Pb.

7/2[514] band: The first $7/2^-$ state at 1002.8 keV is interpreted as the head of the $K = 7/2$ band [Bin90a]. The structure of this band is not as clear as the 9/2[505] band because there are many side-decays. A band up to $13/2^-$ state is suggested: 1002.8-keV($7/2^-$) $\rightarrow$ 1290.8-keV($9/2^-$) $\rightarrow$ 1661.4-keV($11/2^-$?)

$\rightarrow$ 2046.2-keV($13/2^-$?). The 1290.8-keV state decays to 1002.8-keV by a 288.1-keV transition; the 1661.4-keV state connects with $7/2^-$ and $9/2^-$ states by 658.3- and 370.6-keV transitions; and the 2046.2-keV state connects with $9/2^-$ and $11/2^-$(?) states by 755.4- and 384.4-keV transitions.

States set up on the $h_{11/2}$ state: The 1309.3-keV state has a spin and parity of $11/2^-$ and is believed to be the $h_{11/2}$ state corresponding to a hole in a ^{194}Pb core. Fourteen transitions to this level were confirmed by coincident relationships. The 512.6-keV E2+M1 transition placed a negative parity level at 1822.0 keV which is supported by the coincidence between 1064-keV and 393-keV transitions. The 2192.9-keV state is added to the scheme also by the coincidences between 884- and 944-keV transitions and between 1435- and 393-keV transitions. The 2046.2-keV level is added by the coincidence relationships of 384-, 737- and 755-keV transitions and the 2726.3-keV level is placed by the coincidence relationships of 1644- and 1968-keV transitions. Ten other levels (1999.7, 2066.9, 2099.1, 2113.2, 2133.7, 2266.6, 2329.5, 2450.1, 2471.0 and 2552.9 keV) are added because of ten transitions which were only coincident with the 944-keV transition. A quintuplet of levels above the $h_{11/2}$ state are expected due to excitation of the core to its first 2^+ state. The energies of the quintuplet should be near the energy of the $2^+ \rightarrow 0^+$ transition in ^{194}Pb (965-keV). Except for the 512.6-keV transition, the next 5 strongest transitions ($I_{\gamma,Rel.} > 1.9$) are located within a 90 keV (737 $\rightarrow$ 824 keV) energy region, indicating that the core is essentially spherical. (The interpretation of the 2046.2-keV state as a vibration of the spherical core here is somewhat contradictory with its being in the 7/2[514] band. Considering $13/2^-$ members could be mixed, the decays to both deformed and spherical structures are permitted.)

13/2[606] band: The 1494.2-keV state is interpreted as a $13/2^+$ because of the E1 character of 736.0-keV transition [Shi90]. The 1900.6-keV state is the possible $15/2^+$. Other higher spin positive parity states were not observed in this

work.

Other states: All other states connected with the lower states by one or more transitions are supported with the coincidence relationships. 769.5- and 800.3-keV transitions were located in the scheme as possible positions only by the energy relationships; neither was used to place the new levels.

CHAPTER 5

Discussion

5.1 Systematics of the odd-A Pb isotope lower states

Pb isotopes are proton closed-shell nuclei. The shape of Pb isotopes ground state is spherical or near spherical. Most lower states of odd-mass Pb isotopes can be explained by the neutron single-particle motion. The single quasi-neutron coupling with the ground state of the even-mass Pb isotope core creates the ground state and several lower excited states of the odd-A isotope. Below the neutron (126) gap, the order of neutron single particle states is $i_{13/2}$, $p_{3/2}$, $f_{5/2}$ and $p_{1/2}$ from neutron mid-shell to closed-shell. The last single neutron will occupy the particle orbit according to the Nilsson level order at $\varepsilon_2 \approx 0.$ for the ground state. The spin-parity of the odd-mass Pb ground states progress from $3/2^-$ to $5/2^-$ to $1/2^-$ sequentially as the neutron number increases from N = 111 to 125.

The experimental energies and I^π of the lowest 3 negative parity states and first positive parity state of isotopes between ^{193}Pb and ^{205}Pb are displayed in Figure 5.1, except for the case of ^{197}Pb where the possible $1/2^-$ state is still unknown. The $3/2^-$ and $5/2^-$ levels exchange their order around $A = 199$. The $1/2^-$ state starts at quite low excitation energy in ^{205}Pb and its excitation energy increases with A decreasing to ^{201}Pb; the $(1/2, 3/2, 5/2)^-$ levels of ^{199}Pb, ^{195}Pb and ^{193}Pb follows the trend of $1/2^-$ states established in $^{205-201}$Pb, and thus on that basis, they probably are the $1/2^-$ levels in these nuclei. The Fermi surface is higher when the mass of nuclei is increased and the energy difference between the Fermi

surface and the $i_{13/2}$ neutron-hole state is bigger, so the excitation energy of the first positive parity state, with spin 13/2, increases with A.

The modified harmonic-oscillator potential introduced by Nilsson *et al* [Nil69] was used to calculate the first few single particle states of odd-A isotopes. The potential is

$$V = -\kappa\hbar\omega_0[2\mathbf{l_t}\cdot\mathbf{s} + \mu(l_t^2 - \langle l_t^2\rangle_N)] \tag{5.1}$$

where ω_0 is the harmonic-oscillator parameter which incorporates the principle of volume conservation when the nucleus is deformed from spherical shapes; s is the intrinsic nucleon spin and $\mathbf{l}_t$ represents the orbital angular momentum in the stretched coordinate basis [Nil69]. The deduced "universal" (κ, μ) parameters set of different κ,μ values used in the calculation for each oscillator shell were obtained by Bengtsson and Ragnarsson [Ben85, Rag80] which assumes a dependence related to the main oscillator quantum number N, rather than to the mass number A (Table 5.1).

Table 5.1 (κ, μ) values as a function of oscillator shell N used in the calculation for protons and neutrons (from [Ben85]).

	Protons		Neutrons	
N	κ	μ	κ	μ
0	0.120	0.00	0.120	0.00
1	0.120	0.00	0.120	0.00
2	0.105	0.00	0.105	0.00
3	0.090	0.30	0.090	0.25
4	0.065	0.57	0.070	0.39
5	0.060	0.65	0.062	0.43
6	0.054	0.69	0.062	0.34
7	0.054	0.69	0.062	0.26
8	0.054	0.69	0.062	0.26

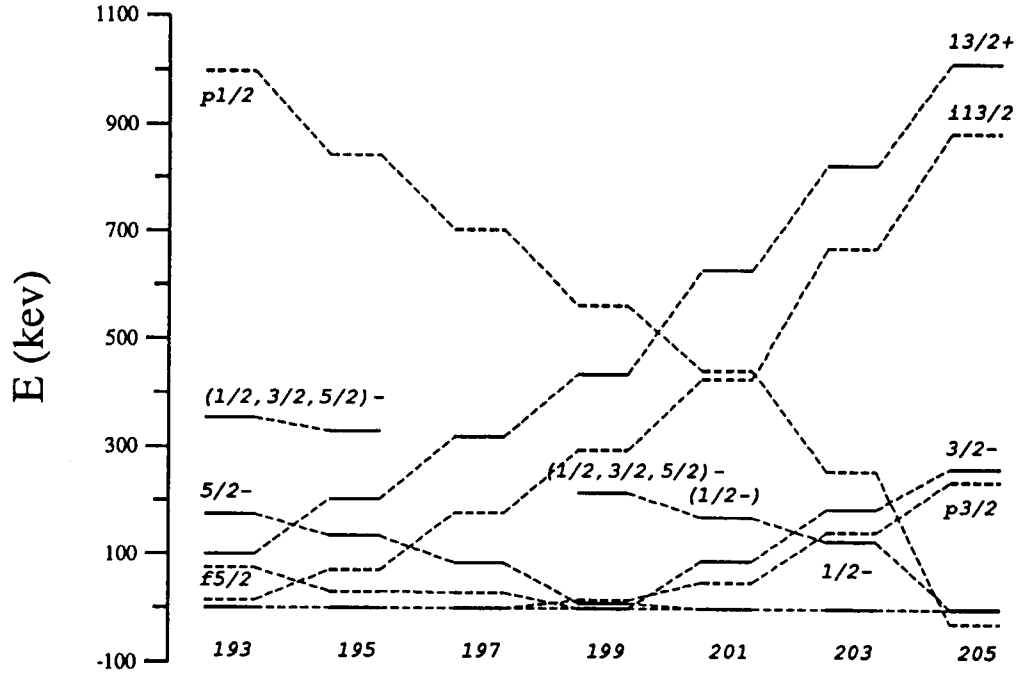

Figure 5.1: Experimental (solid) and calculated (dashed) energy levels for $i_{13/2}$, $f_{5/2}$, $p_{3/2}$ and $p_{1/2}$ states of odd-A Pb nuclides with A = 193 - 205.

Ten single quasi-particle states, $p_{1/2}(K = 1/2), p_{3/2}(K = 1/2, 3/2), f_{5/2}(K = 1/2, 5/2), h_{9/2}(K = 9/2)$ and $i_{13/2}(K = 1/2, 3/2, 11/2, 13/2)$ were considered in the calculations. The potential energy of each single state was extracted from the minimum value on the ε_2–ε_4 two-dimensional surface. The calculated results for $p_{1/2}, p_{3/2}, f_{5/2}$ and $i_{13/2}$ states of odd-A Pb isotopes ($A = 193 - 205$) are shown in Table 5.2 and Figure 5.1 too. Comparing the experimental and theoretical values, the calculations do reproduce the crossing of the $p_{1/2}$ and $f_{5/2}$ orbital states at about $A = 205$ and the crossing of the $p_{3/2}$ and $f_{5/2}$ states at $A = 199$. The predicted levels follow the trend of the experimental levels for the $3/2^-$ and $5/2^-$ levels with excitation energy differences less than about 100 keV and the higher $13/2^+$ levels with less than about 200 keV. Yet if the third negative parity levels of ^{193,195,199}Pb are assigned to the $p_{1/2}$ state, the deviations between experimental and calculated excitation energies are much bigger, becoming about 600 keV in ^{193}Pb. Small

Table 5.2: Comparison between the experimental lower states energies of Pb isotopes (A=193--205) and the theoretical predictions of the Nilsson potential.

	3/2-	$p_{3/2}$			5/2-	$f_{5/2}$			1/2-	$p_{1/2}$			13/2+	$i_{13/2}$		
A	Exp.	Theo.	ε_2	ε_4	Exp.	Theo.	ε_2	ε_4	Exp.	Theo.	ε_2	ε_4	Exp.	Theo.	ε_2	ε_4
193	0	0	.050	.003	175	74	.060	.003	354	996	.000	.001	(100)	16	-.020	.001
195	0	0	.020	.001	134	32	.055	.006	329	842	.005	.001	203	71	-.025	.003
197	0	0	.010	.001	85	29	.025	.001	----	703	.005	.001	319	178	-.025	.003
199	0	16	-.005	.001	11	0	.015	.001	216	562	.005	.001	436	295	-.030	.006
201	89	49	-.020	.001	0	0	-.015	.001	170	443	.005	.001	629	427	-.030	.006
203	187	143	-.015	.001	0	0	-.010	.003	126	256	.005	.001	825	670	-.025	.008
205	263	238	-.015	.001	0	0	-.010	.003	2	-26	.000	.001	1014	885	-.025	.008

alteration of κ and μ do not significantly alter the discrepancy between the theoretical value of $p_{1/2}$ and the experimental energy of the possible $1/2^-$ level.

5.2 Systematics of the shape-coexistence in odd-A Pb isotopes

The phenomenon of shape-coexistence in the odd-mass Pb isotopes was first found in ^{195,197}Pb [Gri91, Van91]. Since pure E0 transitions are found between the different shaped 0^+ states of even-A isotopes, transitions with strong E0 components are expected and observed widely between the shape coexisting states with the same spin and parity both for even-A (other than 0^+ state) and odd-A isotopes. The three very-converted transitions of ^{195}Bi decay at energies of 318, 401 and 890 keV were considered to have E0 components since experimental α_K values were 15(9), 21(11) and 2.0(6) times the theoretical M1 transition conversion coefficient respectively, the three positive parity states (9/2, 11/2 and 13/2) were interpreted as the states with the deformed nuclear shape [Gri91]. From ^{197}Bi β^+-decay, three very-converted transitions at energies of 351, 477 and 1111 keV with experimental α_K values of 2.0(2), 5(2) and 3.6(4) times of the theoretical M1 transition conversion coefficients were also taken as the transitions with E0 components. Three states, $9/2^+$(1525 keV), $11/2^+$(1625 keV) and $13/2^+$(1431 keV), were interpreted as deformed shape states [Van91].

In the present work, similar situations were found in the ^{193}Bi and ^{199}Bi β^+-decays. The 342 and 757 keV transitions in the ^{193}Bi decay, have experimental conversion coefficients (α_K) that are > 5 and 4.5(10) times the theoretical M1 value. Two states (at the 757 and 1023 keV excitation energies over the first positive parity state) were interpreted as the deformed $13/2^+$ and $11/2^+$ states. The 480-keV and 1268-keV transitions in ^{199}Bi decay have α_K values which are about 3.0(2) and 6(3)

times M1 transition conversion coefficients. The 1705-keV state in the ^{199}Pb level scheme was interpreted as deformed $13/2^+$ state and 1754-keV state was assigned as the deformed $9/2^+$ state.

The energies of deformed positive parity states compared with the first positive parity state ($13/2^+$) in the Pb isotopes (A=193–199) are shown in the Figure 5.2. The excitation energies of the deformed states with different spin value increase systematically with the neutron number. This can be understood by comparing the deformed $13/2^+$ states in the odd-A isotopes and the deformed 0^+ states in the even-A Pb isotopes (Fig 5.3). The first $13/2^+$ states and deformed $13/2^+$ states in the odd-A isotopes are interpreted as the $i_{13/2}$ neutron hole coupling with the spherical ground 0^+ and deformed excited 0^+ state of the even core. When the excitation energy of the deformed 0^+ state of even-core increases with the neutron number, the coupling result for the deformed $13/2^+$ state excitation energy will be higher logically.

It would be noticed in detail that the excitation energy of the odd-A deformed state is always lower than the neighboring even-A isotopes, from ^{193}Pb where the 757 keV excitation energy is 174 keV lower than its even-core ^{194}Pb to ^{199}Pb which is 358 keV lower than the even-core. It indicates that the interactions between $i_{13/2}$ neutron-hole state and the ground state of even-core or deformed state of even-core are different systematically. The potential energy of a high j, low K single particle state on the oblate side of the Nilsson diagram will rise as the deformation increases, and hence the $i_{13/2}$ state is closer to the Fermi surface. So the $i_{13/2}$ quasi-particle favors an oblate shape deformed state which has lower excitation energy than the spherical ground state. Or it can be considered that the overlap between the wave function of $i_{13/2}$, low K hole state with the oblate core is bigger than with the spherical core. The stronger interaction between the quasi-neutron and deformed core pulls down the excitation energy of the odd-A deformed state

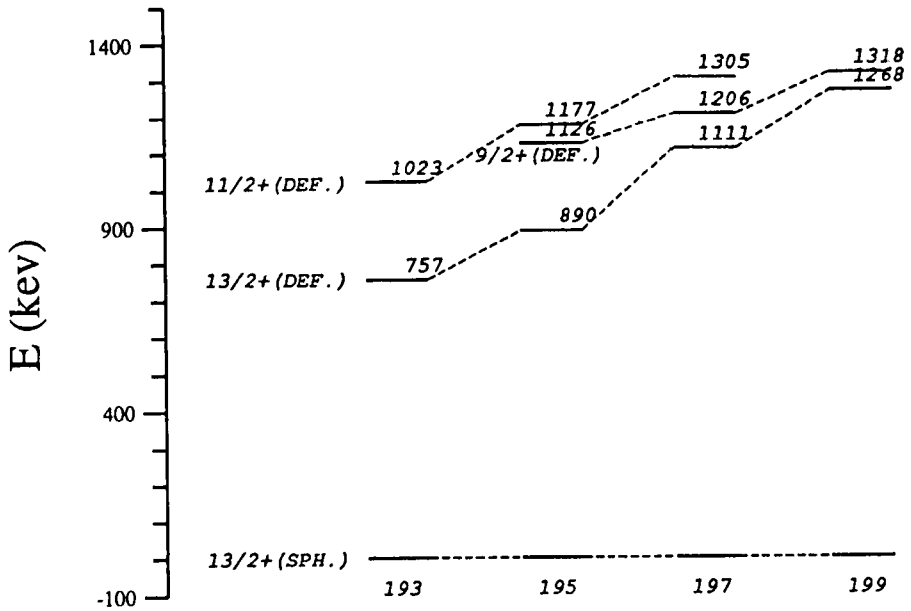

Figure 5.2: Systematics of deformed positive parity states in the odd-mass Pb isotopes (A=193–199). The relative excitation energy is compared with $13/2^+_1$(spherical) state.

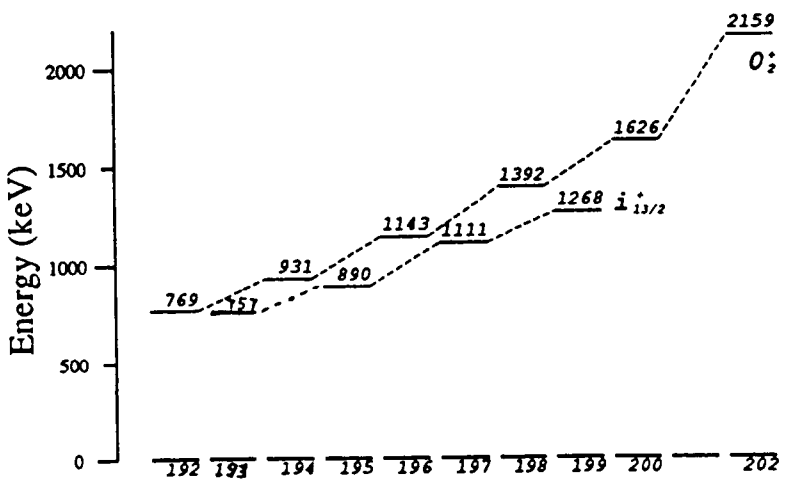

Figure 5.3: Energy systematics for the deformed 0^+_2 states in even-even Pb and deformed $13/2^+$ states in odd-A Pb nuclides. Energy values are relative to the lowest level with the same spin-parity.

relative to the neighboring even isotope.

The deformed states with the lower excitation energy found in the Pb isotopes are interpreted theoretically as two proton holes $(s_{1/2,1/2})^{-2}$ and two proton particles $(h_{9/2,9/2})^2$. In an early Nilsson-Strutinsky calculations [May77], there are possible excited oblate and prolate minima lying above the spherical state. When the neutron number is less than 106, the energy of the prolate state is lower than the oblate state; when the neutron number is more than 106, the oblate state would be lower than the prolate state. In another recent theoretical calculation using a deformed Woods-Saxon field plus the monopole pairing interaction [Ben89], a similar result was obtained: for lower neutron numbers ($N \approx 104$), both oblate and prolate shape states are possibly observed in the experiment; for higher neutron numbers $N \approx 114$), the oblate shape state would be more likely than the prolate shape. The deformation parameter (β_2) of oblate shape is about 0.15.

The same modified Nilsson model and harmonic-oscillator parameters discussed in the last section were used to calculate the ground state potential energy surface here (Fig. 5.4). Similar potential energy curves were obtained with the Woods-Saxon potential calculation [Ben89]. For ^{186}Pb, the clear minima exist on both oblate and prolate sides. The corresponding deformation parameters (ε_2, while ε_4 was varied to keep the energy minimum) are about -0.18 and 0.24. As with the Woods-Saxon potential calculation for ^{196}Pb[Ben89], the local minimum on the prolate side has disappeared and a flat region exists on the oblate side ($\varepsilon_2 \approx -0.15$). For heavier isotopes (A$\approx$202), only a recognizable flat structure in the normal deformation region is left on the oblate side.

For the odd-mass Pb isotopes, the potential energy surface of $i_{13/2}$ was calculated by the same model (Fig. 5.5). On the oblate side, a local minimum for the isotope (A=187) becomes a clear flat region for the isotopes (A=191–199) with A increased, and this flat region disappears as the neutron number approachs

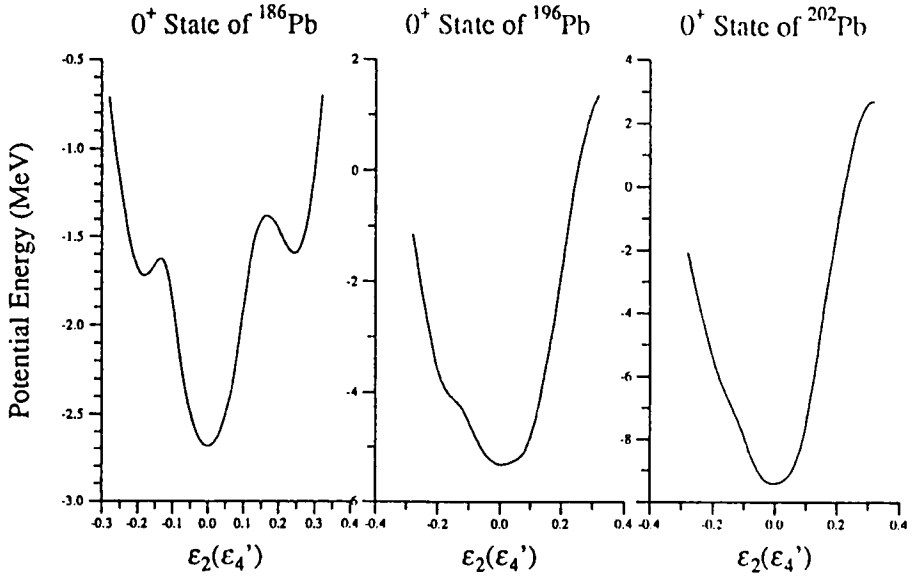

Figure 5.4: Ground state potential energy calculation by Nilsson potential for even-A Pb isotopes.

the closed shell. Just as their even core, all of these occur at ε_2 about -0.15 and the potential energy differences between the flat region on the oblate side and the minimum near the spherical point are about 1 MeV. On the prolate side and at normal deformation region, the deformed minimum disappears very quickly as the neutron number is increased above 106.

As it is known the total routhian surface (TRS) calculation is quite successful in determining the nuclear shapes. The TRS are shown in Figure 5.6 for ^{187,193,197}Pb at low frequencies ($\hbar\omega = 0.0$ and 0.05 MeV). When $\omega = 0.0$, there are no differences between the $\gamma = 60°$ and -60°. From the ^{187}Pb TRS, there is a flat region at $|\beta_2| \approx 0.15$ and $\gamma = -60°$ (oblate); and at a little higher excitation energy region there is a minimum at $\beta_2 \approx 0.20$ and $\gamma = 0°$ (prolate). In both ^{193}Pb and ^{197}Pb TRS's, there is the clear flat region at $\gamma = -60°$ and $|\beta_2| \approx 0.15$; but along the prolate axis the first minimum is in the super-deformation region ($\beta_2 \geq 0.4$).

The different theoretical approaches under the different approximations

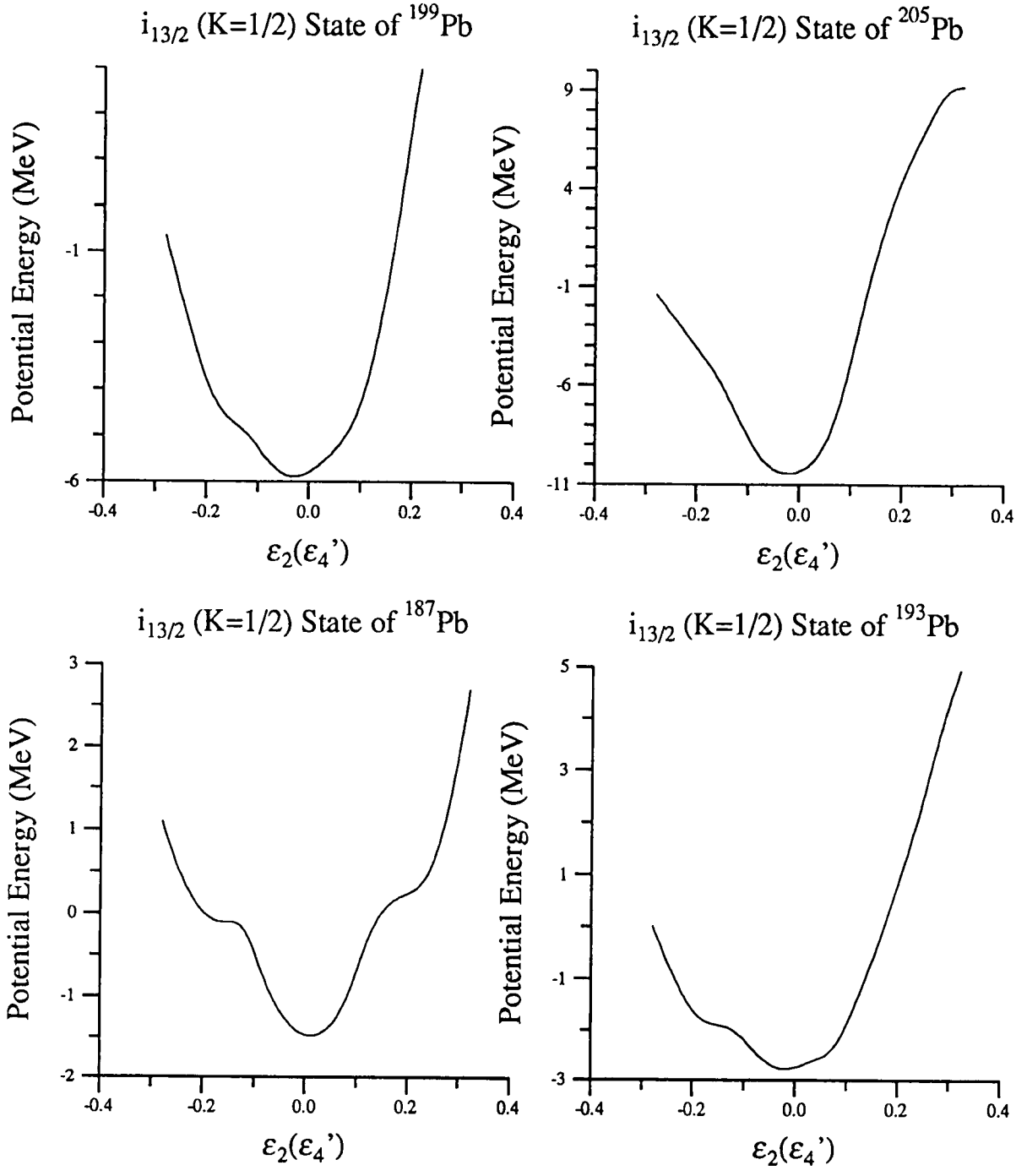

Figure 5.5: The $i_{13/2}$ state potential energy calculation by the Nilsson potential for odd-A Pb isotopes.

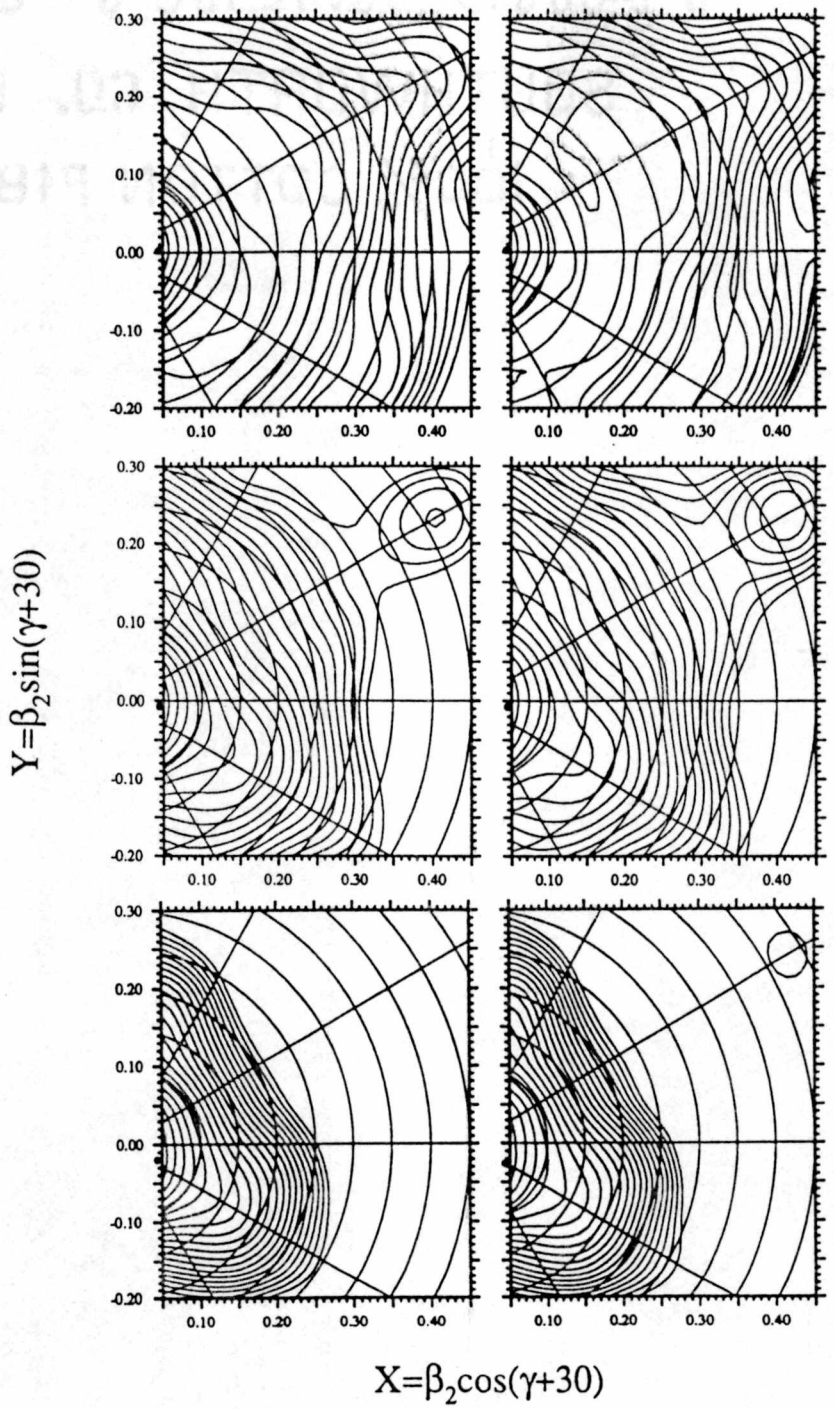

Figure 5.6: Total Routhian Surface (TRS) of ^{187,193,197}Pb at $\hbar\omega = 0.0$ MeV (left column) and 0.05 MeV (right column).

give out the similar deformation results for the 0^+ states of even-A and $13/2^+$ states of odd-A Pb isotopes: when nuclear mass A is larger than 190, there is a normal deformed state on the oblate side at β_2 equal to $\sim$0.15; and when A is smaller than 190, the normal deformed oblate state still exists and a normal deformed prolate state will begin competing with the oblate shape state. The phenomenon of shape coexistence in the odd-A Pb isotopes have been observed experimentally for A=193–199. At the heavier isotope end, the transition energy between the deformed $13/2^+$ state and spherical $13/2^+$ state has increased to 1268 keV, and the conversion coefficient is only 0.05; even so its experimental α_K is 6 times that of a pure M1 transition. For even higher mass number odd-A Pb isotopes, the excitation energy of the deformed state will be higher systematically. Comparing with the relatively simple level structure of even-A isotopes, the odd-A isotopes at higher excitation energy have a higher density of states and the probability of mixture among different states will be much higher. It may be very difficult to find the deformed state by measuring the conversion coefficients. Theoretically, the existing probability will be lower with the smaller flat structure of its potential surface. On the other side ($A \leq 191$), measuring the E0 component at lower transition energy ($\leq$ 700 keV for ^{191}Pb systematically) would be easier. It would be very interesting to observe the normal deformed prolate state beginning to compete with the oblate state and the excitation energy of the spherical $13/2^+$ state will be lower, even becoming the ground state of odd-A Pb isotopes. But the production of very neutron deficient Bi radioactive source has a much lower production cross section and the short half-life will make the measurement much more difficult.

Most of the shape-coexistence phenomena in the odd-A Pb isotopes are found in the positive parity states connected with $i_{13/2}$ single quasi-neutron. In ^{193}Pb one highly converted transition (565 keV) decays to the lowest $5/2^-$ state and serves as the only candidate for shape coexistence among the negative-parity states.

The 739-keV level can be interpreted as a $f_{5/2}$ neutron coupled to the first deformed 0^+ state at 769 keV in the ^{192}Pb core. The lowering of the E0 transitional energy in ^{193}Pb relative to the $0^+ \rightarrow 0^+$ energy in the ^{192}Pb (769 keV) can be explained by the downsloping $f_{5/2}$ orbital on the oblate side of the Nilsson diagram. The $13/2^+_{sph}$ $\rightarrow$ $13/2^+_{def}$ spacing in ^{193}Pb is larger (757 keV), but since the $i_{13/2}$ orbital is nearly full it is interpreted as a hole state in the ^{194}Pb core, which has a $0^+ \rightarrow 0^+$ transition energy of 930 keV.

The shape coexistence phenomenon in the Pb isotopes is very interesting because it is on the proton closed shell. While their ground states are spherical, some excited states are possibly deformed from a broken proton core. At low excitation energy, three negative parity states ($f_{5/2}$, $p_{3/2}$ and $p_{1/2}$) and one positive parity $i_{13/2}$ state are distributed according to their energy difference with the Fermi surface basically with spherical shape. Because the potential energies of the high-j, high-K and high-j, low-K states have large slope in the Nilsson diagram, energetically the nucleus favors large deformation (prolate or oblate) when these orbitals are occupied. It is called the deformation driving effect of the single-particle orbital. In general, the shape-coexistence structure will be more likely in the high-j state. On the oblate side of this mass region, the $i_{13/2}$, low-K hole-state is the energy favored state. Then, the deformed positive parity states in the odd-A Pb isotopes are found in the lower energy region throughout the various isotopes in the experiment. Because of the abundance of spherical negative parity states near 1 MeV, the deformed negative parity states have many states with which to mix. The significant lowering of the 0^+ deformed state in the ^{192}Pb perhaps produced the first such negative parity state with sufficient admixture of the deformed state to be observed by this technique in ^{193}Pb.

When an outside quasi-neutron couples with the spherical 2^+_1 state of an even-core, it will create the multiplet level structure. There are clear observed

level structures from ^{193}Pb to ^{205}Pb showing that there are $\{i_{13/2} \otimes 2_1^+\}$ weak coupling configurations (Fig. 5.7), the full quintuplet was identified in ^{197,199}Pb. The transitions between the $\{i13/2 \otimes 2_1^+\}$ and $\{i13/2 \otimes 0_1^+\}$ should be fairly pure $E2$ characteristic decays; this is confirmed by the experimental data. The corresponding structures cannot be identified in the negative parity states, because the possible $\{p_{3/2} \otimes 2_1^+\}$, $\{f_{5/2} \otimes 2_1^+\}$ and $\{p_{1/2} \otimes 2_1^+\}$ coupling configurations are mixed together in a relative small energy region. As mentioned above the negative parity states might also mix with deformed states thus making simple characterization of any of the negative parity states around 1 MeV excitation difficult. The "crossing" decays with the M1 component are prevalent in the low negative parity states.

5.3 Band structures of ^{193}Tl

The Pb isotopes have a closed proton shell, the low excitation states have spherical or near spherical shape. For the isotopes of Tl, there is a proton quasiparticle outside the closed shell. While many of the configurations are still spherical, some may be easier deformed by the proton-neutron interaction, and other pairing effects promotes a proton to the next major shell ($h_{9/2}$ suborbital) and establishes deformation in the low excitation energy range. Several low spin positive parity states connected with the ground state of ^{193}Tl are believed to be the proton hole states ($s_{1/2}$, $d_{3/2}$) coupling with the spherical Pb core; those are expected from a weak coupling model. There are some high spin positive parity states connected with the $i_{13/2}$ single proton particle state. High spin negative parity states are expected from the coupling of a $h_{11/2}$ proton hole to the Pb spherical core and the coupling of a $h_{9/2}$ proton particle to the Hg oblate core. The mixing between the states from the $h_{11/2}$ and $h_{9/2}$ should be small because the Pb and Hg cores have different deformations. The isolation between the different deformation bands makes it possible to describe

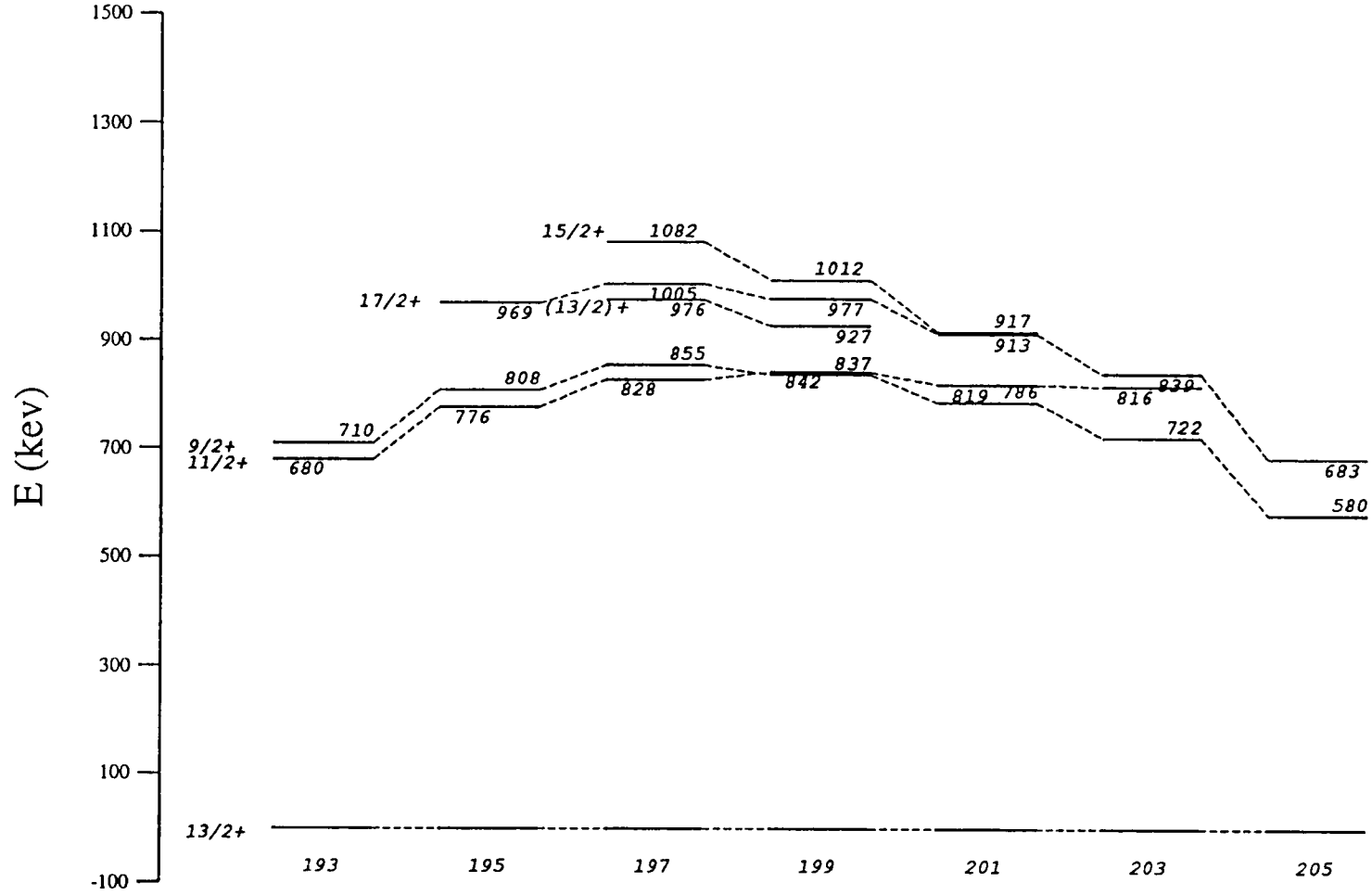

Figure 5.7: The $\{i_{13/2} \times 2_1^+\}$ spherical shape configuration of odd-A Pb isotopes (A=193--205).

the band structure with the theoretical model which couples a single particle to a rigid core. As has been discussed in the chapter of experimental results, four band heads (9/2[505], 7/2[514], 11/2[505] and 13/2[606]) were found in the ^{193}Tl level scheme. Relatively complete quasi-rotational band structures were set up on the 9/2[505] ($9/2^- \rightarrow 17/2^-$)and 7/2[514] ($7/2^- \rightarrow 13/2^-$) states. The rigid triaxial particle-rotor model with a modified oscillator potential was used to calculate the excitation energies and relative transition intensities of these two bands.

A similar calculation has been done on ^{195}Tl [Bin92], in which the quadrupole deformation ε_2 was taken from [Bou85] as -0.14, and the parameter $\gamma = -23°$ was set from fitting the position of the $K = 5/2$ bandhead. In the level scheme of ^{193}Tl, the 5/2[523] state and band were not found. Considering the position of the Tl proton Fermi surface and the lower excitation energy of $h_{9/2}$ and $i_{13/2}$ high Ω states and the coupling Hg core, the nuclear shape should be oblate. The harmonic oscillator potential calculation predicts the minimum of $h_{9/2}$ different Ω states at $\varepsilon_2 \approx -0.14$. For lower Ω values, the nuclear shape is softer and there is a second minimum on the prolate side.

For all these reasons, calculations were made utilizing both an axially symmetric potential ($\gamma = 0°$) and a triaxial rotor potential ($\gamma = -23°$) used in fitting the ^{195}Tl level structure. In both cases the deformation parameter ε_2 was taken as -0.145, Standard values for the g-factors have been used ($g_l = 1.0, g_s = 0.70^* g_s(free), g_R = Z/A$). Another calculation of input parameter E_2 is about half of 2^+ state energy of even core. For the best level energy fit, at $\gamma = 0°$ and $\varepsilon_2 = -0.145$, E2 is 210 keV; at $\gamma = -23°$ and $\varepsilon_2 = -0.145$, E2 is 260 keV. The experimental and theoretical level energies are shown in Figure 5.8 and relative intensities are compared in the Table 5.3.

Usually a nuclear model is more strictly tested by electromagnetic matrix

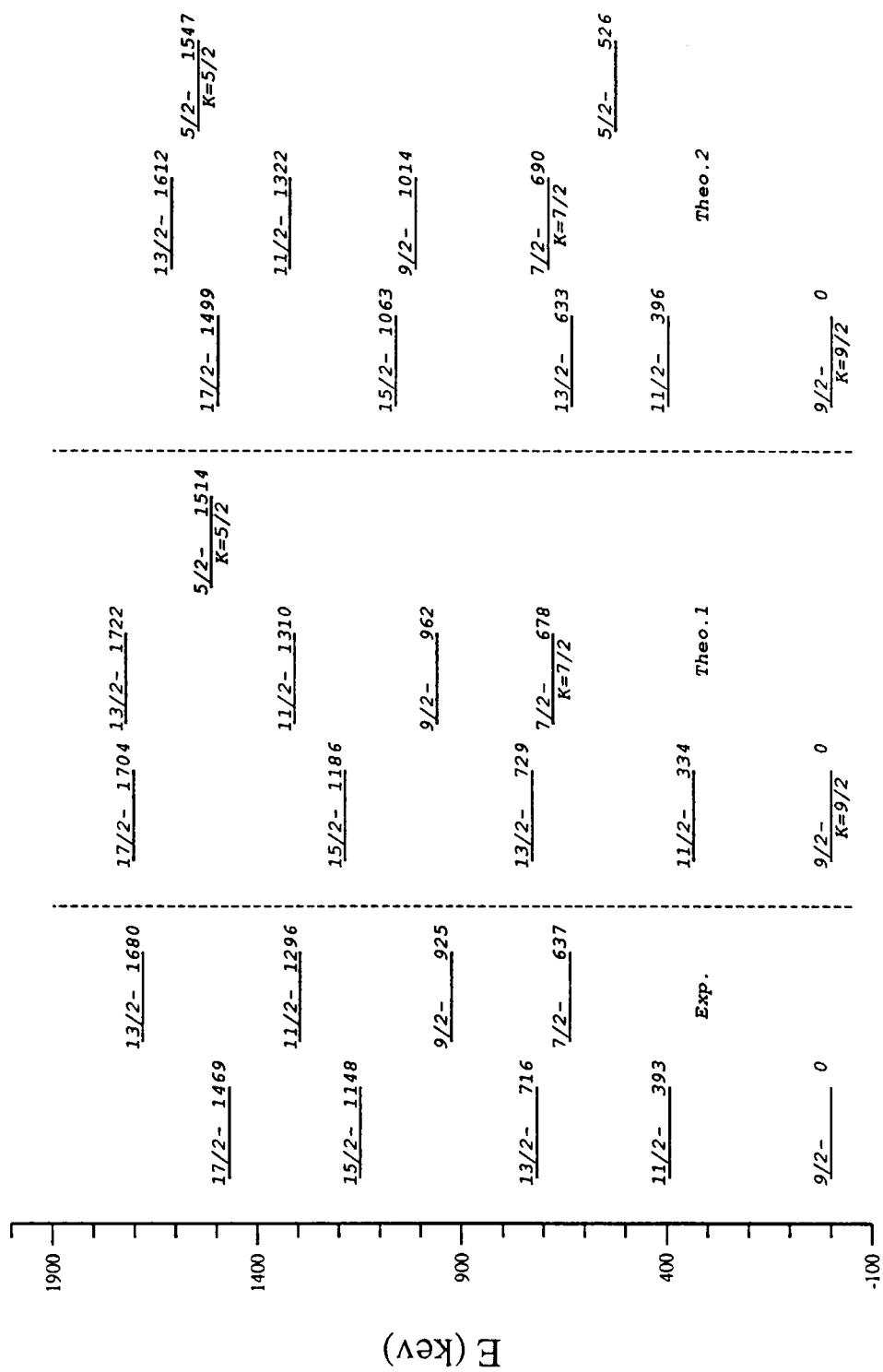

Figure 5.8: The theoretical excitation energy from the Particle-Rotor Model compared with the experimental data of ^{193}Tl. The left part of the figure gives the experimental value. The central and right parts are the theoretical values with different parameters: ($\varepsilon_2 = -0.145$, $\gamma = 0^0$, E2 = 210 keV and $\gamma = -23^0$, E2 =260 keV).

Table 5.3: Comparison of energies and intensities between the Particle-Rotor Model calculations and the experimental data.

Band	Parity: –		Experimental		Theoretical 1 (γ= 0)				Theoretical 2 (γ= -23)			
K	J_i	J_f	Eγ	Rel.Int.	Eγ	B(E2)	B(M1)	Rel.Int.	Eγ	B(E2)	B(M1)	Rel.Int.
9/2	11/2	9/2	393	100	344	.6368	.0822		396	.5352	.0597	
	13/2	9/2	716	100	729	.1182	-----	100	633	.2788	-----	100
	13/2	11/2	324	58	395	.7003	.1292	75	237	.0644	.0339	2.5
	15/2	11/2	755	100	852	.2331	-----	100	667	.3579	-----	100
	15/2	13/2	431	85	457	.6283	.1577	33	430	.3554	.0652	27
	17/2	13/2	753	100	975	.3263	-----	100	866	.3177	-----	100
	17/2	15/2	322	14	518	.5327	.1754	19	436	.3298	.0966	11
7/2	7/2	9/2	637	100	678	.0276	.0540	100	690	.0551	.0411	100
	7/2	11/2	244?	0.	344	.0180	-----	0.3	294	.0007	-----	0.0
	$9/2_2$	7/2	288	42	284	.6238	.1250	21	324	.5212	.0960	20
	$9/2_2$	9/2	925	100	962	.0181	.0079	100	1014	.0214	.0065	100
	$9/2_2$	11/2	533	25	628	.0055	.0484	71	618	.0176	.0405	47
	$11/2_2$	7/2	658	100	632	.1373	-----	100	632	.2830	-----	100
	$11/2_2$	$9/2_2$	371	420	348	.6195	.1817	102	307	.1588	.0752	13
	$11/2_2$	9/2	1296	65	1310	.0054	.0005	160	1322	.0045	.0000	64
	$11/2_2$	11/2	903	104	976	.0176	.0125	234	926	.0111	.0069	54
	$11/2_2$	13/2	579	65	581	.0004	.0458	93	689	.0196	.0366	71

elements than by energy comparisons alone. It is interesting to note that there is not a big difference in the quality of the excitation energy fit for γ equal 0° and -23°; however, the transition intensities are quite different for the different γ. In Table 5.3, the relative intensities from both E2 and M1 contributions are normalized to the strongest γ-ray or the pure E2 transition observed from that particular level. For the predicted transition relative intensities in the K=9/2 band, the γ=0° results gave a much better comparison with those extracted from the experimental data than the $\gamma = -23°$ results. When the intensities of transitions from the first $13/2^-$ state are normalized for the pure E2 decay to the isomer $9/2^-$ state, the prediction of the intensities which decay to the first $11/2^-$ state are 75 for $\gamma = 0°$ and 2.5 for $\gamma = -23°$ compared to the experimental value 58. For the decays from $15/2^-$ and $17/2^-$ states, both calculations give good fits. For the K=7/2 band, the result of $\gamma = -23°$ is improved. The predicted decay intensities from $7/2^-$ and $9/2^-$ states of 7/2[514] band are similar for $\gamma = 0°$ and $-23°$. But for the transitions from the second $11/2^-$ state, the theoretical model gives the better fit for the in band transitions with $\gamma = 0°$; and the better fit for the transitions to the 9/2[505] band with $\gamma = -23°$.

From the Total-Routhian-Surface of ^{193}Tl and ^{195}Tl at the low rotation frequency (Fig. 5.9), there is a real deformation minimum at $\beta_2 \approx 0.14$ and $\gamma \approx -60°$ (same as γ about 0° when ε_2 is a negative number). It is logical that for the K=9/2 band, $\gamma = 0°$ is a very good approximation. But for the ^{195}Tl isotope, the parameter $\gamma = -23°$ was required to get the energy difference of 5/2[523] and 9/2[505] states which was very sensitive to the γ value. A possible explanation is that the nuclear shape is softer for the $h_{9/2}$ middle K states, thus resulting in a K shape dependence. In the Nilsson diagram, the potential energy slope of the 9/2[505] and 7/2[514] single particle states are very big and the 5/2[523] state is basically a flat line. Compared with K=9/2 and 7/2, the nuclear shape of K=5/2 band will be more easily changed,

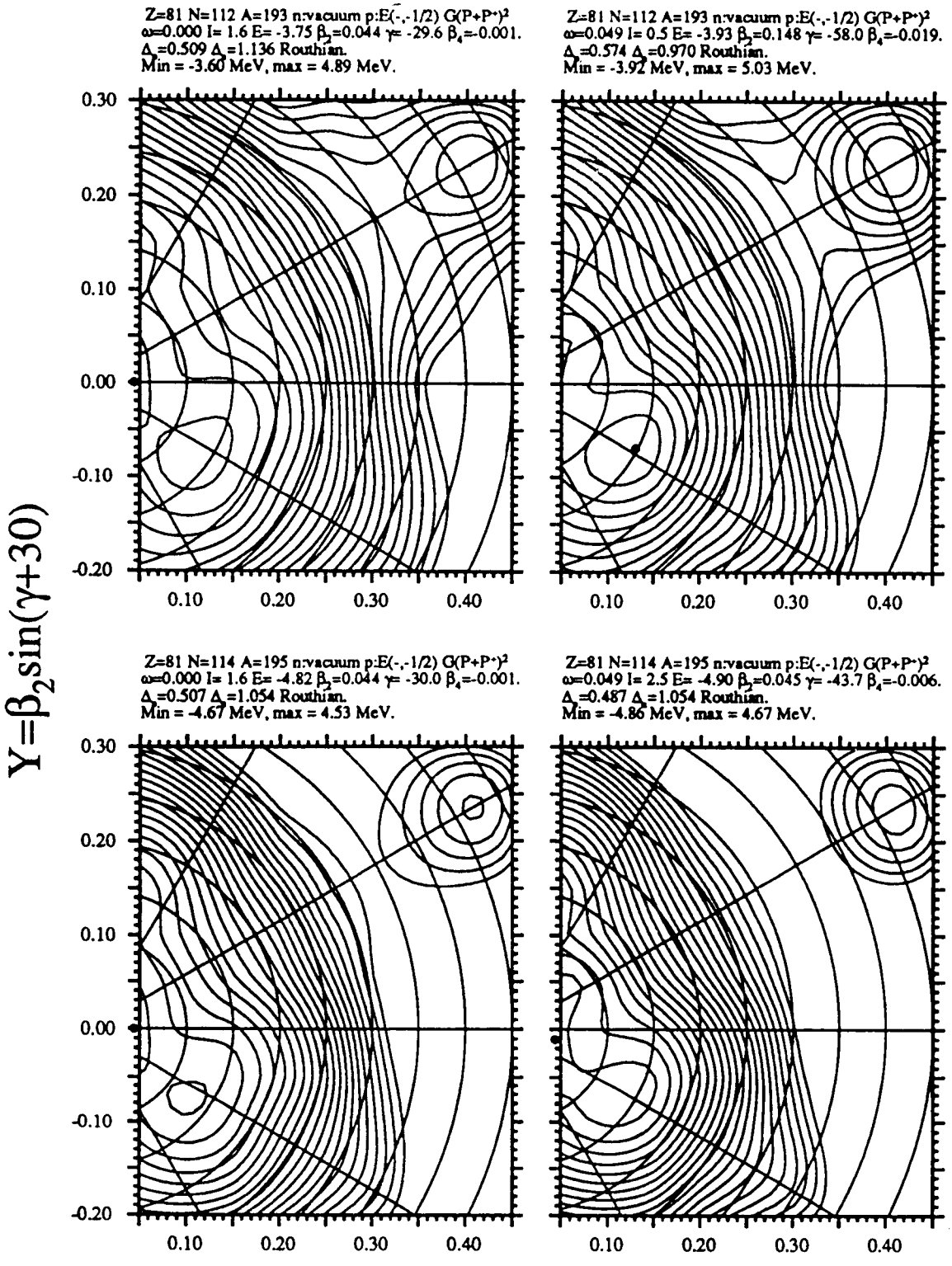

Figure 5.9: The Total-Routhian-Surface of ^{193,195}Tl at low rotation frequency.

perhaps resulting in a different γ value. Under this situation, the different γ value should be assigned to the different K bands or even different states in the same band. The γ-soft rotor should be considered in the calculation. For such a flexible and changing potential, the transition intensity calculation between the different shape bands will be more complicated.

CHAPTER 6

SUMMARY AND CONCLUSION

The β^+/EC decays of mass-separated ^{199}Bi and ^{193}Bi were studied at the Oak Ridge Holifield Heavy-Ion Research Facility. In these experiments the heavy-ion fusion reactions $^{187}Rc(^{16}O, 4n)$ and $^{185}Re(^{16}O, 8n)$ were used. Time-sequenced spectra of γ-rays, X-rays, conversion electrons and $\gamma\gamma$t, γXt, eγt, eXt coincidence data were obtained. The decay schemes were constructed consisting of 67 excited states and 216 transitions in ^{199}Bi and 41 excited states and 61 transitions in ^{193}Bi. Several very-converted transitions interpreted as E0 multipole admixtures, as indicative of shape coexistence, were found to de-excite positive-parity levels at 1705, 1754 keV in ^{199}Bi and 757, 1023 keV higher than the isomer state in ^{193}Bi. One possible deformed state with negative parity, the first one discovered in odd-mass Pb isotopes, was found at 739 keV in ^{193}Bi.

The systematics of the lower excited states in odd-mass Pb isotopes were discussed and interpreted as a single neutron particle or hole coupling with the ground states of their even-core. Good agreement was found for $p_{3/2}$, $f_{5/2}$ and $i_{13/2}$ experimental energies and predictions of the theoretical deformed harmonic-oscillator potential calculation. The theoretical energies of the $p_{1/2}$ states agree with the experimental value at heavy mass region (A$\sim$205), but there are bigger energy differences with the experimental energies of the $(1/2, 3/2, 5/2)^-$ state as neutron number decreases ($\sim$600 keV at A = 193). This state needs more detailed study and the experimental missed one in ^{197}Pb should be found in the 250–300 keV energy region.

The systematics of shape coexistence in odd-mass Pb isotopes with even-mass isotopes were compared and discussed in both positive and negative parities states, and interpreted as single neutron weak-coupling with the spherical and oblate deformed even-core. The Nilsson model and Total Routhian Surface calculations were used to study the nuclear shape of Pb isotopes. The systematics of shape co-existence phenomena in lead isotopes are basically explained by these theory models. Considering the steeper theoretical deformation potential slope, the higher excitation energy of the deformed state, and the resulting lower experimental conversion coefficient on the higher mass side, it will be very difficult to observed the normal shape-deformed state in heavier odd-mass Pb isotopes by the same experimental method. On the lower-mass side, potential minima will appear on both oblate and prolate sides, the experimental α_K value will be bigger at lower transition energy for the same E0 component. Observing the competition between the potential minima on the oblate shape and prolate shape would be quite interesting. More negative parity deformed states are expected in the lower mass region. While production of intense sources will be quite difficult, it would be interesting to pursue these studies to the lower mass region.

As a by-product of the ^{193}Bi experiment, a decay scheme with 56 excited states and 86 transitions in ^{193}Pb was established. Two bands of $\pi h_{9/2}$ $9/2^-[505]$ and $\pi h_{9/2}$ $7/2[514]$ were expanded. The particle-rotor model was applied to the energies and electromagnetic properties of these two bands. Compared with the experimental relative transition intensities, the $\varepsilon_2 = -0.145$ and $\gamma = 0°$ give the better fit for K=9/2 band. This type deformation also agrees with Total Routhian Surface calculation for the $\pi h_{9/2}$ state at low rotation frequency. Comparing with the work of ^{195}Tl [Bin92]. it is suggested that for lower K value(5/2), the Tl nuclei becomes γ-soft shape and a non-zero γ is needed. If true this implies that the deformation variable γ cannot be taken as a constant for the different bands even

in the same nucleus.

Bibliography

[Ben85] R. Bengtsson, T., and I. Ragnarsson, *Nucl. Phys.* **A436** (1985) 14.

[Ben89] R. Bengtsson and W. Nazarewicz, *Z. Phys.*. **A334** (1989) 269.

[Bin90a] C.R. Bingham, M.B. Kassim, H.V. Carmichael, L.L. Riedinger, H.K. Carter, M.O. Kortehlahti, E.F. Zganjar and J.L. Wood, *University of Tennessee Nuclear Physics Progress Report*, (1990) 51.

[Bin90b] C.R. Bingham, M.B. Kassim, H.V. Carmichael, L.L. Riedinger, H.K. Carter, M.O. Kortehlahti, E.F. Zganjar and J.L. Wood, *University of Tennessee Nuclear Physics Progress Report*, (1990) 59.

[Bin92] C.R. Bingham, L.L. Riedinger, G.D. O'Kelly, H.V. Carmichael, L.L. Collins, V.P. Janzen, P.B. Semmes, R.A. Braga, J.L. Wood, R.W.Fink, M. Kortelahti, E.F. Zganjar, I.C. Girit, H.K. Carter and R.L. Mlekodaj, *Studies of the $Z = 81$ Transitional Nucleus ^{195}Tl.*

[Bou85] J.A. Bounds, C.R. Bingham, P. Juncar, H.K. Carter, G.A. Leander, R.L. Mlekodaj, E.H. Spejewski and W.M. Fairbank, *Jr. Phys. Rev. Lett.*. **55** (1985) 2268

[Boh69] A. Bohr, B.R. Mottelson, *Nuclear Structure Vol. I*, (1969) 327.

[Bro64] G.E. Brown, *in:Compt. Rend. Congres Int. de Physique Nucléaire*, de Paris, Vol. 1 (CNRS, Paris, 1964) p. 129.

[Bro66] G.E. Brown and A.M. Green, *Nucl. Phys.* **8** (1966) 87, *Nucl. Phys.* **75** (1966) 401.

[Dup84] P. van Duppen, E. Coenen, K. Deneffe, M. Huyse, K. Heyde and P. van Isacker, *Phys. Rev. Lett.* **55** (1984) 1974.

[Dup87] P. van Duppen, E. Coenen, K. Deneffe, M. Huyse and J.L. Wood, *Phys. Rev.* **C35** (1987) 1861.

[Eji89] H. Ejiri and M.J.A. de Voigt, *Gamma-Ray and Electron Spectroscopy in Nuclear Physics*, (1989).

[Eks76] C. Ekstrom, G. Wannberg, Y.S. Shishodia, *Hyperfine Interactions 1*, (1976), 437.

[Eng65] T. Engeland, *Nucl. Phys.* **72** (1965) 68.

[Fed69] P. Federman, *in: Cargèse Lect. Phys.*, ed. M. Jean (Gordon and Breach, New York, 1969) Vol. 3, p. 21.

[Gri91] J.C. Griffin, R.A. Braga, R.W. Fink, J.L. Wood, H.K. Carter, R.L. Mlekodaj, C.R. Bingham, E. Coenen, M. Huyse and P. van Duppen, *Nucl. Phys.* **A530** (1991) 401.

[Hey83] K. Hyede, P. van Isacker, M. Waroquier, J.L. Wood and R.A. Meyer, *Phys. Rep.* **102** (1983) 291.

[Jel90] N.A. Jelly, *Fundamentals of nuclear physics*, (1990).

[Jin91] H. Jin, "Spectroscopic studies on high-spin states in ^{179,181}Ir and ^{175}Re", *thesis*, (1991).

[May77] F.R. May, V.V. Pashkevich and S. Frauendorf, *Phys. Lett.*. **68B** (1977) 113.

[Mor56] H. Morinaga, *Phys. Rev.* **101** (1956) 254.

[Nat65] O. Nathan and S.G. Nilsson, "Alpha-, Beta-, and Gamma-Ray Spectroscopy", edited by K. Siegbahn, North-Holland Publishing Co., Amsterdam, (1965), 635.

[New74] J.O. Newton, F.S. Stephens, R.M. Diamond, *Nucl. Phys.*. **A236** (1974) 225

[Nil69] S.G. Nilsson, C.F. Tsang, A Sobiczewski, Z. Szymanski, S. Wycech, C. Gustafson, I. Lamm, P. Möller and B. Nilsson, *Nucl. Phys.*. **A131** (1969) 1

[Pau88] M. Pautrat, J.M. Lagrange, J.S. Dionisio, Ch. Vieu and J. Vanhorenbeeck, *Nucl. Phys.*. **A484** (1988) 155.

[Ric78] H. Richel, G. Albouy, G. Auger, F. Hanappe, J.M. Lagrange, M. Pautrat, C. Roulet, H. Sergolle and J. Vanhorenbeeck, *Nucl. Phys.*. **A303** (1978) 483.

[Sch88] M.R. Schmorak, *Nucl. Data Sheet.* **53** (1988) 331.

[Sha53] A. de Shalit and M. Goldhaber, *Phys. Rev.* **92** (1953) 1211.

[Shi90] V.S. Shirley, *Nucl. Data Sheet.* **61** (1990) 519.

[Tho83] R.C. Thompson, M. Anselment, K. Bekk, S. Goring, A. Hanser, G. Meisel, H. Rebel, G. Schatz, B.A. Brown, *J. Phys. (London).* **G9** (1983) 443.

[Tru72] V.F. Trusov, *Nucl. Data Tables.* **10** (1972) 477.

[Van91] J. Vanhorenbeeck, P. del Marmol, E. Coenen, M. Huyse, P. van Duppen and J. Wauters, *Nucl. Phys.* **A531** (1991) 63.

[Woo92] J.L. Wood, K. Heyde, W. Nazarewicz, M. Huyse and P. van Duppen, *Phys. Rep.* **215** (1992) 101.

VITA

Ming Zhang was born in Tianjin, the People's Republic of China, on April 5, 1957. But he grew up in Beijing between 1959 and 1977, and considers it as his home town. He entered the Peihong primary school in September, 1964, and spent the entire primary school and high school education in Beijing, graduating from the Beijing 67th High School in January, 1976. After that, he had to work two years in the countryside before entering Fudan University in Shanghai as an undergraduate in March, 1978. He received his Bachelor of Science degree in Physics in January, 1982. Then he returned to Beijing as a graduate student in the Institute of Atomic Energy and received his Master of Science degree in April, 1985. As a research assistant and research associate, he worked in the same institute for more than four years. In August 1989, he moved to the United States to continue his studies towards a Doctoral degree in Physics at the University of Tennessee, Knoxville. He worked as a research assistant with the nuclear physics group at the university. After receiving his Ph.D. degree, he will study as a post-doctoral scholar in the field of Nuclear Magnetic Resonance Imaging and Spectroscopy.